# A Study of Material Damping in Large Space Structures

Final Technical Report

by

Dr. A.L. Highsmith
Dr. D.H Allen

Department of Aerospace Engineering
Texas A&M University

Submitted to

NASA Johnson Space Center

Grant No. NAG-9-192
April 1989

## Table of Contents

# 1 INTRODUCTION

Because they provide high stiffness and strength and are relatively light weight, continuous fiber reinforced laminated composite materials are candidates for use in large space structures. One of the significant differences between these composites and more conventional engineering materials is that laminated composites develop a considerable amount of large-scale damage. Numerous ply cracks and delaminations may develop in a laminate early in its load history.

Unlike fiber breaks and fiber-matrix debonds, which tend to influence only a small volume of material, ply cracks and delaminations can cause significant changes in the bulk properties of a laminate. Numerous researchers have studied and modelled the influence of ply cracking [1,2,5] and delamination [3,6] on the elastic behavior of laminated composites. But while significant increases in damping have been observed as a result of damage development [7,8], and modelling efforts have predicted that significant changes in the dynamic response of structures can result from changes in material damping [9,10], existing models of damping in composites [11,12] have not included the effects of damage on damping.

This report summarizes the work completed under NASA Grant NAG-9-192. This research effort had as its objective the development of a damage dependent constitutive model for predicting the influence of damage on the damping properties of laminated composites. In particular, the beam bending behavior of cross-ply laminates was studied. The damage mode of interest was ply cracking. The research proceeded along two fronts. The primary effort was to develop a continuum damage model based on internal state variables to describe the viscoelastic behavior of laminates as a function ply cracking. In support of the continuum modelling, an experimental program was implemented to determine stiffness and damping as a function of damage. A second effort involved the development of a micromechanics model of damage dependent damping.

# 2 CONTINUUM DAMAGE MODEL

## 2.1 Theoretical Development

The constitutive model used in this study follows the model developed [4] and used by Allen, et al. to predict the damage dependent elastic response of laminated composites containing ply cracks [5] and delaminations [6]. For a given ply, the uniaxial constitutive equation has the form

$$\sigma_{xx} = E(\epsilon_{xx} - \alpha_1) \quad , \tag{2.1}$$

where E is the modulus of the material, and $\alpha_1$ is an internal state variable which reflects the effect of ply cracking on ply behavior. In general, there would be one internal state variable (ISV) for each different damage mode. Multiaxial behavior requires a tensor quantity to characterize the effect of damage.

In the earliest version of the model [13,14,15], it was assumed that a ply could be modelled as a Voigt material, which has the mechanical analog shown in Fig. 1. For such a material, the constitutive equation has the form

$$\sigma_{xx} = E\epsilon_{xx} + \eta\dot{\epsilon}_{xx} \quad , \tag{2.2}$$

where the term $\eta\dot{\epsilon}_{xx}$ represents the viscous part of the material response. This equation can be made to fit the form Eqn. (1) by taking $\alpha_1 = -\frac{\eta}{E}\dot{\epsilon}_{xx}$ . In fact, two ISV's, one representing stiffness changes due to ply cracking and the other representing damping changes due to ply cracking, were used in the analysis. Strictly speaking continuous fiber reinforced materials do not behave like Voigt materials, within a limited range of frequencies and amplitudes appropriate Voigt material parameters can be chosen to provide a reasonable representation of ply response.

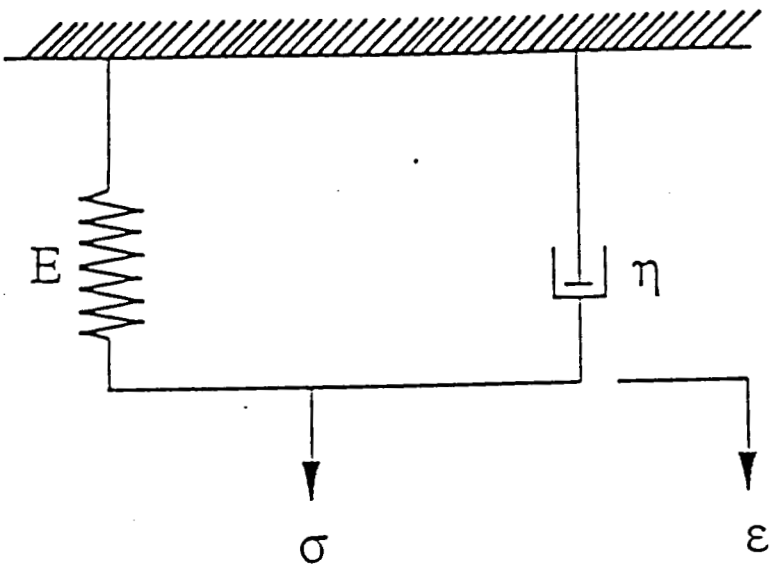


Figure 1.The Voigt model.

While the Voigt model was useful in the early stages of the development of the damage dependent constitutive model, it was somewhat restrictive. For example, Voigt type ply response led to a linear frequency dependence on laminate damping [13,14,15]. This frequency dependence was not observed in subsequent experimental results. A more general formulation has since been developed which uses a complex modulus representation of viscoelastic ply properties [16]. It is this second formulation which will be discussed here. In this formulation, the damage dependent, elastic constitutive relation has the form

$$\sigma_{xx} = E\epsilon_{xx} + I\alpha_1 \quad , \tag{2.3}$$

where now the term $I\alpha_1$ captures the damage dependence. For a linear viscoelastic material under sinusoidal loading, the constitutive relation takes the form

$$\tilde{\sigma}_{xx} = E^*\tilde{\epsilon}_{xx} + I^*\tilde{\alpha}_1 \quad . \tag{2.4}$$

where

$$E^* = E' + iE''$$

$$I = I' + iI''$$

$$\tilde{\epsilon}_{xx} = \epsilon_A e^{i\omega t}$$

$$\tilde{\alpha}_1 = \alpha_{1A} e^{i\omega t} \quad .$$

Using the viscoelastic constitutive relation above, it can be shown that the energy dissipated by a ply per cycle of loading is given by

$$\Delta w = \pi E'' \epsilon_A^2 + \pi I'' \alpha_{1A} \epsilon_A \quad , \tag{2.5}$$

and the stored energy during the peak displacement is given by

$$U = [E' \epsilon_A^2 + I' \epsilon_A \alpha_{1A}]/2 \quad . \tag{2.6}$$

It then follows that the loss factor is

$$\eta = \frac{E'' \epsilon_A^2 + I'' \alpha_{1A} \epsilon_A}{E' \epsilon_A^2 + I' \alpha_{1a} \epsilon_A} \quad . \tag{2.7}$$

With the additional assumptions that

$$\begin{aligned} I'' \alpha_{1A} &= \Delta E'' \epsilon_A \\ I' \alpha_{1A} &= \Delta E' \epsilon_A \quad , \end{aligned} \tag{2.8}$$

we arrive at the expression for the loss factor

$$\eta = \frac{E'' + \Delta E''}{E' + \Delta E'} \quad . \tag{2.9}$$

The complex modulus of a laminate may be determined from the ply level constitutive relations using classical lamination theory [17] to be

$$E^* = \frac{1}{t^3} \sum_{i=1}^{n} (z_k^3 - z_{k-1}^3) E_i^* \quad , \tag{2.10}$$

where $E^*$ is the complex modulus of the laminate, h is the thickness of the laminate, N is the number of plies in the laminate, $E_i^*$ is the damage dependent

complex modulus of ply i, and the $z_i$ are the coordinates of the ply interfaces. For a symmetric cross-ply laminate, a symmetric laminate consisting of 0° and 90° plies, the expression above reduces to

$$E^* = aE_L^* + bE_T^* \tag{2.11}$$

if the laminate is undamaged. In Eqn. (2.11), a and b depend on laminate geometry, and $E_L^*$ and $E_T^*$ are the complex moduli of the 0° and 90° plies, respectively. The flexural damping is given by

$$\tan\phi_E = \eta = \frac{aE''_L + bE''_T}{aE'_L + bE'_T} \ . \tag{2.12}$$

In the present study, it was assumed that ply cracking would affect $E_T^*$ but not $E_L^*$. It follows that for a damaged laminate, the flexural damping is given by

$$\eta = \frac{aE''_L + bE''_T + C\Delta E''_T}{aE'_L + bE'_T + C\Delta E'_T} \ , \tag{2.13}$$

where $C\Delta E''_T$ and $C\Delta E'_T$ are functions of the total crack surface area and location of the cracks. Both $\Delta E''_T$ and $\Delta E'_T$ can be determined from experimental data from a single laminate, and then can be used to predict behavior in other laminates via Eqn. (2.13).

## 2.2 Experimental Program

In order to evaluate the analytical model, damping was measured as a function of damage in a variety of graphite/epoxy cross-ply laminates [14,15]. Damage was introduced into straight sided coupon type specimens under uniaxial tensile loading in an MTS servohydraulic testing machine. Edge replication

was used to monitor the development of 90° ply cracks during tensile loading. At various stages of damage development, the tensile test was interrupted, so that the specimen could be removed and its flexural damping measured.

The experimental setup used in performing the damping measurements is shown schematically in Fig. 2. The specimen was cantilevered from a support housed in a vacuum chamber. All damping data was obtained in vacuum. A motorized wheel with a contacting rod was used to deflect the specimen and excite its first mode of free vibration. Care was used to insure that the initial deflection was small, so that no new damage would be introduced during the damping test. A strain gage mounted on the specimen near the cantilevered support was used to monitor the surface strain in the specimen during free vibration. A personal computer with an A/D board was used to start and stop the motor, and to record strain data.

After capturing the strain data, the peaks in the strain versus time curve were obtained. A representative plot of log strain amplitude versus cycle number is shown in Fig. 3. The decay of strain amplitude is seen to be nearly linear on a semi-log plot. The slope of the best fit straight line to the log strain amplitude data was taken to be the logarithmic decrement, which is directly related to damping.

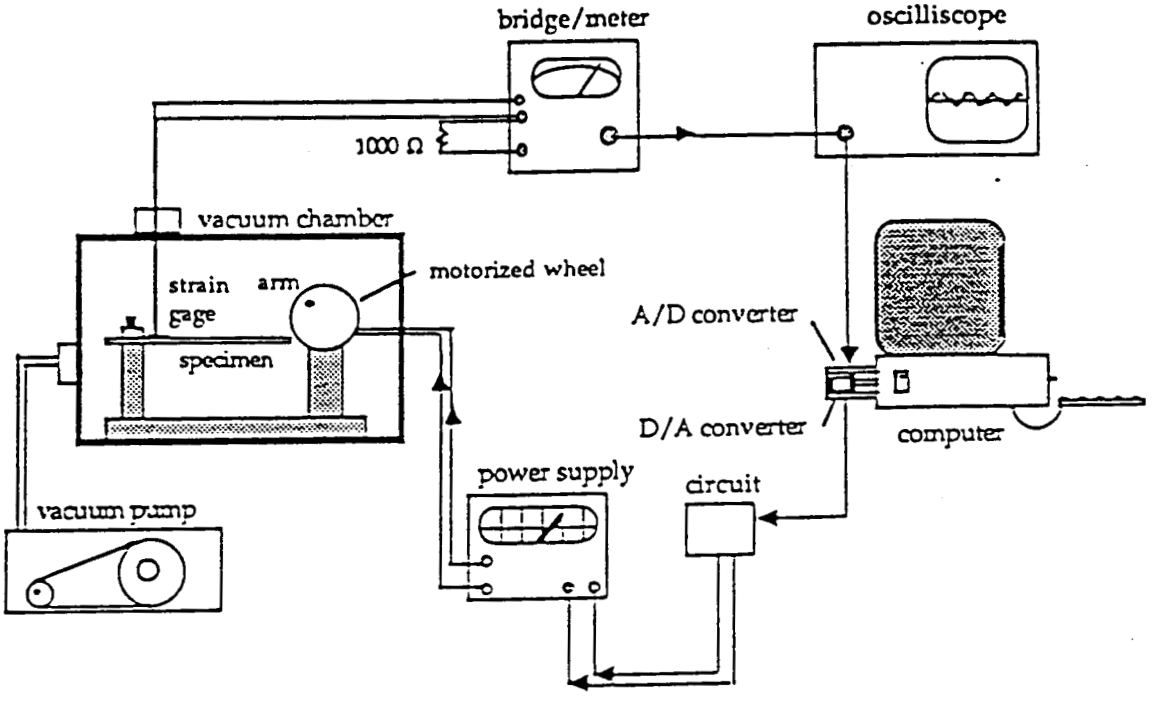


Figure 2. Schematic diagram of the damping measurement system.

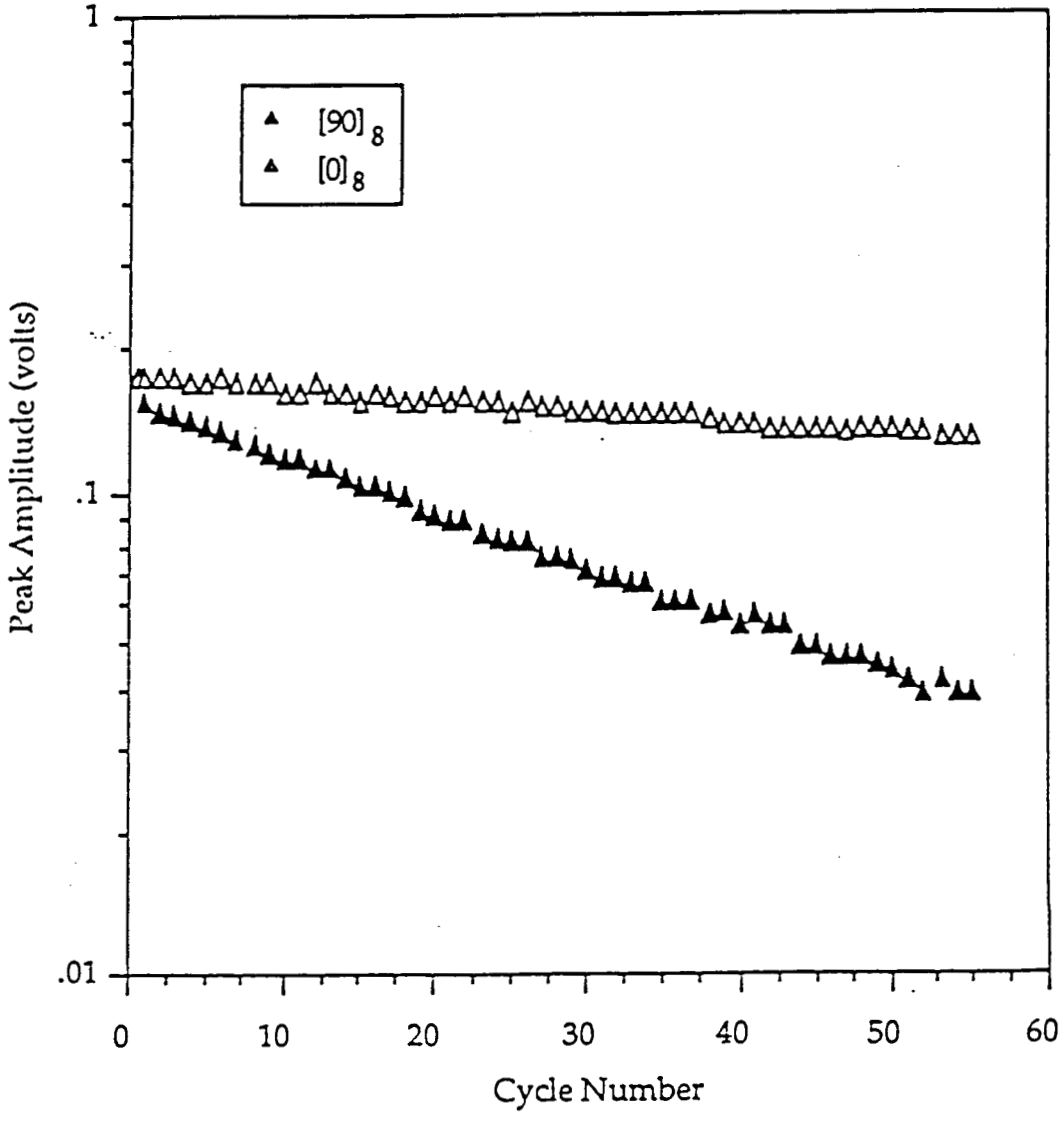


Figure 3. Representative plots of strain amplitude versus cycle for 0° and 90° graphite/epoxy laminates.

## 2.3 Comparison of Theory and Experiment

From measured values of the stiffness and damping of laminates containing all 0° and all 90° plies, the parameters $E'_L$, $E'_T$, $E''_L$, and $E''_T$ can be determined. These parameters can in turn be used to predict the damping of other laminates consisting of combinations of 0° and 90° plies. A comparison of the predicted and observed damping in several cross-ply laminates is presented in Fig. 4. Agreement between theory and experiment is quite reasonable. The 90° plies exhibit matrix dominated behavior, and hence are the primary contributors to damping in laminates. In addition, the effect of a 90° ply increases with distance from the midplane.

In order to predict the influence of damage on damping, it was necessary to determine the parameters $\Delta E'_T$ and $\Delta E''_T$ as a function of crack surface area. Since the elastic properties of the graphite/epoxy laminates are dominated by the 0° plies, $\Delta E'_T$ term was assumed to have a negligible effect on the denominator of the right hand side of Eqn. (2.13). Further, damage dependent damping data from $[0/90/0]_s$ specimens was used to determine

$$\Delta E''_T(s) = 57.97 \times 10^{-6}[0.0002(s) - 1.7108 \times 10^{-5}(s^2)] \ ,$$

where s is the crack surface area in the 90° ply. Using this expression in Eqn. (2.13), damping was predicted as a function of damage in other cross-ply laminates.

Figures 5, 6, and 7 present a comparison between predicted and observed damping values in $[90/0/90]_s$, $[0/90]_{2s}$, and $[90/0/90_2]_s$ laminates at two different damage states. Generally, agreement between theory and experiment is quite good. The effect of damage on the behavior of the $[0/90]_{2s}$ is smaller than the effect of damage on the behavior of the other laminates because the 90° plies are located closer to the midplane. Thus, any influence of the 90° plies on the flexural damping is reduced. This stacking sequence dependence is also reflected in a smaller damping value for the $[0/90]_{2s}$ laminate.

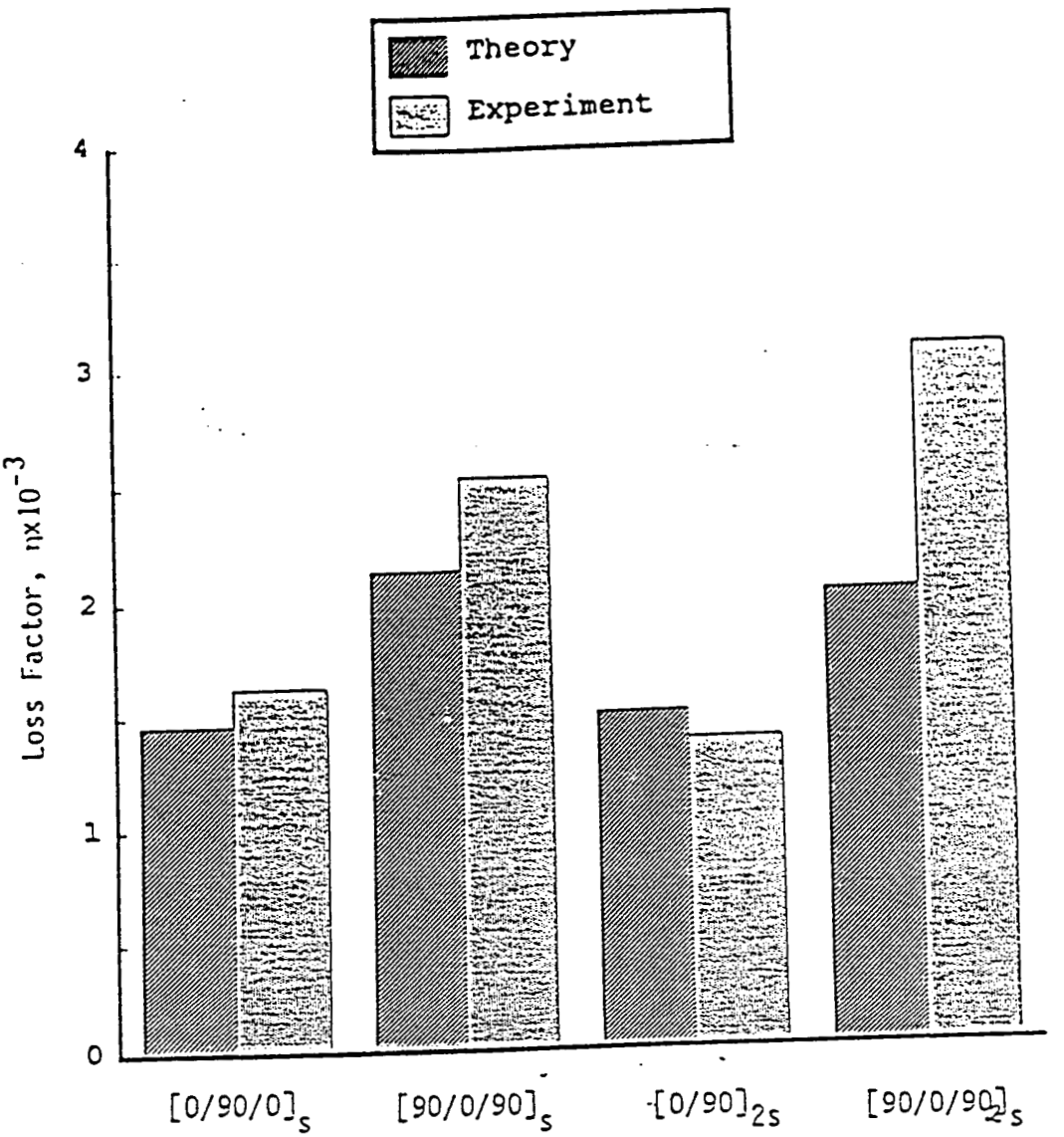


Figure 4. Damping values for various undamaged graphite/epoxy laminates.

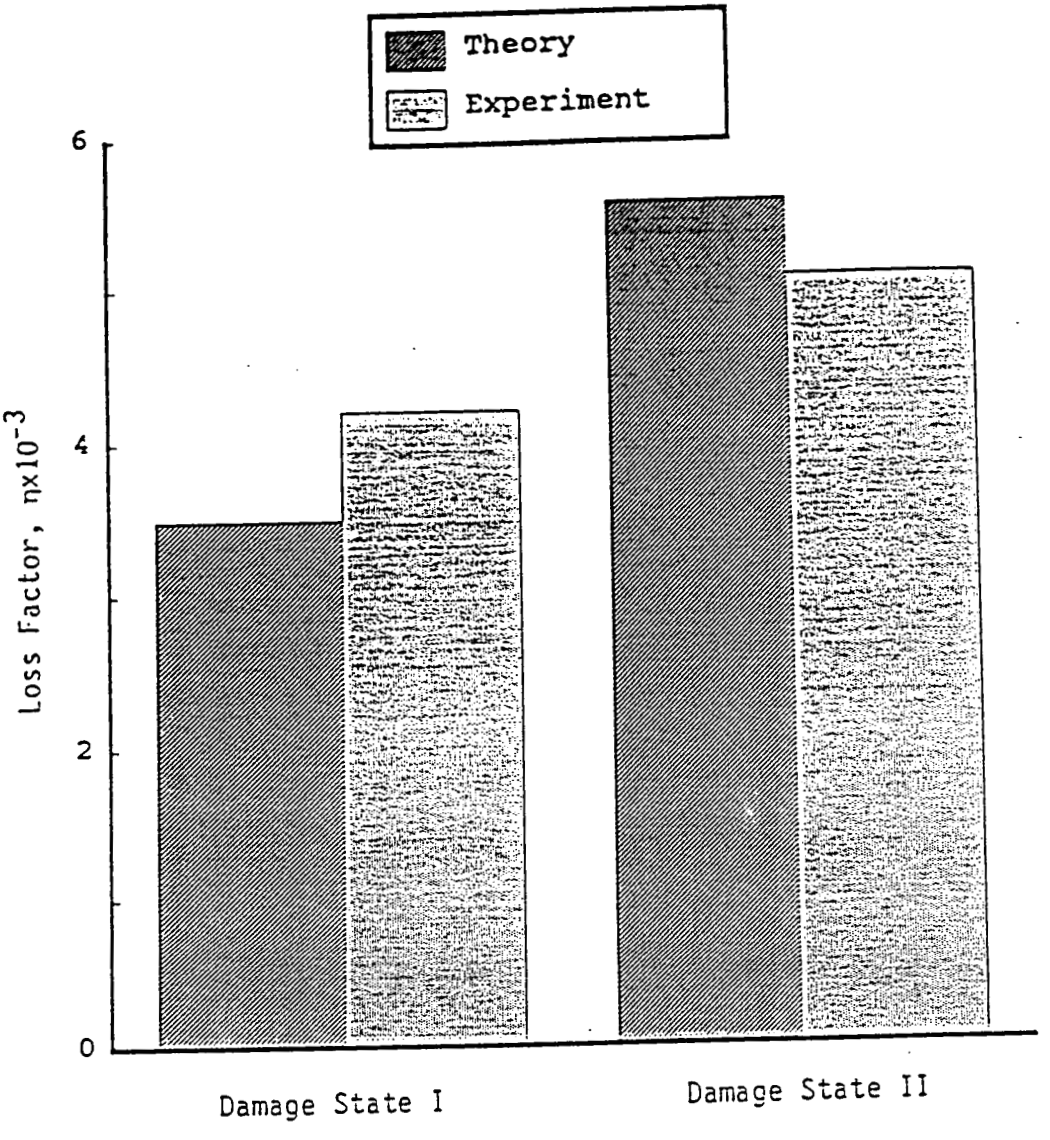


Figure 5. Damage dependent damping values for $[90/0/90]_s$ graphite/epoxy laminates.

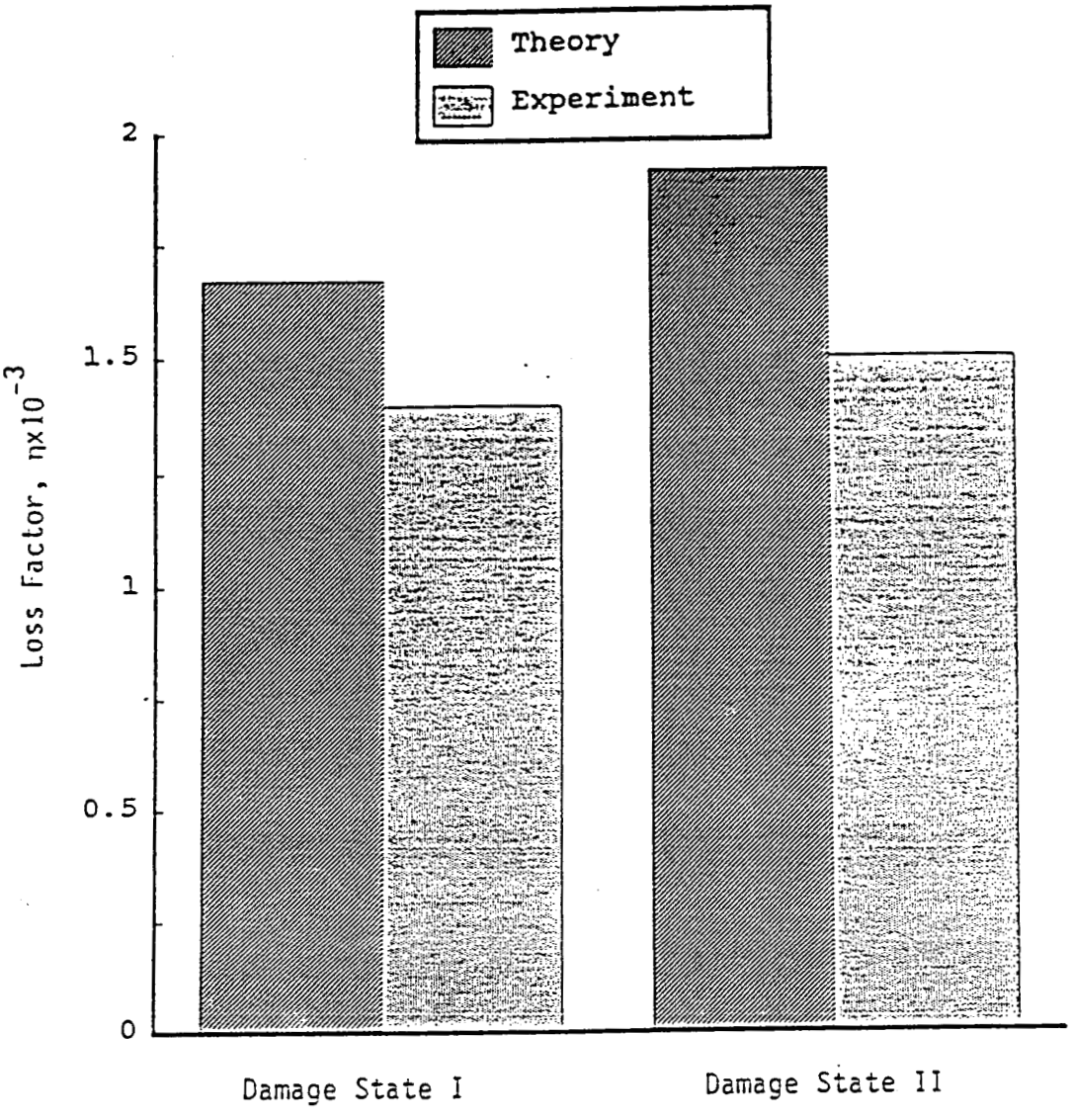


Figure 6. Damage dependent damping values for $[0/90]_{2s}$ graphite/epoxy laminates.

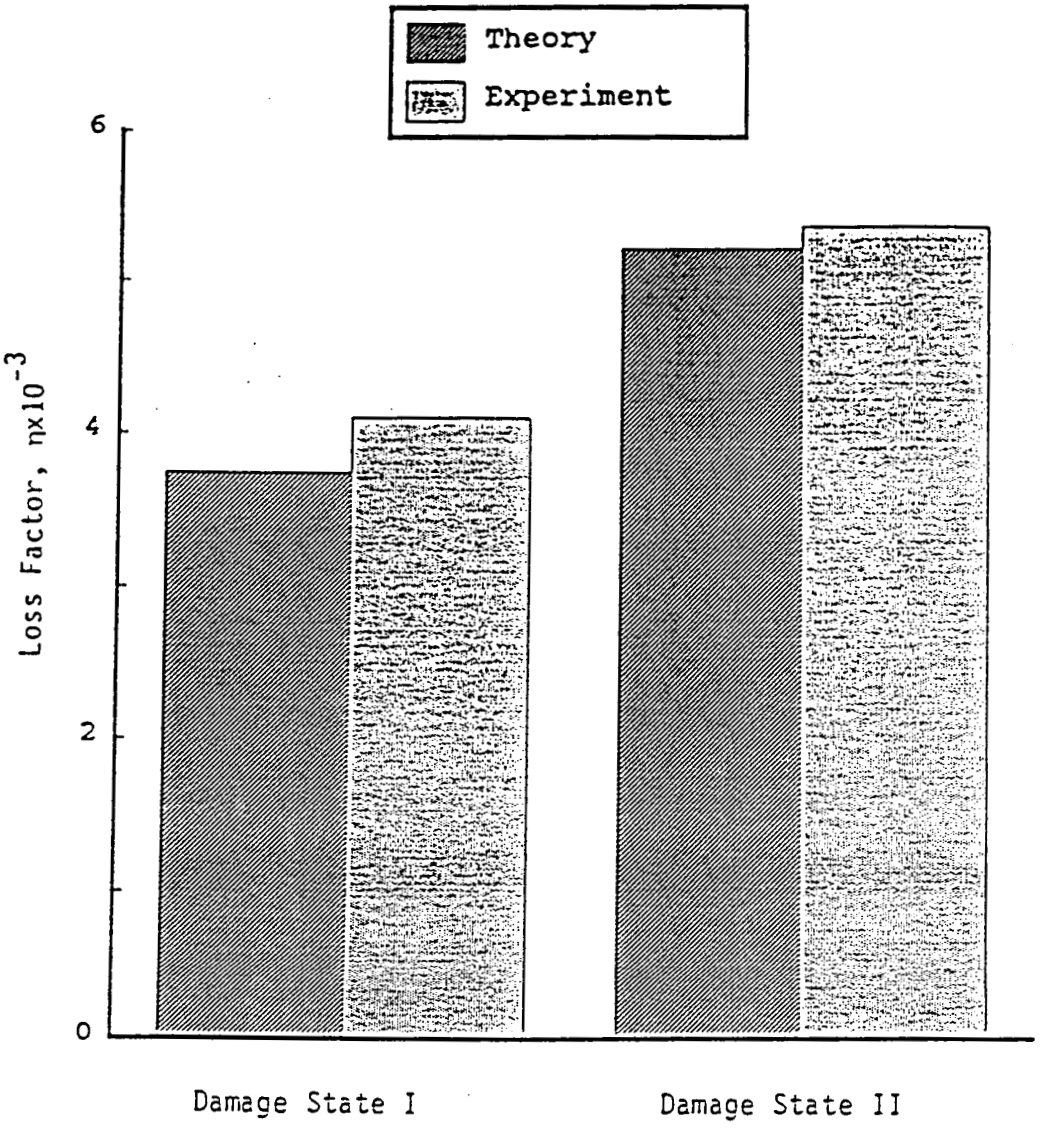


Figure 7. Damage dependent damping values for $[90/0/90_2]_s$ graphite/epoxy laminates.

# 3 MICROMECHANICS MODEL

## 3.1 Theoretical Development

In order to better understand the details of damage-induced damping, a micromechanics model of damaged crossply laminates was developed [19]. The model is based on shear lag theory, and explicitly includes 90° ply cracks. In fact, two versions of the model were developed. In the first, each ply is treated as an Euler-Bernoulli beam, while in the second, each ply is treated as a Timoshenko beam. The Timoshenko beam version will be described below.

For the Timoshenko model, the axial displacement in layer i is given by

$$u_i(x, z_i) = u_{0i}(x) + z k_i(x) \quad , \tag{3.1}$$

where

$$k_i(x) = \beta_i(x) - \frac{dw}{dx} \quad . \tag{3.2}$$

In Eqn. (3.2) w is the deflection of the ply, which is assumed to be the same as the deflection of the laminate. The Euler-Bernoulli model does not include the ply shear term, which is represented by $\beta$.

Ply equilibrium equations are obtained by performing force and moment summations on a differential element taken from the ply. Such an element is shown in Fig. 8. The interlaminar shear stresses shown in this figure are determined using the shear lag assumption, i.e., they are assumed to be proportional to the difference in ply displacements across the interface.

In fact, the shear strain in the interfacial region is given by the difference in the axial displacements of the two plies divided by the thickness of the shear transfer region. Stresses are obtained by multiplying by an appropriate shear modulus for the shear transfer region. Following this procedure, the shear lag assumption yields

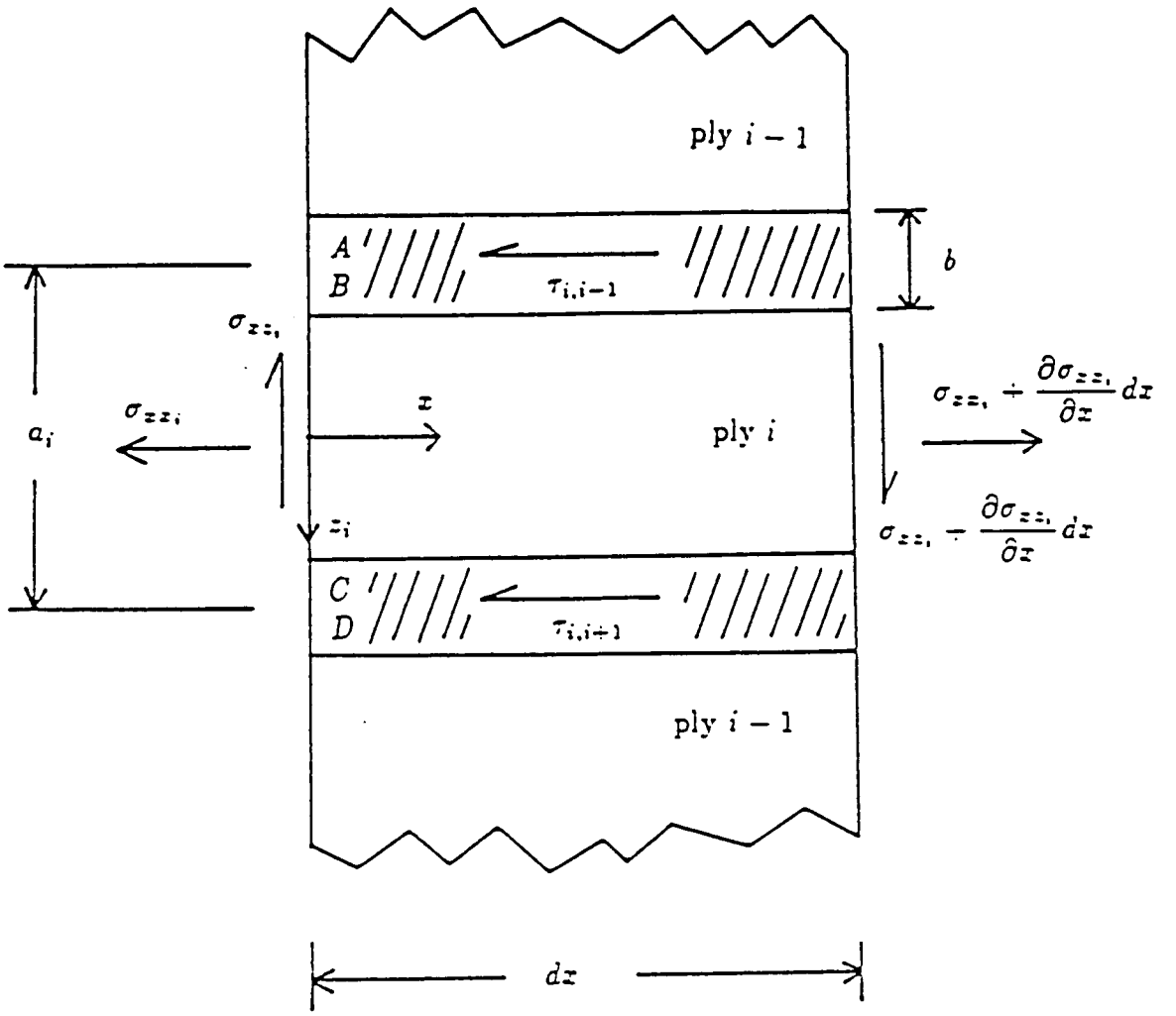


Legend

$a_i$ = Thickness of ply $i$

$b$ = Thickness of shear transfer region

Figure 8. Equilibrium element from ply i for the Timoshenko micromechanics model.

$$\tau_{i,i-1} = \frac{G}{b}\left(u_{0i} - \frac{a_i}{2}k_i - u_{0i-1} - \frac{a_{i-1}}{2}k_{i-1}\right)$$

(3.3)

$$\tau_{i,i+1} = \frac{G}{b}\left(u_{0i} - \frac{a_i}{2}k_i - u_{0i+1} - \frac{a_{i+1}}{2}k_{i+1}\right) \quad .$$

Axial equilibrium for the ply has the form

$$\frac{G}{E_i a_i b}\left(2u_0 i - u_{0i-1} - u_{0i+1} - \frac{a_{i-1}}{2}k_{i-1} + \frac{a_{i+1}}{2}k_{i+1}\right) - u_{oi}'' = 0 \quad . \tag{3.4}$$

equilibrium in the z direction yields

$$\sigma_{xz_i}' = 0 \quad . \tag{3.5}$$

and moment equilibrium has the form

$$\frac{6G}{E_i a_i^2 b}\left(a_i k_i + u_{0i-1} - u_{0i+1} + \frac{a_{i-1}}{2}k_{i-1} + \frac{a_{i+1}}{2}k_{i+1}\right) + \frac{12G_{xz_i}}{E_i a_i^2}k_i$$

(3.6)

$$- \frac{12G_{xz_i}}{E_i a_i^2 \sum_{j=1}^{n} G_{xz_j}}\left(\sum_{j=1}^{n} G_{xz_j}k_j\right) - k_i'' = - \frac{12G_{xz_i}V}{E_i a_i^3 \sum_{j=1}^{n} G_{xz_j}} \quad .$$

Exterior plies have slightly different equilibrium equations owing to the fact that on one side of such a ply there is no neighboring ply, and thus there are no interlaminar shear stresses.

The equilibrium equations for the plies within a laminate can be assembled into a system of coupled, second order differential equations in the form

$$B\{y\} - \{y''\} = \{c\} \quad . \tag{3.7}$$

where the column vector {y} has as its components the midply displacements $u_{0i}$ and the ply rotations $k_i$. These governing equations are applied to a region of the laminate which corresponds to one-half of the crack spacing. Such a region is shown in Fig. 9. At x=0, the displacement in the uncracked plies is zero, while in the cracked plies, the crack surfaces are stress-free. A symmetry condition at x=1 requires that ply displacements be equal at the ply interfaces. Applied loads then determine the midplane displacement and rotation at this end.

The system of linear ordinary differential equations was solved using techniques commonly used for analyzing dynamic systems [20]. This approach requires the determination of eigenvalues and eigenvectors of the coefficient matrix [B]. The solution takes the form of a linear combination of "mode shapes":

$$\{y\} = \sum_{i=1}^{2n} A_i \; e^{\alpha_i x} \{\psi_i\} \quad , \tag{3.8}$$

where the $\alpha_i$ are the eigenvalues and the $\{\psi_i\}$ are the eigenvectors. Boundary conditions determine the coefficients $A_i$ in the solution.

The viscoelastic problem was also solved in order to determine the effect of cracking on damping. This was accomplished using complex moduli in the analysis described above, and obtaining the corresponding solution. Note that only material viscoelastic behavior was included, and that other dissipation mechanisms, such as friction, were ignored.

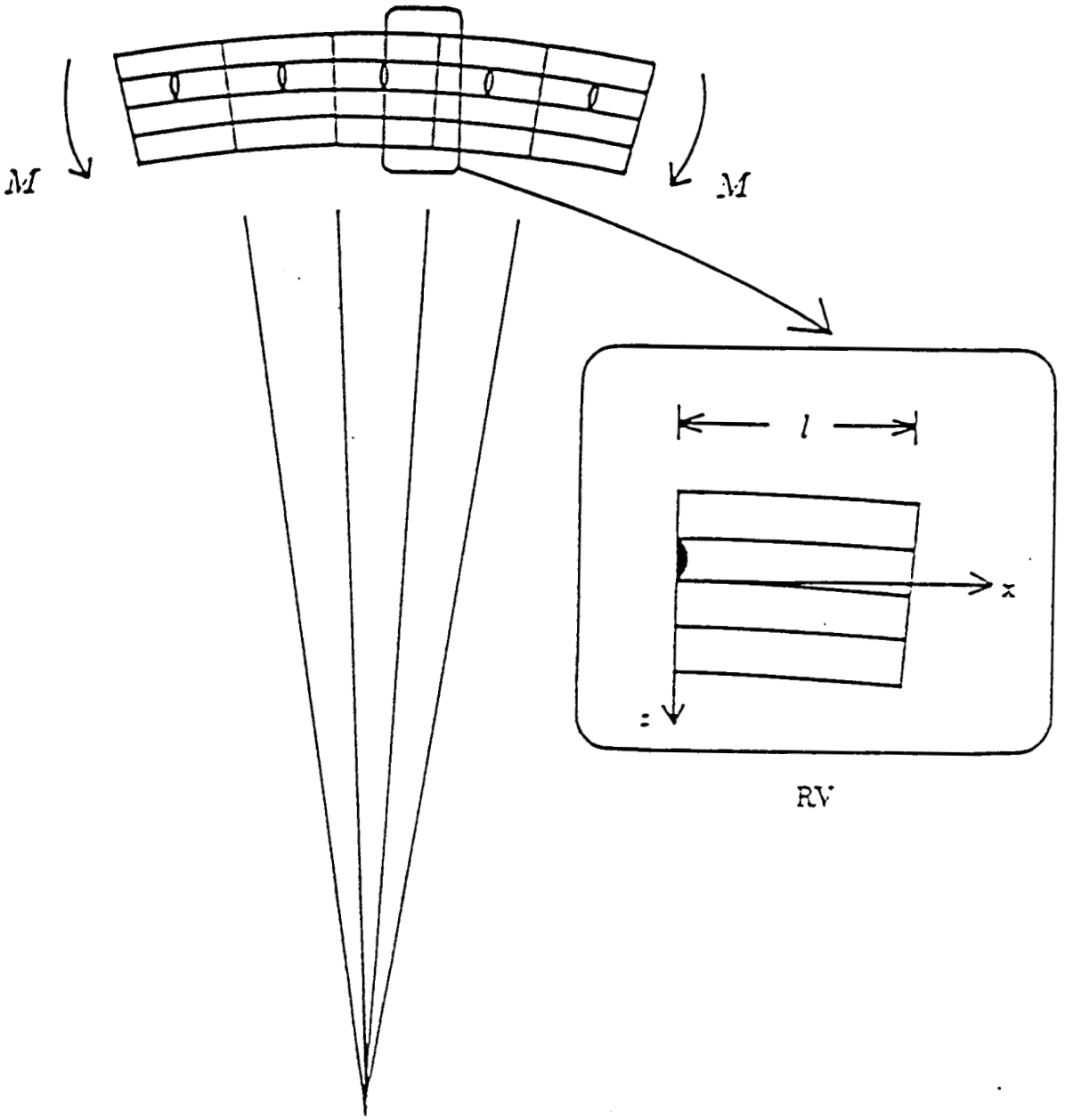


Figure 9. Representative volume within a damaged laminate.

### 3.2 Comparison with Experiment

Experimental data for bending stiffness as a function of crack density was obtained for $[0/90_3]_s$ and $[90_2/0_2]_s$ glass/epoxy laminates. A glass/epoxy system was chosen because it is a less fiber dominated system than graphite/epoxy, and thus should exhibit larger property changes due to damage development. Specimens were loaded in quasi-static tension in order to introduce damage, which was monitored using edge replication. Four-point bending tests were used to determine the bending stiffness at a variety of damage states. This data was compared to model predictions.

Figures 10 and 11 present the theoretical and experimental bending stiffness data for the $[0/90_3]_s$ and $[90_2/0_2]_s$ laminates, respectively. Note that in Fig. 10, there is little bending stiffness reduction observed. This is because the 0° plies are located at the exterior of the laminate. In light of this small stiffness reduction, the predicted responses are in reasonable agreement with experiment. The Timoshenko model provides slightly better predictions than the Euler-Bernouli model. The $[90_2/0_2]_s$ laminate (Fig. 11) exhibits larger stiffness changes. The Timoshenko model provides a reasonable estimate of laminate response up to crack densities of about 13 cracks/in., at which point delaminations begin to develop.

Fig. 12 shows the predictions of loss factor as a function of crack density in a $[90_2/0_2]_s$ laminate. At low crack densities, the damping increases with cracking. But at larger crack densities, damping decreases with cracking. It is believed that this behavior is a result of excessive load transfer from the relatively viscoelastic 90° plies to the relatively elastic 0° plies that occurs at high crack densities. At lower crack densities, stress concentrations in the shear transfer region are able to generate an increase in damping. This decrease in damping is not observed in the laboratory. At present, it is believed that other dissipation mechanisms, such as friction between rubbing crack faces, account for the discrepancy. With

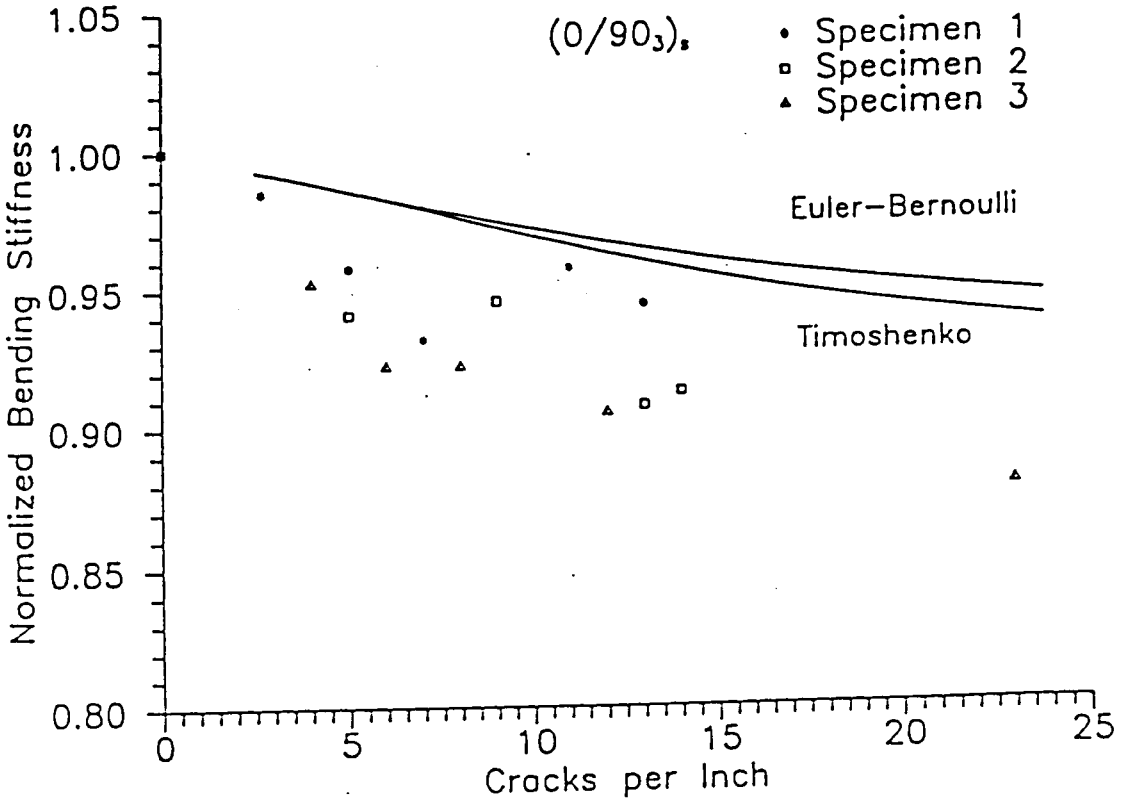


Figure 10.Damage dependent bending stiffness in $[0/90_3]_s$ glass/epoxy laminates.

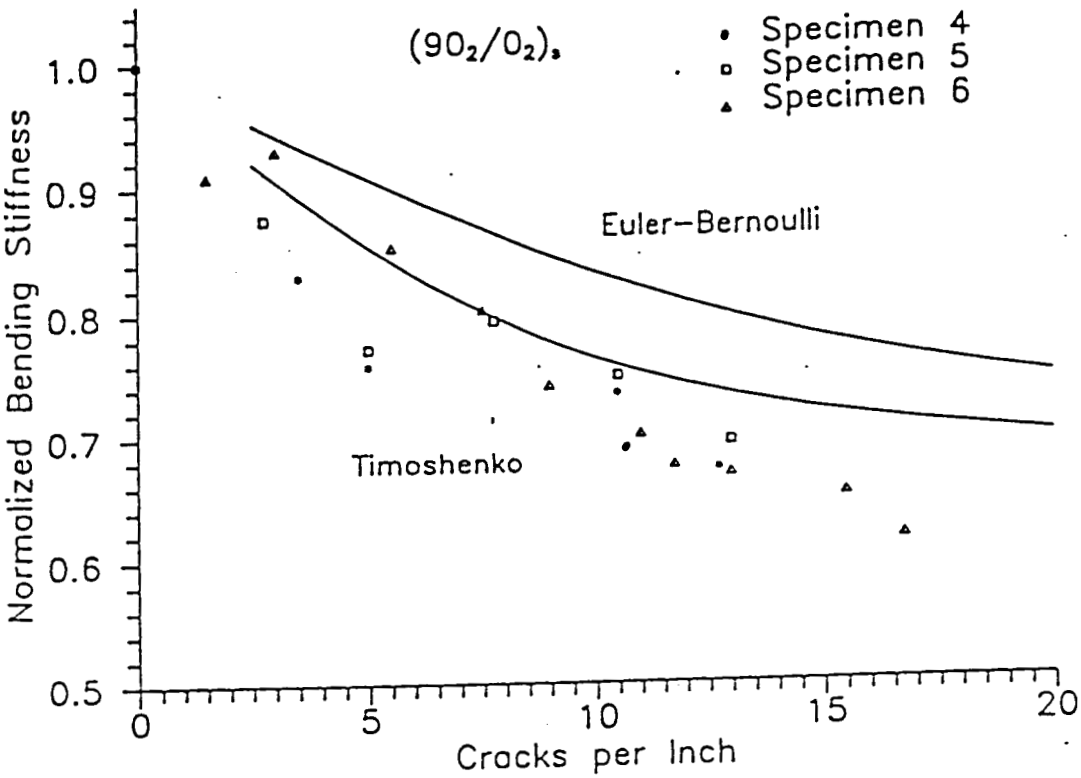


Figure 11. Damage dependent bending stiffness in $[90_2/0_2]_s$ glass/epoxy laminates.

additional effort, it should be possible to use the micromechanics model to estimate frictional dissipation.

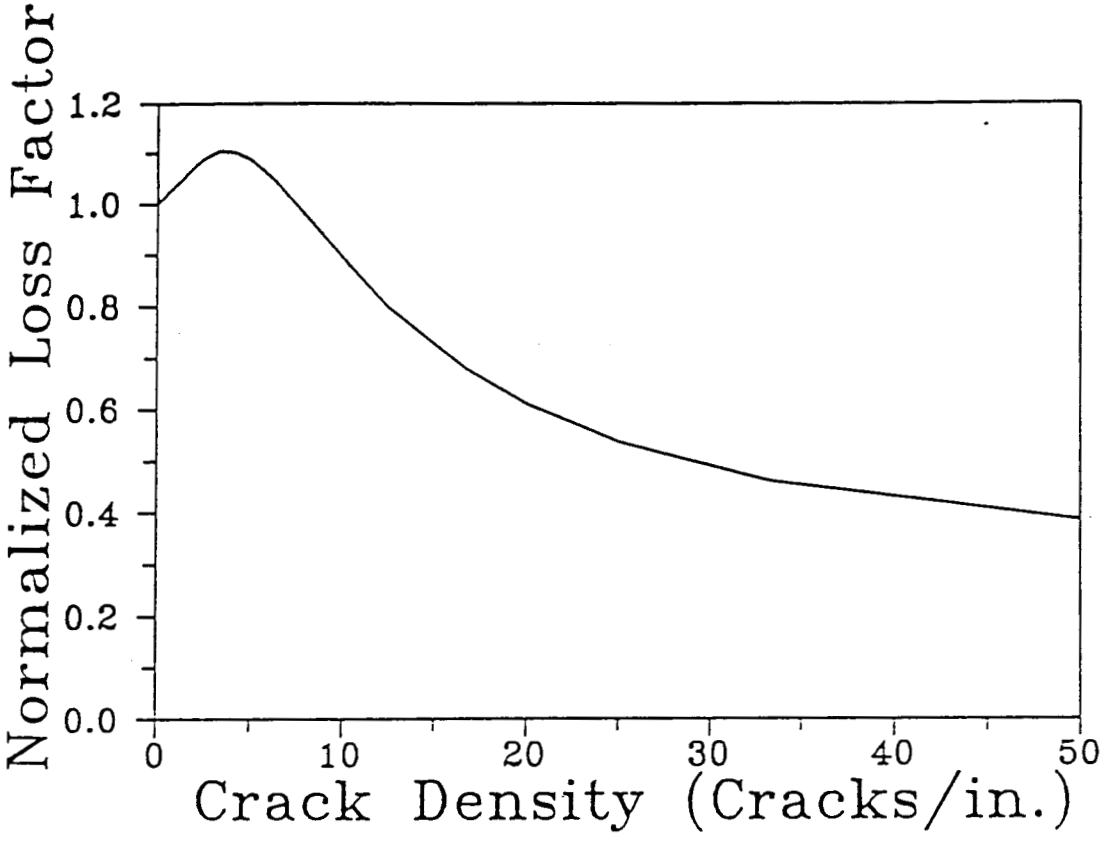


Figure 12. Predictions of loss factor as a function of damage using the Timoshenko model.

# 4 CONCLUSIONS

A constitutive model has been developed for predicting damping as a function of damage in continuous fiber reinforced laminated composites. The damage model is a continuum formulation, and uses internal state variables to quantify damage and its subsequent effect on material response. The model is sensitive to the stacking sequence of the laminate. Given appropriate baseline data from unidirectional material, and damping as a function of damage in one crossply laminate, damping can be predicted as a function of damage in other crossply laminates. Agreement between theory and experiment has been quite good.

A micromechanics model has also been developed for examining the influence of damage on damping. This model explicitly includes crack surfaces. The model provides reasonable predictions of bending stiffness as a function of damage. Damping predictions are not in agreement with experiment. This is thought to be a result of dissipation mechanisms such as friction, which are not presently included in the analysis.

## 5 REFERENCES


[1] Highsmith, and Reifsnider, K.L., "Stiffness Reduction Mechanisms in Composite Laminates," Damage in Composite Materials, ASTM STP 775, K.L. Reifsnider, Ed., ASTM, 1982, pp. 103-117.

[2] Norvell, R.G., "An Investigation of Damage Accumulation in Graphite/Epoxy Laminates," Texas A&M University Thesis, August, 1985.

[3] O'Brien T.K., "Characterization of Delamination Onset and Growth in a Composite Laminate," Damage in Composite Materials, ASTM STP 775, K.L. Reifsnider, Ed., ASTM, 1982, pp. 140-167.

[4] Allen, D.H., Allen, C.E., and Groves, S.E., "A Thermomechanical Constitutive Theory for Elastic Composites with Distributed Damage - Part I. Theoretical Development," International Journal of Solids and Structures

[5] Allen, D.H., Allen, C.E., and Groves, S.E., "A Thermomechanical Constitutive Theory for Elastic Composites with Distributed Damage - Part I. Application to Matrix Cracking in Laminated Composites," International Journal of Solids and Structures

[6] Allen, D.H., Groves, S.E., and Harris, C.E., "A Cumulative Damage Model for Continuous Fiber Composite Laminates with Matrix Cracking and Interply Delaminations," ASTM STP ___, 8th Symposium on Composites: Testing and Design

[7] Plunkett, R., "Damping in Fiber Reinforced Laminated Composites at High Strain," J. Composite Materials Supplement, Vol. 14, pp. 109-117, 1980.

[8] Edberg, D.L., "Material Damping of Sample Structures in a Simulated Space Environment,", Journal of Spacecraft and Rockets, Vol. 23, pp. 288-296, 1986.

[9] Kalyanasundaram, S., Lutz, J.D., Haisler, W.E., and Allen D.H., "Effect of Degradation of Material Properties on the Dynamic Response of Large Space Structures," Journal of Spacecraft and Rockets, Vol. 23, pp. 297-302, 1986.

[10] Chang, H.T., and Allen, D.H., "Predicted Dynamic Response of a Composite Beam with History Dependent Damage," Texas A&M University Mechanics and Materials Center, MM 4875-86-17, July, 1986.

[11] Gibson, R.R., and Plunkett, R., "Dynamic Mechanical Behavior of Fiber-Reinforced Composites: Measurement and Analysis," Journal of Composite Materials, Vol. 10, pp. 325-341, 1976.

[12] Ni, R.G., and Adams, R.D., "The Damping and Dynamic Moduli of Symmetric Laminated Composite Beams - Theoretical and Experimental Results," Journal of Composite Materials, Vol. 18, pp. 104-121, 1984.

[13] Allen, D.H., Harris, C.E., and Highsmith, A.L., "Prediction and Experimental Observation of Damage Dependent Damping in Laminated Composite Beams," The Role of Damping in Vibration and Noise Control, DE-Vol. 5, L. Rogers, ed., ASME, 1987, pp. 253-263.

[14] Smith, S.A., "An Experimental Investigation of Damage-Dependent Material Damping of Laminated Composites," Texas A&M University Thesis, May 1988.

[15] Smith, S.A., Allen, D.H., and Harris, C.E., "An Experimental Investigation of Damage-Dependent Material Damping in Laminated Composites," Proc. AIAA/ASME/ASCE/AHS 29th Structures, Structural Dynamics, and Materials Conference, pp. 1501-1510, 1988.

[16] Kalyanasundaram, S., and Allen, D.H., "A Model for Predicting Damage Dependent Damping in Laminated Composites," Computers and Structures, Vol. 30, No. 1/2, pp. 113-118, 1988.

[17] Jones, R.M., Mechanics of Composite Materials, Hemisphere, New York, 1975.

[18] Kalyanasundaram, S., Allen, D.H., and Schapery, R.S., "Dynamic Response of a Viscoelastic Timoshenko Beam," Proc. AIAA/ASME/ASCE/AHS 28th Structures, Structural Dynamics, and Materials Conference, 1987.

[19] Frailey, J.A., "Matrix Cracking and Bending Stiffness Reduction in Composite Laminates," Teexas A&M University Thesis, December, 1988.

[20] Junkins, J.L., and Turner, J.D., Optimal Spacecraft Rotational Maneuvers, Elsevier, Amsterdam, 1986.

## 6 BIBLIOGRAPHY


[1] Allen, D.H., Harris, C.E., and Highsmith, A.L., "Prediction and Experimental Observation of Damage Dependent Damping in Laminated Composite Beams," The Role of Damping in Vibration and Noise Control, DE-Vol. 5, L. Rogers, ed., ASME, 1987, pp. 253-263.

[2] Smith, S.A., Allen, D.H., and Harris, C.E., "An Experimental Investigation of Damage-Dependent Material Damping in Laminated Composites," Proc. AIAA/ASME/ASCE/AHS 29th Structures, Structural Dynamics, and Materials Conference, pp. 1501-1510, 1988.

[3] Kalyanasundaram, S., and Allen, D.H., "A Model for Predicting Damage Dependent Damping in Laminated Composites," Computers and Structures, Vol. 30, No. 1/2, pp. 113-118, 1988.

[4] Kalyanasundaram, S., Allen, D.H., and Schapery, R.S., "Dynamic Response of a Viscoelastic Timoshenko Beam," Proc. AIAA/ASME/ASCE/AHS 28th Structures, Structural Dynamics, and Materials Conference, 1987.

[5] Smith, S.A., "An Experimental Investigation of Damage-Dependent Material Damping of Laminated Composites," Texas A&M University Thesis, May 1988.

[6] Frailey, J.A., "Matrix Cracking and Bending Stiffness Reduction in Composite Laminates," Teexas A&M University Thesis, December, 1988.

# 7 THESIS AND DISSERTATION ABSTRACTS

# ABSTRACT

An Experimental Investigation of Damage-Dependent Material Damping of Laminated Composites. (May 1988)

Scott Andrew Smith, B.S., Texas A&M University

Co-Chairs of Advisory Committee: Dr. Alton L. Highsmith
Dr. Charles E. Harris

An experimental program was developed in which the material damping of laminated graphite/epoxy specimens was measured as a function of matrix cracking. The damping test apparatus was designed to measure the first mode free vibration response of a cantilevered beam. Matrix cracks were introduced into cross-ply laminates, and damping, calculated by the logarithmic decrement method, was measured at several levels of damage.

The 90 degree plies were found to have a greater damping capacity than the 0 degree plies, and placement of the 90 degree plies away from the mid-plane of the laminate thickness resulted in a higher damping measurement. Matrix cracks in the 90 degree plies were seen to significantly increase the damping of the cross-ply laminates. In addition, the matrix cracks which formed in 90 degree plies near the specimen surface, caused a greater increase in damping than matrix cracks near the mid-plane. Finally, a damage-dependent material damping model was applied, which closely predicted the measured damping values.

# ABSTRACT

Matrix Cracking and Bending Stiffness Reduction
in Composite Laminates. (December 1988)
James Alan Frailey, B.S., Texas A&M University
Chair of Advisory Committee: Dr. Alton L. Highsmith

Shear-lag theory was used in the development of two mathematical models to predict the behavior of cracked, cross-ply, laminated composites. One model used Euler-Bernoulli beam theory to model the deformation of each ply while the other used the Timoshenko beam theory. Solutions to the governing system of differential equations provide displacements and stresses throughout a representative volume of the laminate. The models were used to predict the response of laminates under two loading conditions: axial, pure bending.

Analytical results were compared to experimental data for axial and bending stiffness reductions with matrix crack density. Glass/epoxy $[0/90_3]_s$ and $[90_2/0_2]_s$ laminates were selected for the analytical-experimental comparison.

# ABSTRACT

An Investigation of Damping Behavior of

Fiber Reinforced Composite Materials. (May 1989)

Shankar Kalyanasundaram, B.Tech., Madras Institute of Technology

M.S., Oklahoma State University

Co-Chairmen of Advisory Committee: Dr. David H. Allen
Dr. Walter E. Haisler

Advanced fibrous composite materials are known to exhibit viscoelastic behavior, which in turn contributes to the damping of these materials. This study has investigated the effect of shear deformations, rotary inertia and matrix crack damage on the damping characteristics of composite materials. For a composite beam the influence of shear deformation and rotary inertia depend on the ratios of $E'/G'$ , $Tan\Phi_G/Tan\Phi_E$, the length to thickness ratio and mode number. For highly anisotropic beams the loss factors in shear are substantially higher than longitudinal loss factor. This leads to large differences between the damping predictions obtained from Euler-Bernoulli and Timoshenko beam theories. The results of this study show that for highly anisotropic slender beams in which the ratio of $Tan\Phi_G/Tan\Phi_E$ and $E'/G'$ are high, the influence of shear damping is important even in low vibrational modes. A constitutive model has been developed for predicting the effect of microstructural damage on the dynamic response of composite materials. This model is valid for a fixed damage state and small amplitude vibrations. The theoretical formulation has been verified for crossply graphite-epoxy laminates with transverse matrix crack damage. For crossply laminates the loss factor in shear is of the same

order as the longitudinal loss factor and Euler-Bernoulli theory has been found to be adequate for obtaining dynamic properties. Damage dependent material constants obtained from $[0/90/0]_s$ laminates have been used to predict the increase in damping in $[90/0/90]_s$, $[0/90]_{2s}$ and $[90/0/90_2]_s$ laminates for different matrix crack damage states. Damping has been found to be more sensitive to matrix crack damage than the stifness loss. Thus, damping measurements hold some promise for further studying the damage development in composite structural components.

# 8 TECHNICAL REPORTS

## 8.1 Dynamic Response of a Viscoelastic Timoshenko Beam

# DYNAMIC RESPONSE OF A VISCOELASTIC TIMOSHENKO BEAM

by

S. Kalyanasundaram*
D.H. Allen**
and
R.A. Schapery***

Texas A&M University
College Station, TX 77843

## Abstract

The analytical determination of the steady state and transient flexural vibrations of beams is often based on the Euler-Bernoulli equation. In this theory what are normally secondary effects, such as shear deformations and rotary inertia are not included; but these effects may significantly influence the vibrational response under certain conditions.

Advanced fibrous composite materials are known to exhibit viscoelastic behavior, which in turn contributes to the damping of these materials. The analysis presented in this study deals with the vibratory response of viscoelastic Timoshenko beams under the assumption of small material loss tangents. The appropriate method of analysis employed here may be applied to more complex structures.

This study compares the damping ratios obtained from the Timoshenko and Euler-Bernoulli theories for a given viscoelastic material system. From this study the effect of shear deformation and rotary inertia on damping ratios can be identified.

*Research Assistant, Aerospace Engineering Department
Student Member AIAA

**Associate Professor, Aerospace Engineering Department
Member AIAA

***Professor, Civil and Aerospace Engineering Department
Member AIAA

## Nomenclature

| | |
|---|---|
| $E^*$ | Complex Longitudinal Modulus |
| $G^*$ | Complex Shear Modulus |
| $A$ | Cross Sectional Area |
| $\rho$ | Mass Density |
| $w$ | Total Deflection |
| $\psi$ | Bending Slope |
| $L$ | Length of the Beam |
| $I$ | Area Moment of Inertia of Cross Section |
| $k$ | Numerical Shape Factor for Cross Section |
| $n$ | Mode number |
| $E'$ | Longitudinal Storage Modulus |
| $G'$ | Shear Storage Modulus |
| $\tan\delta_E$ | Longitudinal Loss Factor |
| $\tan\delta_G$ | Shear Loss Factor |
| $h$ | Thickness of the Beam |
| $b$ | Width of the Beam |

## Introduction

The study of vibration damping properties of advanced composites is important for several reasons. An automatically controlled flexible space structure may act either docile or unmanageable depending on the level of damping in higher vibration modes[1]. It is also known that damping is sensitive to microstructural detail so that damping measurements can be used to study damage development in composite members[2].

The analytical determination of the dynamic properties of beams generally employs the Euler-Bernoulli equation. For highly anisotropic beams, neglecting shear deformations and rotary

inertia can result in relatively large errors in the predicted dynamic properties. For long slender beams composed of undirectional composite laminae in which the ratio of longitudinal modulus ($E_{11}$) to the shear modulus ($G_{12}$) is high, transverse shear deformations can become significant even in lower vibrational modes.

In experiments[3] conducted on unidirectional E-glass composite beams, the measured values of longitudinal loss modulus are typically 50 to 80 percent higher than the prediction obtained from Euler-Bernoulli beam theory. Adams, et al.[4-6] have also indicated that the measured damping values may depend on shear effects. Schultz and Tsai[7,8] have used the damping ratios measured for three fiber orientation angles to predict the damping ratio for any angle. The damping ratios exhibited qualitative but not quantitative agreement with the predicted properties.

There is a need to develop an improved model for the analysis of large space structures which is capable of describing global structural response including accurate representation of damping characteristics of structural components. The global dynamic response of space structures can be modelled with equivalent continuum beam and plate models. Sun, et al.[9] have presented procedures for constructing several equivalent continuum models. It was found that the Timoshenko beam and Mindlin plate theories were suitable for equivalent continuum modelling. Material damping[10] of structural members can be included in such formulations. For small material loss tangents the dynamic steady-state and transient response of a viscoelastic Timoshenko beam and other structures can be predicted by simple techniques described by Schapery[11].

The Timoshenko beam theory[12], which includes the effects of shear deformation and rotary inertia, has been used to predict flexural resonance frequencies obtained for anisotropic specimens such as wood[13] and fiber reinforced composites[14]. Although the Timoshenko theory was originally developed for isotropic materials, it may be applied to anisotropic beams, providing the appropriate longitudinal and shear moduli and associated loss factors are employed in the model. When the wave lengths of the deformation response are relatively small, a higher order shear deformable theory may be necessary in order to accurately predict dynamic properties of composite beams[15,16].

The goal of the present investigation is to compare the free-vibration damping obtained from Timoshenko and Euler-Bernoulli beam theories for a simply supported beam. From this study the effect of shear deformation and rotary inertia on damping can be identified. The results of the study can be used to interpret the difference between experimental and predicted damping values for beams and to guide a more general study of passive damping in large space structures.

## Analysis

The governing differential equation of the free vibrations of an elastic Euler-Bernoulli beam is given by

$$EI \frac{\partial^4 w}{\partial x^4} + \rho A \frac{\partial^2 w}{\partial t^2} = 0 \qquad (1)$$

The solution for free vibrations can be written in the form

$$w(x,t) = W(x) \exp(i\omega t) \qquad (2)$$

where $W(x)$ is the displacement amplitude at any point in the beam. For sufficiently small damping, free vibrations of a viscoelastic structure decay very slowly, which permits the use of an approximation wherein stress-strain equations for steady-state harmonic vibration are employed. Thus, by the correspondence principle of linear viscoelasticity, the elastic Young's modulus $E$ is replaced by the corresponding complex modulus $E^*$, where

$$E^* = E'(1+i \tan\phi_E) \qquad (3)$$

which, in general, depends on frequency. The boundary conditions for the simply supported Euler-Bernoulli beam are

$$w = \frac{\partial^2 w}{\partial x^2} = 0 \qquad \text{at } x=0,\ L \tag{4}$$

The deflection of the nth mode of vibration is given by

$$w_n(x,t) = A_n \sin \frac{n\pi x}{L}\, e^{i\omega_n t} \qquad (n=1,2,\ldots) \tag{5}$$

The frequency equation is given by

$$n^4\pi^4 = \frac{\rho A L^4}{E^* I}\,\omega_n^2 \tag{6}$$

Since $E^*$ is complex, the frequency values are also complex and can be written as

$$\omega_n = \omega_n' + i\,\omega_n'' \tag{7}$$

Observe that when $\omega_n'' > 0$, the displacement, equation (5), is predicted to decay exponentially. Separating the real and imaginary parts of equation (6) results in

$$E' = \frac{\rho A L^4}{n^4\pi^4 I}\,\omega_n'^2\left(1 - \frac{\omega_n''^2}{\omega_n'^2}\right)$$

If $(\omega_n''/\omega_n')^2 \ll 1$,

$$E' = \frac{\rho A L^4}{n^4\pi^4 I}\,\omega_n'^2 \tag{8}$$

Also,

$$\text{Tan}\phi_E = \frac{2\,\omega_n'\,\omega_n''}{\omega_n'^2(1 - \omega_n''^2/\omega_n'^2)} = \frac{2\,\omega_n''}{\omega_n'} \tag{9}$$

which shows that $\omega_n''/\omega_n'$ is small when the material loss tangent $\tan\phi_E$ is small.

The coupled equations for the total deflection $w$ and bending slope $\psi$ for the Timoshenko beam[17] are as follows:

$$EI\,\frac{\partial^2 \psi}{\partial x^2} + k\left(\frac{\partial w}{\partial x} - \psi\right) AG - I\rho\,\frac{\partial^2 \psi}{\partial t^2} = 0 \tag{10}$$

$$\rho A\,\frac{\partial^2 w}{\partial t^2} - k\left(\frac{\partial^2 w}{\partial x^2} - \frac{\partial \psi}{\partial x}\right) AG = 0 \tag{11}$$

Eliminating $\psi$ from equations (10) and (11), the following equation in $w$ is obtained:

$$\frac{EI}{\rho A}\,\frac{\partial^4 w}{\partial x^4} + \frac{\partial^2 w}{\partial t^2} - \frac{I}{A}\,(1+E/kG)\,\frac{\partial^4 w}{\partial x^2 \partial t^2} + \frac{\rho I}{kGA}\,\frac{\partial^4 w}{\partial t^4} = 0 \tag{12}$$

The boundary conditions for the simply supported Timoshenko beam are given by

$$w = \frac{\partial \psi}{\partial x} = 0 \qquad \text{at } x=0,L \tag{13}$$

The deflection of the nth mode of vibration is given by

$$w_n(x,t) = A_n \sin \frac{n\pi x}{L}\, e^{i\omega_n t} \tag{14}$$

As in the Euler-Bernoulli theory for small damping, the complex frequency equation is obtained by using equation (14) in (12) and by replacing E and G by the complex moduli $E^*$ and $G^*$, where

$$E^* = E'(1 + i \tan\phi_E) \qquad (15)$$

and

$$G^* = G'(1 + i \tan\phi_G) \qquad (16)$$

Therefore,

$$\frac{E^* I}{\rho A}\frac{n^4\pi^4}{L^4} - \left[1 + \frac{n^2\pi^2}{L^2}\frac{I}{A}\left(1 + \frac{E^*}{kG^*}\right)\right]\omega_n^2 + \frac{\rho I}{kG^* A}\omega_n^4 = 0 \qquad (17)$$

Now consider again equation (7) and the small loss tangent approximation, such that

$$\frac{\omega_n''^2}{\omega_n'^2} \ll 1, \quad \tan^2\phi_E \ll 1, \quad \tan^2\phi_G \ll 1 \qquad (18)$$

$$\omega_n^2 = \omega_n'^2\left(1 + 2i\frac{\omega_n''}{\omega_n'}\right)$$

$$\omega_n^4 = \omega_n'^4\left(1 + 4i\frac{\omega_n''}{\omega_n'}\right) \qquad (19)$$

Using (19) in (17) and separating the real and imaginary parts results in two equations. Setting the real part equal to zero gives the following equation:

$$\frac{E' I}{\rho A}\frac{n^4\pi^4}{L^4} - \omega_n'^2\left\{\left[1 + \frac{n^2\pi^2}{L^2}\frac{I}{A}\left(1 + \frac{E'}{kG'}\right)\right] + \left[\frac{2n^2\pi^2}{L^2}\frac{I}{A}\frac{E'}{kG'}(\tan\phi_E - \tan\phi_G)\frac{\omega_n''}{\omega_n'}\right]\right\} + \frac{\rho I}{kG' A}\omega_n'^4\left\{1 + \frac{4\omega_n''}{\omega_n'}\tan\phi_G\right\} = 0 \qquad (20)$$

or

$$\frac{E' I}{\rho A}\frac{n^4\pi^4}{L^4} - \left[1 + \frac{n^2\pi^2}{L^2}\frac{I}{A}\left(1 + \frac{E'}{kG'}\right)\right]\omega_n'^2 + \frac{\rho I}{kG' A}\omega_n'^4 = 0 \qquad (21)$$

which is identical to the frequency equation for an elastic beam except $E'$ and $G'$ appear in place of elastic constants. Similarly, by setting the imaginary part equal to zero, the following equation is obtained:

$$\omega_n'' = \left\{\left[\frac{EI}{\rho A}\frac{n^4\pi^4}{L^4} - \frac{n^2\pi^2 IE'}{kG' A L^2}\omega_n'^2\right]\tan\phi_E + \left[\frac{n^2\pi^2 E' I}{L^2 kG' A}\omega_n'^2 - \frac{\rho I}{kG' A}\omega_n'^4\right]\tan\phi_G\right\} \Big/ \left\{\left[1 + \frac{n^2\pi^2}{L^2}\frac{I}{A}\left[1 + \frac{E'}{kG'}\right]\right] 2\omega_n' - 4\frac{\rho I}{kG' A}\omega_n'^3\right\} \qquad (22)$$

Observe that $\omega_n'$ can be obtained from equation (21) for each n. This value can then be substituted into equation (22) to obtain $\omega_n''$. $\omega_n'$ can be easily estimated when $n^2\pi^2 I/L^2 A$ is a small quantity. Using this approximation, it can be shown [12] that the last term in equation (21) is small compared to $n^2\pi^2 I/L^2 A$. Neglecting the last term, the frequency $\omega_n'$ is given by

$$\omega_n' = \sqrt{EI/\rho A}\,\frac{n^2\pi^2}{L^2}\left(1 - \frac{1}{2}\frac{n^2\pi^2}{L^2}\frac{I}{A}\left[1 + \frac{E'}{kG'}\right]\right) \qquad (23)$$

Tan$\phi$ for the viscoelastic Timoshenko beam is defined as,

$$\tan\phi = \frac{2\omega_n''}{\omega_n'} \qquad (24)$$

where $\omega_n'$ and $\omega_n''$ are found from equation (22). This loss tangent provides a measure of the decay per cycle of free vibration, which can be shown by substituting equation (7) into (5). and replacing $\omega_n''$ in favor of $\tan\phi$ by means of equation (24). The ratio of displacement at time $t + 2\pi/\omega_n'$ to that at time t is found to be $\exp(-\pi\tan\phi)$. Note that $\tan\phi = \tan\phi_E$ for the Euler-Bernoulli theory, equation (9).

## Discussion of Results

The influence of shear deformation on the damping will depend on the ratios of $E'/G'$, $\tan\phi_G/\tan\phi_E$, the length to thickness ratio, and mode number. For unidirectional composites, the ratios $E'/G'$ and $\tan\phi_E/\tan\phi_G$ depend on the volume fraction of fibers and matrix and the moduli of fibers and matrix. By considering different material systems and different orientation angles it is possible to have wide variations in the ratios $E/G$ and $\tan\phi_E/\tan\phi_G$. In the continuum model of large space structures, the effective shear and longitudinal moduli can be varied independently of each other by changing the configuration of the individual cells. All the results presented in this study will be given in a dimensionless form.

The material properties and dimensions of the beam are given in Table 1. For the purpose of illustration the loss factors and storage modulus are assumed to be independent of the frequency.

Table 1

Typical Properties of A Composite Beam

$E' = 20\times10^6$ psi $\qquad \frac{E'}{G'} = 10\text{-}40$

$L = 50$ in $\qquad \frac{L}{h} = 20\text{-}100$

$\tan\phi_G = 0.05 \qquad \frac{\tan\phi_G}{\tan\phi_E} = 100\text{-}1$

$\rho = 0.065$ lb/in$^3$ $\qquad$ width $b = 1.0$ in

shape factor $k = 5/6$

The influence of $E'/G'$, $\tan\phi_G/\tan\phi_E$, L/h and mode numbers on the ratio of damping predicted by the Timoshenko and Euler-Bernoulli theories are shown in Figs. 1 through 8.

Figure 1 is a plot of $\tan\phi/\tan\phi_E$ for $\tan\phi_G/\tan\phi_E$ varying from 100 to 1. The first mode of vibration (n=1) is considered. The length to thickness ratio of the beam is 100. It is found that for large values of $\tan\phi_G/\tan\phi_E$(100) the damping values predicted by Timoshenko theory are 9% to 38% higher than the prediction by Euler-Bernoulli theory depending on the ratio of $E'/G'$. Increasing $E'/G'$ increases the shear effects.

The third mode of vibration (n=3) is considered in Fig. 2. The effect of shear damping is more pronounced than in the first mode. Figures 3 and 4 illustrate similar trends for a beam of smaller length to thickness ratio (50). The damping $\tan\phi$ predicted by the Timoshenko theory is substantially higher than $\tan\phi_E$ (38% to 1300% for $\tan\phi_G/\tan\phi_E = 100$). It is interesting to note that when the difference between $\tan\phi_G$ and $\tan\phi_E$ becomes small the difference in predicted damping values obtained from the Timoshenko and Euler-Bernoulli theories is very small.

In Figs. 5 and 6 damping is predicted for different modes while keeping the ratio of

$E'/G'$ constant. For higher modes the shear effects become important and this effect is enhanced as the ratio of $Tan\phi_G/Tan\phi_E$ is increased.

Figures 7 and 8 illustrate the effect of the variation of length to thickness ratio on damping. For small L/h ratios the damping predicted by Timoshenko theory is higher than the prediction by Euler-Bernoulli beam theory.

## Conclusions

This study has investigated the effects of shear deformations and rotary inertia on the damping characteristics of beams. For typical longitudinally reinforced composite beams, the loss factors in shear ($Tan\phi_G$) are substantially higher than $Tan\phi_E$. This leads to large differences between the predictions obtained from Euler-Bernoulli and Timoshenko beam theory. The results of this study indicate that for long slender beams in which the ratio of $Tan\phi_G/Tan\phi_E$ and $E'/G'$ is large, the influence of shear damping is important even in low vibrational modes. The methods and results from this investigation can be used to study the role of shear damping in higher modes of vibration of large space structures.

## Acknowledgement

The authors gratefully acknowledge the support provided for this research by NASA Johnson Space Center under grant no. NAG 9-140.

## References

[1] Golla D.F., and Hughes P.C., "Dynamics of Viscoelastic Structures, A Time-Domain, Finite Element Formulation", Journal of Applied Mechanics, Vol. 52, Dec. 1985.

[2] Schultz, A.B., and Warwick, D.N., "Vibration Response: A Non-Destructive Test for Fatigue Crack Damage in Filament-Reinforced Composites," Journal of Composite Materials, Vol. 5., July 1971.

[3] Gibson, R.F., and Plunkett R., "Dynamic Mechanical Behavior of Fiber-Reinforced Composites: Measurement and Analysis," Journal of Composite Materials, Vol. 10, Oct. 1976.

[4] Adams, R.D., and Bacon D.G.C., "Effect of Fibre Orientation and Laminate Geometry on the Dynamic Properties of CFRP," Journal of Composite Materials, Vol. 7, Oct. 1973.

[5] Adams, R.D., Fox, M.A.O., Flood R.J.L., Friend, R.T., and Hewitt, R.L., "The Dynamic Properties of Unidirectional Carbon and Glass Fibre Reinforced Plastics in Torsion and Flexure," Journal of Composite Materials, Vol. 3, 1969.

[6] Ni, R.G., and Adams, R.D., "The Damping and Dynamic Moduli of Symmetric Laminated Composite Beams - Theoretical and Experimental Results," Journal of Composite Materials, Vol. 18, March 1984.

[7] Schultz, A.B., and Tsai, S.W., "Dynamic Moduli and Damping Ratios of Fibre-Reinforced Composites," Journal of Composite Materials, Vol. 2, July 1968.

[8] Schultz, A.B., and Tsai, S.W., "Measurements of Complex Dynamic Moduli for Laminated Fibre-Reinforced Composites," Journal of Composite Materials, Vol. 3, July 1969.

[9] Sun, C.T., Kim, B.J., and Bogdanoff, J.L., "On The Derivation of Equivalent Simple Models for Beam and Plate Like Structures in Dynamic Analysis," Proceedings AIAA 22nd Structures Structural Dynamics and Materials Conference and AIAA Dynamics Specialists Conference, Atlanta, Georgia, 1981.

[10] Sun, C.T., and Juang, J.N., "Modeling Global Structual Damping in Trusses Using Simple Continum Models," Proceedings AIAA 24th Structures, Structural Dynamics, and Materials Conference, Lake Tahoe, Nevada, May 1983.

[11] Schapery, R.A., "Viscoelastic Behavior and Analysis of Composite Materials," Chapter 4, Composite Materials, Vol. 2, G.P., Sendecky, Ed., Academic Press, New York, 1974.

[12] Timoshenko, S.P., Vibration Problems in Engineering, Third Edition, D. Van Nostrand Company, Inc., New York, 1955.

[13] Hearmon, R.F.S., "The Influence of Shear and Rotary Inertia on the Free Flexural Vibrations of Wooden Beams," British Journal of Applied Physics, Vol. 9, 1958.

[14] Dudek, T.J., "Young's and Shear Moduli of Unidirectional Composites by a Resonant Beam Method," Journal of Composite Materials, Vol. 4, 1970.

[15] Biot, M.A., "A New Approach to the Mechanics of Anisotropic Multilayered Plates," Int. J. Solids Structures, Vol 8., 1972.

[16] Biot, M.A., "Simplified Dynamics of Multilayed Orthotropic Viscoelastic Plates," Int. J. Solids Structures, Vol. 8, 1972.

[17] Huang, T.C., "The Effect of Rotary Inertia and of Shear Deformation on the Frequency and Normal Mode Equations of Uniform Beams With Simple End Conditions," Journal of Applied Mechanics, Vol. 28, No. 4, 1961.

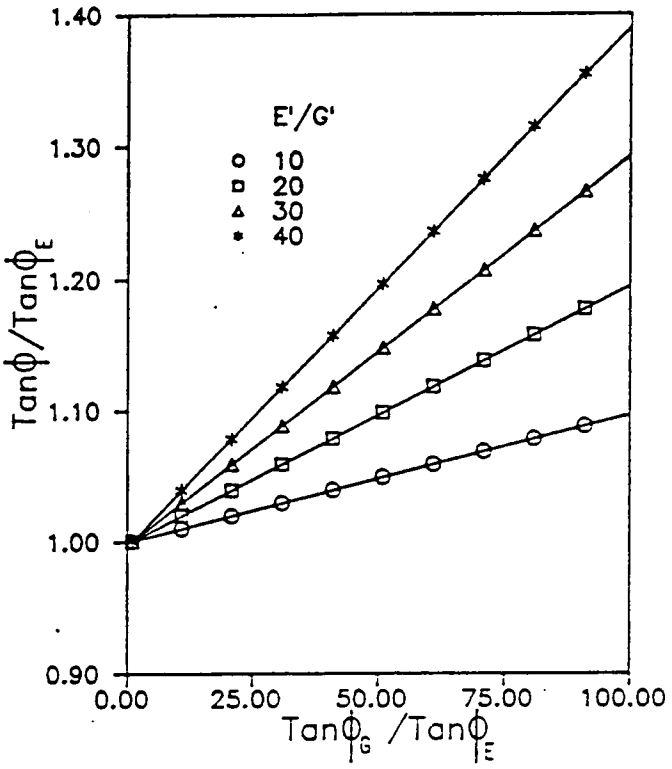


Fig. 1 Effect of shear deformation on damping as a function of $\tan\phi_G/\tan\phi_E$ for various values of E'/G' (L/h = 100, n=1)

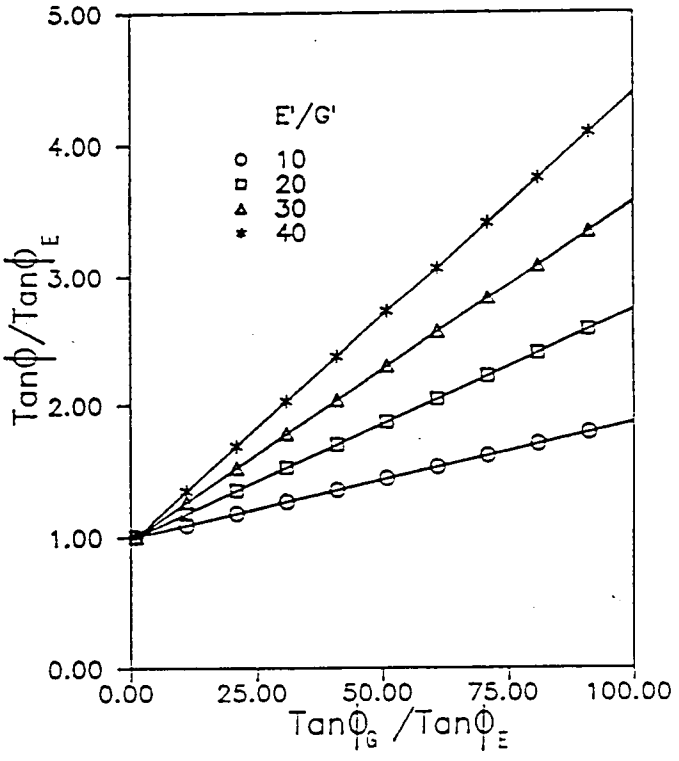


Fig. 2 Effect of shear deformation on damping as a function of $\tan\phi_G/\tan\phi_E$ for various values of E'/G' (L/h = 100, n=3)

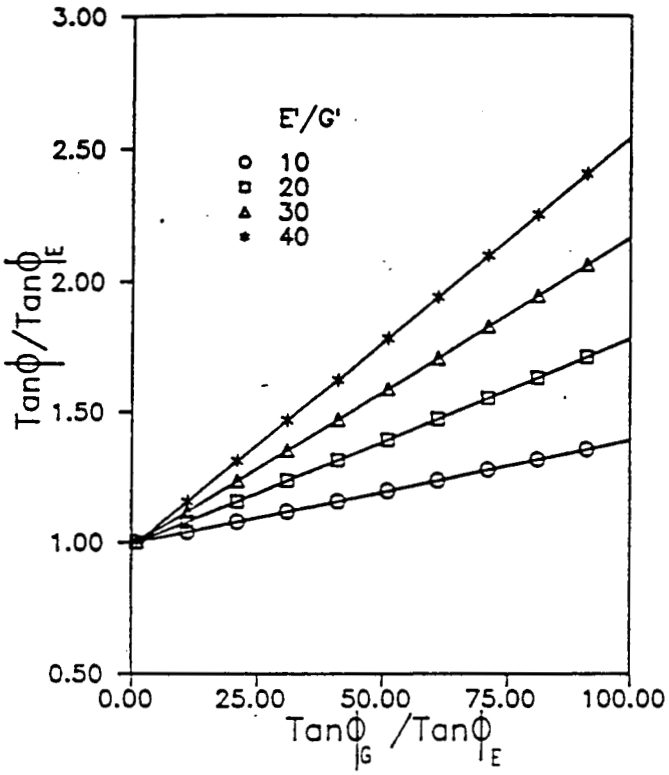


Fig. 3 Effect of shear deformation on damping as a function of $\tan\phi_G/\tan\phi_E$ for various values of E'/G' (L/h = 50, n=1)

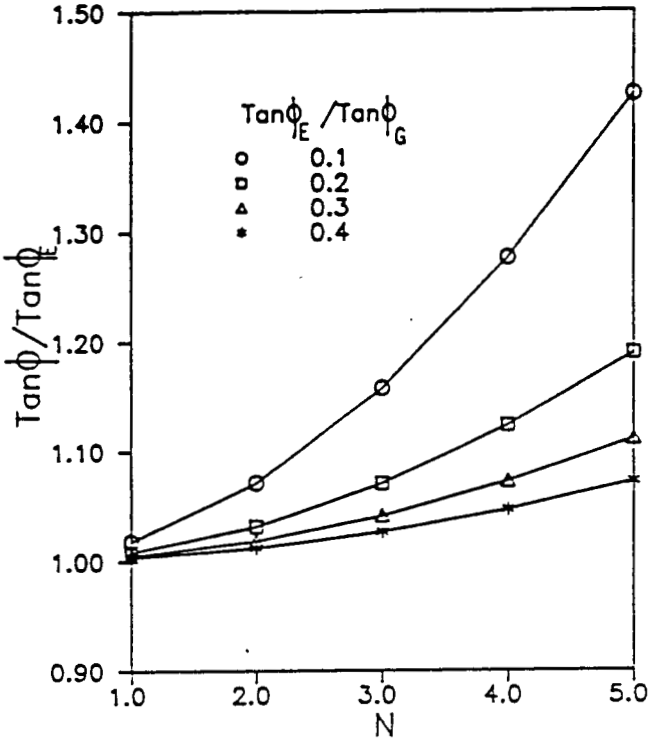


Fig. 5 Effect of shear deformation on damping as a function of n for various values of $\tan\phi_E/\tan\phi_G$ (L/h = 100, E'/G' = 20)

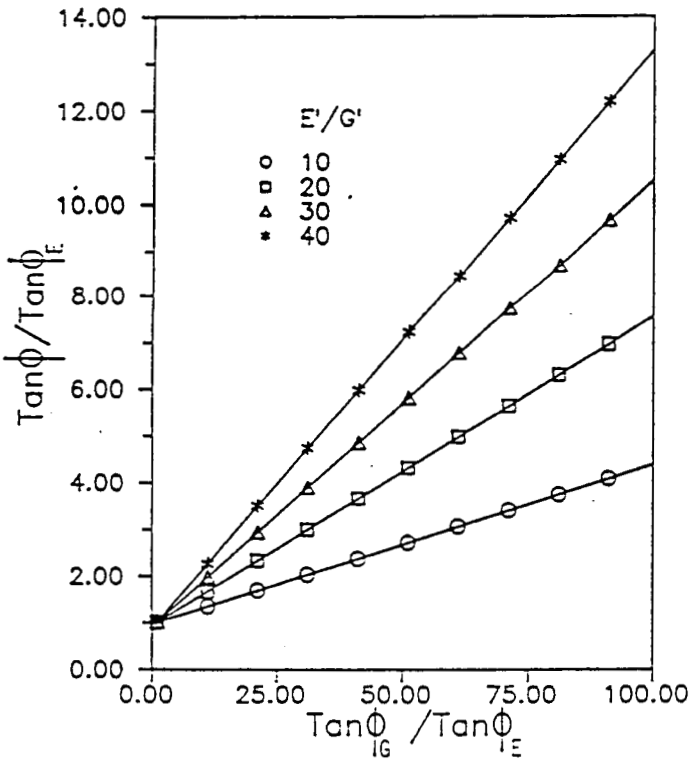


Fig. 4 Effect of shear deformation on damping as a function of $\tan\phi_G/\tan\phi_E$ for various values of E'/G' (L/h = 50, n=3)

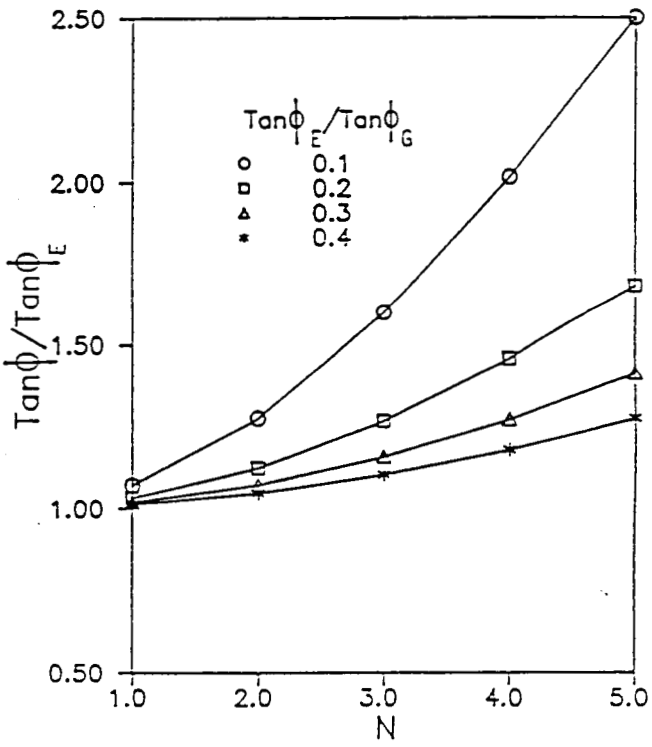


Fig. 6 Effect of shear deformation on damping as a function of n for various values of $\tan\phi_E/\tan\phi_G$ (L/h = 50, E'/G' = 20)

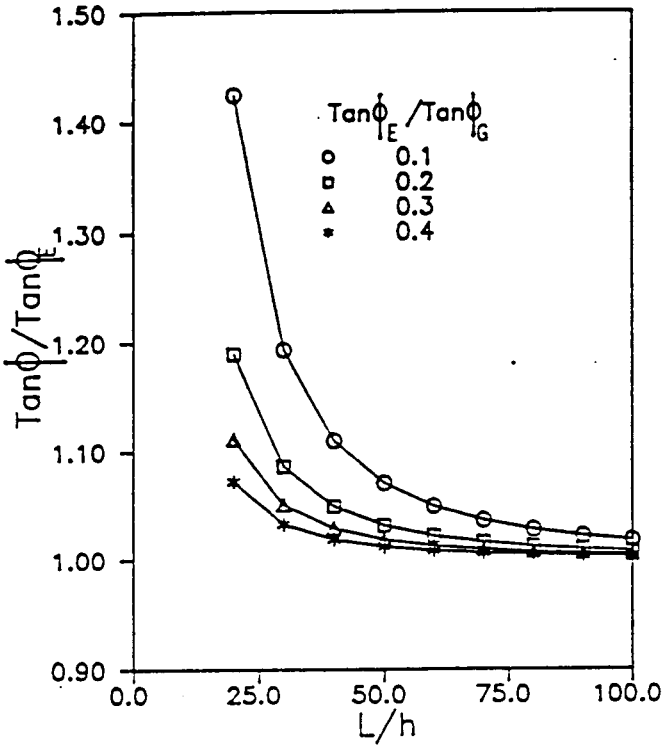


Fig. 7 Effect of shear deformation on damping as a function of L/h for various values of $Tan\phi_E/Tan\phi_G$ (n=1, E'/G' = 20)

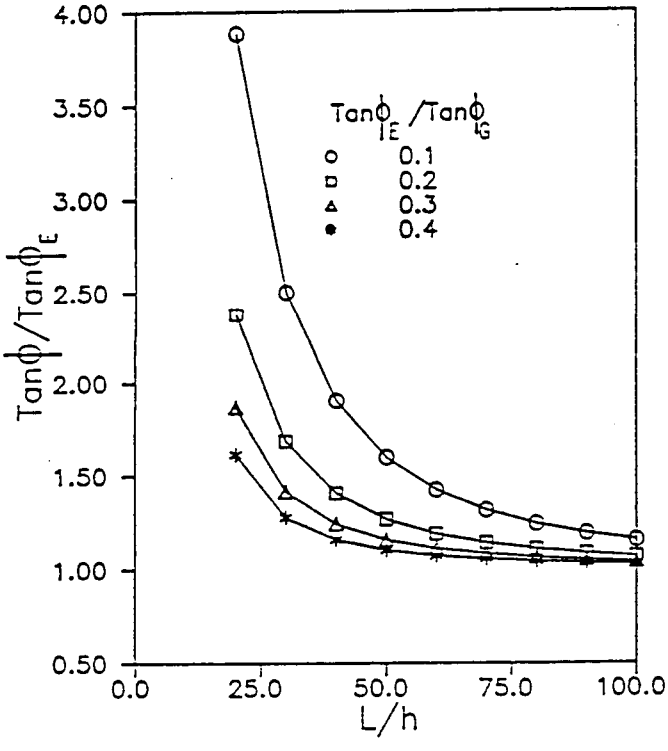


Fig. 8 Effect of shear deformation on damping as a function of L/h for various values of $Tan\phi_E/Tan\phi_G$ (n=3, E'/G' = 20)

## 8.2 Prediction and Experimental Observation of Damage Dependent Damping in Laminated Composite Beams

# PREDICTION AND EXPERIMENTAL OBSERVATION OF DAMAGE DEPENDENT DAMPING IN LAMINATED COMPOSITE BEAMS

D. H. Allen, C. E. Harris, and A. L. Highsmith
Aerospace Engineering Department
Texas A&M University
College Station, Texas

ABSTRACT

The equations of motion are developed herein for laminated composite beams with load-induced matrix cracking. The damage is accounted for by utilizing internal state variables. The net result of these variables on the field equations is the introduction of both enhanced damping, and degraded stiffness. Both quantities are history dependent and spatially variable, thus resulting in nonlinear equations of motion. It is explained briefly how these equations may be quasi-linearized for laminated polymeric composites under certain types of structural loading. The coupled heat conduction equation is developed, and it is shown that an enhanced Zener damping effect is produced by the introduction of microstructural damage. The resulting equations are utilized to demonstrate how damage dependent material properties may be obtained from dynamic experiments. Finally, experimental results are compared to model predictions for several composite layups.

NOMENCLATURE

| | |
|---|---|
| $A$ | - beam cross-sectional area |
| $A_i$ | - cross-sectional area of ith lamina |
| $A^*$ | - modulus weighted beam cross-sectional area |
| $A_m$, $a_m$ | - coefficients in cantilever beam displacement field |
| $b$ | - beam width |
| $C$ | - viscoelastic modulus |
| $C_v$ | - specific heat at constant volume |
| $C_1$, $C_2$ | - coefficients in cantilever beam displacement field |
| $E_o$, $E_1$, $n_1$ | - viscoelastic material parameters |
| $E$ | - axial modulus of elasticity |
| $E_i$ | - axial modulus of elasticity of ith lamina |
| $E_1$ | - reference axial modulus of elasticity |
| $F$ | - transverse load applied to free end of cantilever beam |
| $F_A$ | - transverse load amplitude |
| $h$ | - beam depth |
| $I^*_{yy}$ | - modulus weighted moment of inertia about y axis |
| $k$ | - material constant in internal state variable growth law |
| $k_{ij}$ | - coefficient of heat conduction |
| $k_{Dij}$ | - loss in heat conduction coefficient due to damage |
| $L$ | - beam length |
| $M_y$ | - beam moment resultant about y axis |
| $M^T_y$ | - beam moment resultant about y axis due to temperature change |
| $N$ | - number of cycles of applied load |
| $n$ | - number of plies in laminate |
| $n_2$ | - material constant in internal state variable growth law |
| $P$ | - beam axial resultant |
| $P^T$ | - beam axial resultant due to temperature change |

$p_x$ - beam axial load per unit length

$p_z$ - beam transverse load per unit length

$\bar{q}$ - heat flux vector

$r$ - heat source

$S$ - term used to obtain laminate damping coefficient

$S_c$ - surface area of matrix cracks in local volume element

$T$ - temperature

$T_r$ - reference temperature

$t$ - time

$u$ - axial displacement

$u_c$ - crack opening displacement

$u_o$ - axial displacement of neutral surface

$u_L^c$ - internal energy dissipation per unit volume due to matrix cracking

$U_L^c$ - total internal energy dissipation due to matrix cracking

$V_z$ - beam shear resultant in z direction

$w_o$ - transverse displacement of neutral surface

$x$ - beam axial coordinate direction

$z$ - beam transverse coordinate direction

$\bar{z}^*$ - z component of modulus weighted centroidal axis

$\bar{z}_i$ - z component of distance from centroid of ith ply to modulus weighted centroid

$\bar{\alpha}$ - coefficient of thermal expansion

$\alpha_D$ - internal state variable (ISV) due to damage

$\alpha_1$ - axial component of matrix cracking damage ISV

$\alpha_{1i}$ - axial component of matrix cracking damage ISV in ith lamina

$\delta$ - initial displacement applied to free end of cantilever beam

$\varepsilon_{xx}$ - axial strain component

$\varepsilon_{xxi}^A$ - average axial strain in ith lamina

$\eta$ - damping coefficient

$\eta_{A1}$ - axial damping coefficient in ith lamina

$\eta_{B1}$ - bending damping coefficient in ith lamina

$\nu_{A1}$ - axial stiffness loss coefficient in ith lamina

$\nu_{B1}$ - bending stiffness loss coefficient in ith lamina

$\omega_m$ - modal frequency of mth resonant mode

$\rho$ - mass density

$\sigma_A$ - stress amplitude of cyclic loading

$\sigma_{xx}$ - axial stress component

$\sigma_{xz}$ - shear stress component

$\theta$ - temperature minus reference temperature

$\theta_y$ - beam rotation about y axis

## INTRODUCTION

Microstructural damage in laminated fibrous composites has been studied by several researchers in the past decade. It has been observed that this damage can result in significant stiffness loss [1-3]. Furthermore, experimental results indicate that material damping may increase by an order of magnitude or more as a result of damage [4,5]. Recent research has indicated that this damage induced stiffness loss may have a substantial effect on the dynamic response of both truss structures [6] and beams in bending [7]. However, to these authors' knowledge, no concerted effort has been previously reported to model the effect of damage induced damping on dynamic structural response. While there have been models [8,9] developed for damping in laminated composites, these models do not include the effects of microstructural damage. The primary objective of the research described herein is to develop models that explicitely account for the effect of microstructural damage on the stiffness and damping in the structural dynamics equations of motion.

In this paper a model is developed for predicting the structural dynamics response of composite beams in both bending and extension, where microstructural damage induces both damping and stiffness loss. The equations of motion are formulated using the theory of internal state variables (ISV's) to account for damage [10-12]. The resulting equations are cast in such a way that experimental data can be readily implemented to the model.

## DEVELOPMENT OF THE EQUATIONS OF MOTION

Consider a free body diagram of a laminated composite beam, as shown in Fig. 1.

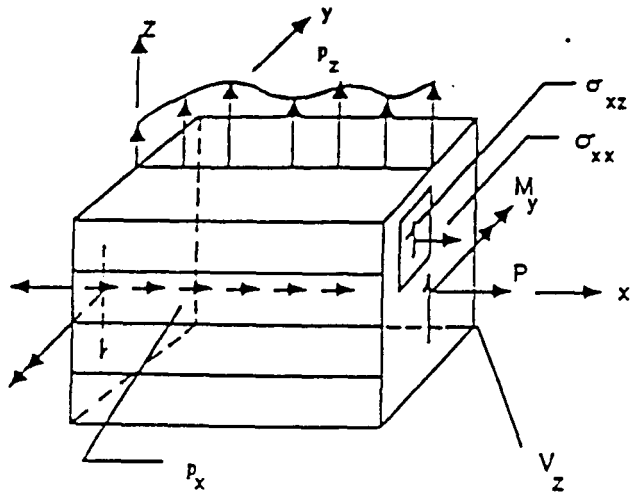


Fig. 1. Free Body Diagram of Laminated Composite Beam

The governing equations are

1) resultant loads [13]

$$P \equiv \int_A \sigma_{xx} dA \tag{1a}$$

$$V_z \equiv \int_A \sigma_{xz} dA \tag{1b}$$

$$M_y \equiv \int_A \sigma_{xx} z dA \tag{1c}$$

2) equilibrium [13], neglecting rotatory inertia [14]

$$\frac{\partial P}{\partial x} = -p_x + \frac{\partial}{\partial t}(\rho A \frac{\partial u_o}{\partial t}) \tag{2a}$$

$$\frac{\partial V_z}{\partial x} = -p_z + \frac{\partial}{\partial t}(\rho A \frac{\partial w_o}{\partial t}) \tag{2b}$$

$$\frac{\partial M_y}{\partial x} = V_z \tag{2c}$$

3) kinematic [13,15]

$$\varepsilon_{xx} = \frac{\partial u}{\partial x} \tag{3a}$$

$$\theta_y = \frac{\partial w_o}{\partial x} \tag{3b}$$

$$u = u_o + \theta_y z, \; u = u_o(x), \; \theta_y = \theta_y(x) \tag{3c}$$

where equation (3c) is the Euler-Bernoulli assumption.

4) thermomechanical constitution [10,11]

$$\sigma_{xx} = E(\varepsilon_{xx} - \alpha_1 - \bar{\alpha}\theta), \; \theta \equiv T - T_R \tag{4a}$$

$$q_i = -(k_{ij} - k_{Dij})T_{,j} \tag{4b}$$

$$\dot{\alpha}_1 = a_1(\varepsilon_{xx}, \dot{\varepsilon}_{xx}, T, \alpha_1) \tag{4c}$$

$$k_{Dij} = k_{Dij}(\alpha_1) \tag{4d}$$

where $\alpha_1$ is an internal state variable representing matrix cracking in each ply [9]. It can be shown that $\alpha_1$ is a kinematic description of the locally averaged microcrack geometry [10,11]; that is,

$$\alpha_1 = \frac{1}{V_L} \int_{S_c} u_c ds \tag{5}$$

where $V_L$ is a local characteristic volume which is large enough to encompass statistically homogeneous damage. Furthermore, $u_c$ is the normal component of crack opening displacement, and $S_c$ is the surface area of cracks in $V_L$, as shown in Fig. 2. $V_L$ may typically be taken as one square inch in the x-y plane for laminated polymeric composites [3]. For matrix cracking the z coordinate is taken to be one ply thickness [11]. Equation (4c) is termed the internal state variable growth law.

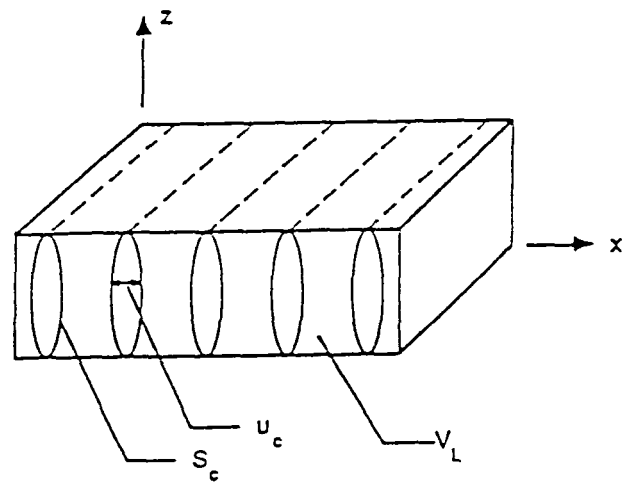


Fig. 2. Kinematics of Matrix Cracking

5) thermodynamics [16,17]

$$\dot{u}_L^c - \rho C_v \frac{\partial T}{\partial t} - q_{i,i} + \dot{\rho} r = 0 \tag{6}$$

which is a statement of conservation of energy for the material described by equations (4). Although specific forms may be given for $u_L^c$ as a function of $\varepsilon_{xx}$ and $\alpha_1$, this is covered in a later section. Note that although the mechanical formulation is one-dimensional in the spatial coordinate x, multi-dimensionality must be retained in thermodynamic equation (6).

Now substitute (3c) into (3a) to obtain

$$\varepsilon_{xx} = \frac{\partial u_o}{\partial x} + z \frac{\partial \theta_y}{\partial x} \tag{7}$$

Substituting the above result into (4a) gives

$$\sigma_{xx} = E\left(\frac{\partial u_o}{\partial x} + z\frac{\partial \theta_y}{\partial x} - \alpha_1 - \bar{\alpha}\theta\right) \quad (8)$$

Now substitute (8) into (1a) and (1c) to obtain

$$P = E_1 A^* \frac{\partial u_o}{\partial x} + E_1 \frac{\partial \theta_y}{\partial x}\int_A \frac{E}{E_1} z dA - \sum_{i=1}^{n} E_i \alpha_{1i} A_i - P^T \quad (9a)$$

$$M_y = E_1 \frac{\partial u_o}{\partial x}\int_A \frac{E}{E_1} z dA + E_1 \frac{\partial \theta_y}{\partial x} I^*_{yy} - \sum_{i=1}^{n} E_i \alpha_{1i} \bar{z}_i A_i - M_Y^T \quad (9b)$$

where $\alpha_{1i}$ is assumed to be independent of y and z in the ith ply [11], and

$$A^* \equiv \int_A \frac{E}{E_1} dA \quad (10a)$$

$$I^*_{yy} \equiv \int_A \frac{E}{E_1} z^2 dA \quad (10b)$$

Furthermore,

$$P^T \equiv \int_A E\bar{\alpha}\theta dA \quad (11a)$$

$$M_y^T \equiv \int_A E\bar{\alpha}\theta z dA \quad (11b)$$

The term containing $\alpha_{1i}$ in equation (9b) does not go to zero even for a symmetric layup because $\alpha_{1i}$ is not symmetric (due to the crack opening displacements in equation (5)) during bending.

Now, suppose the modulus weighted centroidal axis is utilized, such that,

$$\bar{z}^* = \int_A \frac{E}{E_1} z dA = 0 \quad (12)$$

Note that since E is the initial undamaged modulus, $\bar{z}^*$ represents the initial modulus weighted centroidal axis, which is not damage dependent. Therefore, using equations (3b) and (12), equations (9a) and (9b) simplify to the following for symmetric layups

$$P = E_1 A^* \frac{\partial u_o}{\partial x} - \sum_{i=1}^{n} E_i \alpha_{1i} A_i - P^T \quad (13a)$$

$$M_y = E_1 I^*_{yy} \frac{\partial^2 w_o}{\partial x^2} - \sum_{i=1}^{n} E_i \alpha_{1i} \bar{z}_i A_i - M_y^T \quad (13b)$$

The term containing $\alpha_{1i}$ in equation (13b) represents a shift in the centroidal axis due to matrix cracking, which is nonzero when the matrix crack displacements are not symmetric through the thickness. This is generally the case in bending and with asymmetric layups [15].

Now substitute (13a) into (2a) to obtain

$$\frac{\partial}{\partial x}\left(E_1 A^* \frac{\partial u_o}{\partial x} - \sum_{i=1}^{n} E_i \alpha_{1i} A_i - P^T\right) = -p_x + \frac{\partial}{\partial t}\left(\rho A \frac{\partial u_o}{\partial t}\right) \quad (14)$$

which is the governing equation of motion for axial displacement.

Similarly, substitute (13b) into (2c) to obtain

$$\frac{\partial}{\partial x}\left(E_1 I^*_{yy} \frac{\partial^2 w_o}{\partial x^2} - \sum_{i=1}^{n} E_i \alpha_{1i} \bar{z}_i A_i - M_y^T\right) = V_z \quad (15)$$

Substituting (15) into (2b) thus gives

$$\frac{\partial^2}{\partial x^2}\left(E_1 I^*_{yy} \frac{\partial^2 w_o}{\partial x^2} - \sum_{i=1}^{n} E_i \alpha_{1i} \bar{z}_i A_i - M_y^T\right) = -p_z + \frac{\partial}{\partial t}\left(\rho A \frac{\partial w_o}{\partial t}\right) \quad (16)$$

which is the governing equation of motion for transverse displacement.

Now consider a simple example for the constitutive behavior. Suppose that the stress-strain relation can be modelled by a Voigt element, shown in Fig. 3.

The governing differential equation for the analog is

$$\sigma_{xx} = E\varepsilon_{xx} + \eta\dot{\varepsilon}_{xx} - E\bar{\alpha}\theta \quad (17)$$

Suppose we let

$$\alpha_{1i} = -\frac{\eta_i}{E_i}\dot{\varepsilon}^A_{xxi} \quad (18)$$

Then equation (17) may be written

$$\sigma_{xx} = E(\varepsilon_{xx} - \alpha_{1i} - \bar{\alpha}\theta) \quad (19)$$

which is equivalent to (4a), and (18) replaces (4c); that is,

$$\alpha_{1i}(t_1) = \int_{--}^{t_1} \alpha_1(\varepsilon^A_{xxi}, \dot{\varepsilon}^A_{xxi}, T, \alpha_{1i})dt = -\frac{\eta_i}{E_i}\dot{\varepsilon}^A_{xxi}(t_1) \quad (20)$$

Substituting (7) and (3b) into (18) gives

$$\alpha_{1i} = -\frac{\eta_{Ai}}{E_i}\frac{\partial^2 u_o}{\partial t \partial x} - \frac{\eta_{Bi}}{E_i}\bar{z}_i \frac{\partial^3 w_o}{\partial t \partial x^2} \quad (21)$$

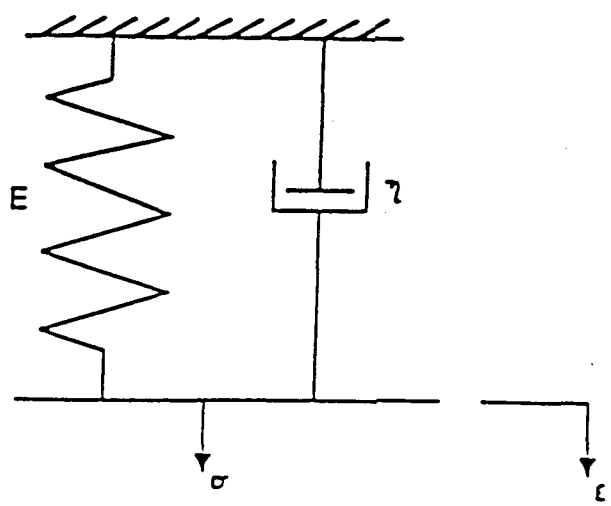


Fig. 3. Voigt Model

Therefore, substituting (21) into (14) gives

$$\frac{\partial}{\partial x}\left[(E_1 A^* \frac{\partial u_o}{\partial x}) + \sum_{i=1}^{n} \eta_{Ai} A_i \frac{\partial u_o^2}{\partial t \partial x} + \eta_{Bi} \bar{z}_i A_i \frac{\partial^3 w_o}{\partial t \partial x^2}\right]$$

$$- \frac{\partial}{\partial t}(\rho A \frac{\partial u_o}{\partial t}) = p_x + \frac{\partial p^T}{\partial x} \qquad (22)$$

Furthermore, substituting (21) into (16) gives

$$\frac{\partial^2}{\partial x^2}(E_1 I_{yy}^* \frac{\partial^2 w_o}{\partial x^2}) + \frac{\partial^2}{\partial x^2}\left[\sum_{i=1}^{n} (\bar{z}_i A_i \eta_{Ai}) \frac{\partial^2 u_o}{\partial t \partial x}\right.$$

$$\left. + \eta_{Bi} \bar{z}_i^2 A_i \frac{\partial^3 w_o}{\partial t \partial x^2}\right] - \frac{\partial}{\partial t}(\rho A \frac{\partial w_o}{\partial t}) =$$

$$-p_z + \frac{\partial^2 M_y^T}{\partial x^2} \qquad (23)$$

Therefore, if $\eta_{Ai}$ and $\eta_{Bi}$ are constants in time t, the above reduces to linear theory.

Experimental evidence indicates that polymeric composites may not be represented by simple mechanical analogs such as the Voigt model [18]. For small displacements a single integral model of the following form has been shown to be accurate [19]:

$$\sigma_{xx} = \int_{-\infty}^{t_1} C(t-\tau) \frac{\partial}{\partial \tau}(\varepsilon_{xx} - \bar{\alpha}\theta) d\tau \qquad (24)$$

where the kernel function C is a power law in time, and is also a weak function of damage (for near-constant amplitude vibrations); that is,

$$C(t) = E_o + E_1 (t)^{n_1} \qquad (25)$$

where $E_o = E_o(\sigma_1)$, $E_1 = E_1(\sigma_1)$ and $n_1 = n_1(\sigma_1)$.

In general, the constitutive model represented by equation (4a) is not in agreement with equation (24). However, it is our intent to show that this assumption is at least approximately correct. To do this, first recall that equation (24) may be represented by an infinite order differential equation:

$$\sigma_{xx} = E(\varepsilon_{xx} - \bar{\alpha}\theta) + \sum_{i=1}^{\infty} E_i \frac{d^i \varepsilon_{xx}}{dt^i} \qquad (26)$$

Equation (26) may be written in the same form as equation (17), where in this case

$$\eta = \eta(\dot{\varepsilon}_{xx}, \bar{\varepsilon}_{xx}, \ldots, \sigma_1) \qquad (27)$$

Therefore, equations (22) and (23) may still be used except that the damping coefficients are not constant. For near-constant amplitude load histories, it is now assumed that

$$\dot{\varepsilon}_{xx} = \dot{\varepsilon}_{xx}(\omega, \sigma_A)$$
$$\bar{\varepsilon}_{xx} = \dot{\varepsilon}_{xx}(\omega, \sigma_A)$$
$$\vdots \qquad (28)$$

Furthermore, experimental evidence [20] indicates that for constant amplitude cyclic loading

$$\dot{\sigma}_1 = k\sigma_A^{n_2} \qquad (29)$$

where k and $n_2$ are material constants. For $n_2 >> 1$, the above may be integrated in time to give

$$\sigma_1 = \sigma_1(N, \sigma_A) \qquad (30)$$

so that equation (27) may be simplified to

$$\eta = \eta(\sigma_A, \omega, N) \qquad (31)$$

Now, consider a more general representation of equation (21) given by

$$\sigma_{1i} = \nu_{Ai} \frac{\partial u_o}{\partial x} + \nu_{Bi} \bar{z}_i \frac{\partial^2 w_o}{\partial x^2} - \frac{\eta_{Ai}}{E_i} \frac{\partial^2 u_o}{\partial t \partial x}$$

$$- \frac{\eta_{Bi}}{E_i} \bar{z}_i \frac{\partial^3 w_o}{\partial t \partial x^2} \qquad (32)$$

where

$$\eta_{Ai} = \eta_{Ai}(\sigma_A, \omega, N), \quad \eta_{Bi} = \eta_{Bi}(\sigma_A, \omega, N)$$
$$\nu_{Ai} = \nu_{Ai}(\sigma_A, \omega, N), \quad \nu_{Bi} = \nu_{Bi}(\sigma_A, \omega, N) \qquad (33)$$

Substituting (32) into (14) gives

$$\frac{\partial}{\partial x}\left[(1-\bar{\nu}_{A0})E_1A^*\frac{\partial u_o}{\partial x}\right] + \frac{\partial}{\partial x}\left(\bar{n}_{A0}A^*\frac{\partial^2 u_o}{\partial t\partial x}\right)$$

$$- \frac{\partial}{\partial x}\left(\bar{\nu}_{B1}he_1A^*\frac{\partial^2 w_o}{\partial x^2} + \frac{\partial}{\partial x}\left(\bar{n}_{B1}hA^*\frac{\partial^3 w_o}{\partial t\partial x^2}\right)\right.$$

$$- \frac{\partial}{\partial t}\left(\rho A\frac{\partial u_o}{\partial t}\right) = -p_x + \frac{\partial p^T}{\partial x} \qquad (34)$$

where

$$\bar{\nu}_{A0} \equiv \frac{\sum_{i=1}^{n}\nu_{Ai}E_iA_i}{E_1A^*} \qquad (35a)$$

$$\bar{\nu}_{B1} \equiv \frac{\sum_{i=1}^{n}\nu_{Bi}E_iA_i\bar{z}_i}{hE_1A^*} \qquad (35b)$$

and

$$\bar{n}_{A0} \equiv \frac{\sum_{i=1}^{n}n_{Ai}A_i}{A^*} \qquad (36a)$$

$$\bar{n}_{B1} \equiv \frac{\sum_{i=1}^{n}n_{Bi}\bar{z}_iA_i}{hA^*} \qquad (36b)$$

Substituting (32) into (16) gives

$$\frac{\partial^2}{\partial x^2}\left[(1-\bar{\nu}_{B2})E_1I^*_{yy}\frac{\partial^2 w_o}{\partial x^2}\right] - \frac{\partial^2}{\partial x^2}\left(\bar{\nu}_{A1}hE_1A^*\frac{\partial u_o}{\partial x}\right)$$

$$+ \frac{\partial^2}{\partial x^2}\left(\bar{n}_{A1}E_1hA^*\frac{\partial^2 u_o}{\partial t\partial x}\right) + \frac{\partial^2}{\partial x^2}\left(\bar{n}_{B2}I^*_{yy}\frac{\partial^3 w_o}{\partial t\partial x^2}\right)$$

$$- \frac{\partial}{\partial t}\left(\rho A\frac{\partial w_o}{\partial t}\right) = -p_z + \frac{\partial^2 H^T_y}{\partial x^2} \qquad (37)$$

where

$$\bar{\nu}_{A1} \equiv \frac{\sum_{i=1}^{n}\nu_{Ai}E_iA_i\bar{z}_i}{hE_1A^*} \qquad (38a)$$

$$\bar{\nu}_{B2} \equiv \frac{\sum_{i=1}^{n}\nu_{Bi}E_iA_i\bar{z}_i^2}{E_1I^*_{yy}} \qquad (38b)$$

and

$$\bar{n}_{A1} \equiv \frac{\sum_{i=1}^{n}n_{Ai}E_iA_i\bar{z}_i}{hE_1A^*} \qquad (39a)$$

$$\bar{n}_{B2} \equiv \frac{\sum_{i=1}^{n}n_{Bi}A_i\bar{z}_i^2}{I^*_{yy}} \qquad (39b)$$

The last term in each of equations (34) and (37) will produce Zener-like damping due to thermomechanical coupling in equation (6). To consider these two terms, the fully coupled field problem must be solved. That is, equations (6), (34), and (37) comprise a set of three coupled equations in three unknowns, $u_o$, $w_o$, and T.

Determination of Material Damping Constants

The energy dissipation due to damage must be at least first order in damage [10]; that is,

$$u^c_L = u^c_L(\epsilon_{xx}, T, \alpha_1) = u^c_{L1}(\epsilon_{xx}, T)\cdot\alpha_1 \qquad (40)$$

Therefore, assuming that Zener damping may be neglected, a first order approximation is given by [10,11]

$$\dot{u}^c_L = E\,\epsilon_{xx}\dot{\alpha}_1 \qquad (41)$$

Thus, the total energy dissipation during a simple cycle in a specimen of length L is given by

$$U^c_L = \int_{t_1}^{t_1+2\pi/\omega}\int_0^L\int_A E\,\epsilon_{xx}\dot{\alpha}_1\,dA\,dx\,dt \qquad (42)$$

Substituting equation (3) for the case of pure bending thus gives

$$U^c_L = \int_{t_1}^{t_1+2\pi/\omega}\int_0^L\sum_{i=1}^{n}E_iA_i\bar{z}_i\frac{\partial^2 w_o}{\partial x^2}\dot{\alpha}_{1i}\,dx\,dt \qquad (43)$$

Thus, substituting (32) into the above results in

$$U^c_L = \int_{t_1}^{t_1+2\pi/\omega}\int_0^L\sum_{i=1}^{n}E_iA_i\bar{z}_i\frac{\partial^2 w_o}{\partial x^2}\left(\nu_{Bi}\bar{z}_i\frac{\partial^3 w_o}{\partial t\partial x^2} - \frac{n_{Bi}}{E_i}\bar{z}_i\frac{\partial^4 w_o}{\partial t^2\partial x^2}\right)dx\,dt \qquad (44)$$

The above neglects energy losses due to shearing [21], which may not be negligible in laminated composites [18].

Now consider the case where the damage is independent of x and no new damage is introduced during the cycle of interest. It follows that for symmetric vibrations, the first term in the above equation is zero, and equation (44) reduces to

$$U^c_L = -S\sum_{i=1}^{n}n_{Bi}A_i\bar{z}_i^2 \qquad (45)$$

where

$$S \equiv \int_{t_1}^{t_1+2\pi/\omega}\int_0^L\frac{\partial^2 w_o}{\partial x^2}\frac{\partial^4 w_o}{\partial t^2\partial x^2}\,dx\,dt \qquad (46)$$

Substituting equation (39b) and rearranging thus results in

$$\bar{n}_{B2} = -\frac{U^c_L}{I^*_{yy}S} \qquad (47)$$

Therefore, for a beam of given geometry and boundary conditions, equation (47) can be used to obtain $\eta_{B2}$. Equation (39b) can then be utilized to extract $\eta_{B1}$ for certain simplified stacking sequences. This information may then be utilized to predict the damping coefficients $\eta_{B1}$ and $\eta_{B2}$ as a function of damage in other stacking sequences by using equation (39b) for other conditions.

Although it is in principal possible to obtain the other coefficients described by equations (35), (36), (38) and (39), it is difficult to accurately measure $U_L^c$ during dynamic axial tests, so that $\bar{\eta}_{A0}$ and $\bar{\eta}_{A1}$ are not easily evaluated by the method described here. However, the stiffness loss coefficients $\nu_{A0}$, $\nu_{B1}$, $\nu_{A1}$, and $\nu_{B2}$ may be obtained from direct static testing [11,12].

## Experimental Determination of Damping

Because of its relative simplicity, a cantilevered beam has been selected as the current test configuration for studying material damping. (It should be noted that the theoretical development described in the previous section is valid for all beam boundary conditions. We are also investigating other beam boundary conditions such as the free-free beam but will confine the present discussion to the behavior of a cantilever beam). The laboratory setup is shown schematically in Fig. 4. A coupon 1.0 in. (25.4 mm) wide and 12.0 in. (304.8 mm) long is clamped in a beam bending fixture to achieve a cantilever of the desired length. The beam is set into vibratory motion by a motorized wheel which rotates until a post engages the free end of the beam, achieves a preselected deflection and then releases the free end. Therefore, the frequency and amplitude of the beam are controlled by varying the length of the beam and the initial deflection. The free decay response is recorded by a strain gage mounted on the beam near the clamp. The bend fixture is housed in a vacuum chamber and the test is initiated externally by a computer which also acquires the strain gage data in digital form. The output of the strain gage is recorded at 1500 data points per second. The amplified signal from the 1000 ohm strain gage is filtered to improve the data reduction accuracy. The damping of the beam is calculated by the logarithmic decrement method.

In the present study the outer fiber strain amplitude was selected so that the logarithmic decement response of the beam is linear. The system (joint) damping has been estimated from tests on several well known materials and has been subtracted from the experimental damping values measured from the composite. It is recognized by the writers that the cantilever beam may not be the most desirable test configuration for a study of material damping. However, our primary objective is to study damping as a function of microstructural damage. Therefore, by constructing carefully controlled laboratory experiments, the relative change in damping due to a progression of microstructural damage will be relatively independent of the system damping which should remain constant.

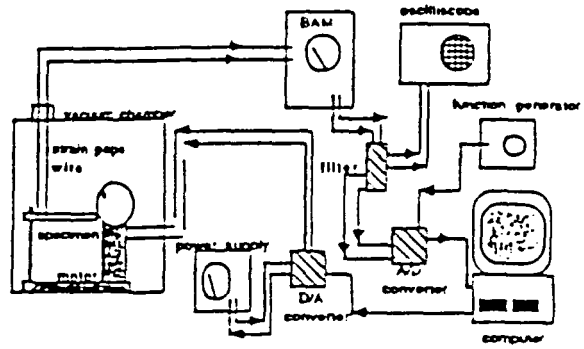


Fig. 4. Schematic Drawing of Testing Apparatus

## Analysis of a Cantilevered Beam

This section provides the specialization of the damage-dependent beam theory for the cantilever beam. The analytical procedure for determining the material damping constants from the experimental data is also described.

For an undamped prismatic cantilever beam undergoing free vibrations, the solution is of the form [22]

$$w_o(t,x) = \sum_{m=1}^{\infty} f_m(t)\phi_m(x) \tag{48}$$

where

$$f_m(t) = C_1 \sin \omega_m t + C_2 \cos \omega_m t \tag{49}$$

and

$$\phi_m(x) = A_m\left[\left(-\frac{\cos \varepsilon_m L + \cosh \varepsilon_m L}{\sin \varepsilon_m L + \sinh \varepsilon_m L}\right)\right.$$
$$(\sinh \varepsilon_m x - \sin \varepsilon_m x)$$
$$\left. + \cosh \varepsilon_m x - \cos \varepsilon_m x\right] \tag{50}$$

Also

$$\varepsilon_m L = \begin{cases} 1.875 & m=1 \\ (m-1/2)\pi & m>1 \end{cases} \tag{51}$$

and

$$\omega_m = (0.597\pi/L)^2[(1-\nu_{B2})E_1 I^*_{yy}/\rho A]^{1/2} \quad m=1$$

$$= [(m-\tfrac{1}{2})\pi/L]^2[(1-\bar{\nu}_{B2})E_1 I^*_{yy}/\rho A]^{1/2} \quad m>1 \qquad (52)$$

Furthermore, $A_m$ depends on the maximum tip deflection and $C_1$ and $C_2$ depend on the initial conditions. Equation (52) may be used to determine the laminate bending coefficient $\bar{\nu}_{B2}$ when $\omega_m$ can be obtained from an experimental test.

In our initial phase of research, the damage-dependent constants are more easily determined if we consider only the first mode of vibration and confine our experiments to the first mode. (Later research will include other modes of vibration.) Considering only the first mode and a beam with the following initial conditions:

$$w_o(0,L) = \delta \qquad (53a)$$

$$\frac{\partial w_o}{\partial t}(0,x) = 0 \qquad (53b)$$

Then $C_1 = 0$ and $C_2 = 1$. Furthermore,

$$\phi_1(x) = A_1[(0.7341)(\sinh 1.875\tfrac{x}{L} - \sin 1.875\tfrac{x}{L}) + \cosh 1.875\tfrac{x}{L} - \cos 1.875\tfrac{x}{L}] \qquad (54)$$

Substituting the above into (48) gives

$$w_o(t,x) = A_1 \cos \omega_1 t\,[(0.7341)(\sinh 1.875\tfrac{x}{L} - \sin 1.875\tfrac{x}{L} + \cosh 1.875\tfrac{x}{L} - \cos 1.875\tfrac{x}{L}] \qquad (55)$$

Satisfying initial condition (53) gives

$$A_1 = \frac{\delta}{5.2734} \qquad (56)$$

Therefore,

$$w_o(t,x) = \frac{\delta}{5.2734}\cos \omega_1 t\,[0.7341\,(\sinh 1.875\tfrac{x}{L} - \sin 1.875\tfrac{x}{L}) + \cos 1.875\tfrac{x}{L} - \cos 1.875\tfrac{x}{L}] \qquad (57)$$

Substituting (57) into (46) thus gives

$$S = -\int_0^{2\pi/\omega_1}\int_0^L \omega_1^2 \left(\frac{1.875}{L}\right)^4 \frac{\delta^2}{5.2734^2}\cos^2\omega_1 t\,[0.7341\,(\sinh 1.875\tfrac{x}{L} + \sin 1.875\tfrac{x}{L}) + \cosh 1.875\tfrac{x}{L} + \cos 1.875\tfrac{x}{L}]^2 dx dt \qquad (58)$$

Integrating the above equation and substituting into equation (47) thus gives

$$\bar{n}_{B2} = \frac{U_L^C}{20.12\, I^*_{yy}\,\frac{\omega_1\delta^2}{L^3}} \qquad (59)$$

The energy dissipated per cycle, $U_L^C$, of a vibrating beam is related to the experimentally determined logarithmic decrement, $\Delta$, by the following relationship

$$\Delta = \frac{U_L^C}{2\,U_s} \qquad (60)$$

where $U_s$ is the maximum strain energy of the beam. The strain energy of the beam is given by

$$U = \frac{1}{2}\int_0^L \int_A E\left(\frac{\partial^2 w_o}{\partial x^2}\right)^2 z^2\, dA dx \qquad (61)$$

and for a cantilever vibrating in the first mode with an initial tip deflection, $\delta$,

$$U_s = 3.2016\,\frac{\delta^2}{L^3}\sum_{i=1}^{n} E_i A_i \bar{z}_i^2 \qquad (62)$$

Substituting equations (108), (60), and (62) into (59) gives

$$\bar{n}_{B2} = 0.31827\left(\frac{E_1\Delta}{\omega_1}\right) \qquad (63)$$

The procedure used herein to determine the damping constants, $n_{Bi}$, is to experimentally measure the logarithmic decrement for a $[0/90/0]_s$ laminate and calculate $n_{B1}$ from equations (63) and (39B). Since we are only considering matrix crack damage at present, we will assume that all the damping may be attributed to the 90° plies of the $[0/90/0]_s$ laminate. This will provide an experimental measure of the damping in a single 90° ply with matrix crack damage. Substituting equation (39B) into equation (63) and rearranging gives the following expression for the logarithmic decrement

$$\Delta = 3.142\,\omega_1\,\frac{\sum_{i=1}^{n} n_{Bi} A_i \bar{z}_i^2}{\sum_{i=1}^{n} E_i A_i \bar{z}_i^2} \qquad (64)$$

Once $n_{B1}$ is determined as a function of damage,

equation (64) can be used to predict the damping of a cantilever beam of any cross-ply laminate stacking sequence. While equation (64) appears linear in damping this is not the case because the damping constants, $n_{Bi}$ are also function of frequency. (See equation 33).

## Comparison of Experimental and Analytical Results

Experimental results have been obtained from cross-ply laminates with various combinations of 0° and 90° plies of AS-4/3502 graphite/epoxy. The laminates were fabricated using a standard prepreg tape layup and hot press curing process following the curing procedure recommended by the prepreg tape vendor. The approximate per ply thickness of the cured laminates was 0.005" (0.127 mm) and the fiber volume fraction was approximately 62%. The measured lamina properties are given in Table 1. These properties are typical of this material system.

The theory presented herein was developed only for material damping. Therefore, it was essential to separate the system damping from the measured values of logarithmic decrement to determine material damping constants and to compare theoretical predictions to experimental values. Using test results for a variety of materials, the system damping for the current configuration of a cantilevered beam vibrating predominantly in the first mode has been determined to be approximately $3.52 \times 10^{-3}$. This value of system damping was considered to be a constant for all laminates in this study.

Table 1. Material Properties for Hercules AS4/3502

Lamina Properties

| | |
|---|---|
| $E_{11}$ | $21.0 \times 10^6 \pm 2.0\%$ psi (144.8 GPa) |
| $E_{22}$ | $1.39 \times 10^6 \pm 2.1\%$ psi (9.58 GPa) |
| $G_{12}$ [1] | $0.694 \times 10^6$ psi (4.79 GPa) |
| $\nu_{12}$ | $0.310 \pm 3.7\%$ |
| $F_{tu}$ | $326000 \pm 3.5\%$ psi (2.248 MPa) |
| $F_{tu}$ | $11085 \pm 9.8\%$ psi (76.4 MPa) |
| $\epsilon_{tu}$ | $0.0144 \pm 4.6\%$ in/in |
| $\epsilon_{tu}$ | $0.00773 \pm 6.7\%$ in/in |

[1] Theoretically calculated from test data for a $[\pm 45]_{2s}$ laminate.

Considerable attention was given to the experimental test parameters that yielded the most repeatable results and held constant those parameters which influenced damping such as frequency and stress amplitude. This procedure allows for the most direct comparison between theory and experiment for the laminates discussed herein. All test results reported herein were obtained at the frequency of the first mode of vibration. The initial tip deflection was selected so that the outer fiber stress near the root was within the stress amplitude range where damping was constant and the free decay was linear when plotted on a log scale, as shown in Fig. 5.

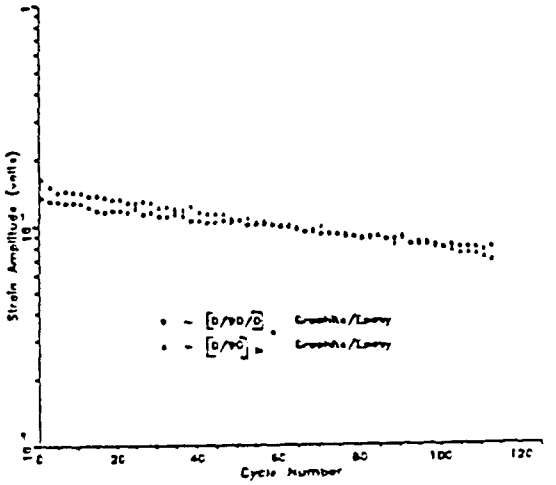


Fig. 5. Logarithmic Peak Value Decay

Since the contribution to material damping of the matrix material is considered to be substantially greater than that of the graphite fibers, as a first approximation, the assumption is made that all the material damping of the cross-ply laminates may be attributed to the 90° layers. Furthermore, we are confining the present study to the single damage mode of matrix cracks in the 90° plies. Therefore, it is necessary to specify only one material damping constant, $n_{B_1}$ in equation 39b, to determine the damping of any cross-ply laminate. Using the experimental results for the $[0/90/0]_s$ laminate, $n_{B_1}$ for a single 90° ply was calculated from equations (63) and (39b) to be 3.86 lbs-sec/in$^2$ for an undamaged laminate. This value of $n_{B_1}$ and equation (64) was used to predict the undamaged material damping of the $[0/90]_{2s}$, $[0/90_3]_s$ and $[0/90_2]_{3s}$ laminates. The comparison of the predicted values of damping to the experimentally measured values for the undamaged laminates is given in Table 2. The predicted values are within ±8% of the experimental values. This is consistent with the range of repeatability of the experimental data as measured by the standard deviation of numerous replicate tests.

A complete characterization of the damage dependent material damping of graphite/epoxy laminates is in progress. The experimental results confirm a strong relationship between material damping and microstructural damage. Figure 6 shows the relationship between material damping and microstructural damage. Figure 6 shows the relationship between material damping and matrix crack damage in the 90° layer of a

Table 2. Predicted and Experimental Values of Damping Determined by the Logarithmic Decrement Method

| LAMINATE STACKING SEQUENCE | FIRST MODE FREQUENCY | EXPERIMENTAL DAMPING | PREDICTED DAMPING |
|---|---|---|---|
| $[0/90]_{2s}$ | 18.5 | $4.52\times10^{-3}$ | $4.20\times10^{-3}$ |
| $[0/90_3]_s$ | 18.7 | $5.11\times10^{-3}$ | $5.56\times10^{-3}$ |
| $[0/90_2]_{3s}$ | 25.3 | $10.64\times10^{-3}$ | $10.42\times10^{-3}$ |

$[0/90_3]_s$ laminate. (The damage states were developed in uniaxial tension-tension fatigue.) As can be seen in Fig. 6, damping, normalized by the initial value of damping for the undamaged laminate, increases by about a factor of 2 as the matrix crack damage state progresses to the crack saturation state.

## Summary and Conclusions

Equations of motion for a vibrating beam have been developed for composite materials which account for the influence of microstructural damage on beam stiffness and material damping. This new theoretical approach introduces damage-dependence into the constitutive relationships via internal state variables which characterize the current microstructural damage state. Since the constitutive relationship is time dependent, the equations of motion contain explicit terms representing the damage-dependent material damping. The equations of motion are developed for a laminated composite beam by employing standard lamination theory and assuming that individual ply contributions to material damping can be represented by a rule-of-mixtures formulation. The equations of motion may be solved to determine the damage-dependent natural frequencies and mode shapes of the beam. The beam theory is also used to construct a mathematical model of damage-dependent material damping at the laminate level which is the primary subject of this paper.

Damage-dependent material damping constants are obtained from baseline experimental data. Once the material constants are determined for a particular material system, the mathematical model of the laminate material damping is used to predict the damping of any other laminate stacking sequence.

In order to verify the validity of the theoretical formulation, experimental results were obtained from cross-ply graphite/epoxy laminates with a variety of stacking sequences. A cantilevered beam was selected for experimental study and the test results to date are confined to the first mode of vibration and at initial tip deflections that produced damping values relatively independent of stress amplitude. Because our study is currently only addressing the behavior of cross-ply laminates with the single damage mode of matrix cracks in the 90° layers, we have assumed that all the material damping can be attributed to the 90° layers. The

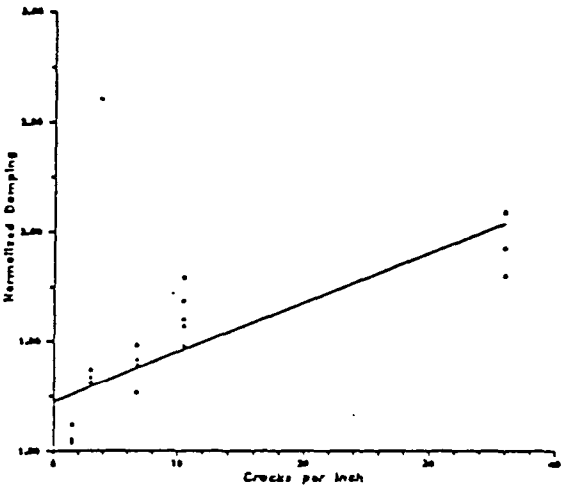


Fig. 6. Normalized Damping vs. Crack Density $[0/90_3]_s$, Graphite/Epoxy

undamaged damping constants for a 90° ply were determined from the experimental data of the $[0/90/0]_s$ laminate. The undamaged damping of the $[0/90]_{2s}$, $[0/90_3]_s$ and $[0/90_2]_{3s}$ laminates was predicted by the theoretical model of damping. The predicted values for these laminates were within ±8% of the measured values. While damage-dependent data are not fully developed at this time, the excellent agreement between the theory and experiment for the undamaged damping provides verification of the theoretical formulation.

ACKNOWLEDGEMENTS

The writers wish to acknowledge the financial support provided by a grant from NASA Johnson Space Center.

REFERENCES

1. Highsmith, A.L., Stinchcomb, W.W., and Reifsnider, K.L., "Stiffness Reduction Resulting from Transverse Cracking in Fiber-Reinforced Composite Laminates," Virginia Polytechnic Institute and State University, VPI-E-81.33, November, 1981.

2. O'Brien, T.K., "An Evaluation of Stiffness Reduction as a Damage Parameter and Criterion for Fatigue Failure in Composite Materials," Ph.D. Dissertation, Virginia Polytechnic Institute and State University, October, 1978.

3. Norvell, R.G., "An Investigation of Damage Accumulation in Graphite/Epoxy Laminates," Texas A&M University Thesis, August, 1985.

4. Plunkett, R., "Damping in Fiber Reinforced Laminated Composites at High Strain," J. Composite Materials Supplement, Vol. 14, pp. 109-117, 1980.

5. Edberg, D.L., "Material Damping of Sample Structures in a Simulated Space Environment," Journal of Spacecraft and Rockets, Vol. 23, pp. 286-296, 1986.

6. Kalyanasundaram, S., Lutz, J.D., Haisler, W.E., and Allen, D.H., "Effect of Degradation of Material Properties on the Dynamic Response of Large Space Structures," Journal of Spacecraft and Rockets, Vol. 23, pp. 297-302, 1986.

7. Chang, H.T., and Allen, D.H., "Predicted Dynamic Response of a Composite Beam with History Dependent Damage," Texas A&M University Mechanics and Materials Center, MM 4875-86-17, July, 1986.

8. Gibson, R.R., and Plunkett, R., "Dynamic Mechanical Behavior of Fiber-Reinforced Composites: Measurement and Analysis," J. Composite Materials, Vol. 10, pp. 325-341, 1976.

9. Ni, R.G. and Adams, R.D., "The Damping and Dynamic Moduli of Symmetric Laminated Composite Beams - Theoretical and Experimental Results," J. Composite Materials, Vol. 18, pp. 104-121, 1984.

10. Allen, D.H., Harris, C.E., and Groves, S.E., "A Thermomechanical Constitutive Theory for Elastic Composites with Distributed Damage - Part I. Theoretical Development," to appear in International Journal of Solids and Structures, 1987.

11. Allen, D.H., Harris, C.E., and Groves, S.E., "A Thermomechanical Constitutive Theory for Elastic Composites with Distributed Damage - Part II: Application to Matrix Cracking in Laminated Composites," to appear in International Journal of Solids and Structures, 1987.

12. Allen, D.H., Harris, C.E., Groves, S.E., and Norvell, R.G., "Characterization of Stiffness Loss in Crossply Laminates with Curved Matrix Cracks," to appear in Journal of Composite Materials, 1987.

13. Allen, D.H., and Haisler, W.E., Introduction to Aerospace Structural Analysis, Wiley, New York, 1985.

14. Timoshenko, S.P., Vibration Problems in Engineering, 2nd edition, Van Nostrand, New York, 1937.

15. Allen, D.H., Groves S.E., and Harris, C.E., "A Cumulative Damage Model for Continuous Fiber Composite Laminates with Matrix Cracking and Interply Delaminations," to appear in ASTM Special Technical Publication, 8th Symposium on Composite Materials: Testing and Design, American Society for Testing and Materials, 1987.

16. Allen, D.H., "A Prediction of Heat Generation in a Thermoviscoplastic Uniaxial Bar," International Journal of Space Structures, Vol. 21, No. 4, pp. 325-342, 1985.

17. Allen, D.H., "Predicted Axial Temperature Gradient in a Viscoplastic Uniaxial Bar Due to Thermomechanical Coupling," International Journal for Numerical Methods in Engineering, Vol. 23, No. 5, pp. 903-917, 1986.

18. Schapery, R.A., "Viscoelastic Behavior and Analysis of Composite Materials," Mechanics of Composite Materials, Vol. 2, G.P. Sendeckyj, Ed., Academic Press, N.Y., pp. 85-167, 1974.

19. Schultz, A.B., and Warwick, D.N., "Vibration Response: A Non-Destructive Test for Fatigue Crack Damage in Filament-Reinforced Composites," Journal of Composite Materials, Vol. 5, pp. 394-404, 1971.

20. Chou, P.C., Wang, A.S.D., and Miller, H., "Cumulative Damage Model for Advanced Composite Materials," AFWAL-TR-82-4-83, September, 1982.

21. Adams, R.D., and Bacon, D.G.C., "The Dynamic Properties of Unidirectional Fibre Reinforced Composites in Flexure and Torsion," J. Composite Materials, Vol. 7, pp. 53-67, 1973.

22. Biggs, J.M., Introduction to Structural Dynamics, McGraw-Hill, New York, 1964.

## 8.3 An Experimental Investigation of Damage-Dependent Material Damping in Laminated Composites

# AN EXPERIMENTAL INVESTIGATION OF DAMAGE-DEPENDENT MATERIAL DAMPING IN LAMINATED COMPOSITES

S. A. Smith *
D. H. Allen **
C. E. Harris ***
Texas A&M University
College Station, Texas

## Abstract

An experimental program is reported in which the material damping of laminated graphite/epoxy specimens was measured as a function of matrix cracking. The damping test apparatus is designed to measure the first mode free vibration response of a cantilevered beam. Damping is calculated by the logarithmic decrement method. Matrix cracks are introduced into the material, and damping is measured at several levels of damage. The results from six different laminate stacking sequences are recorded and compared to each other. Damping is found to be significantly affected by the laminate ply stacking sequence, and is also seen to increase dramatically with the presence of matrix cracks. Finally, mathematical model predictions are compared to the experimental results.

## Nomenclature

| | |
|---|---|
| $A$ | - beam cross-sectional area |
| $A_i$ | - cross-sectional area of the ith lamina |
| $E$ | - axial modulus of elasticity |
| $E_1$ | - reference axial modulus of elasticity |
| $E_i$ | - axial modulus of elasticity of ith lamina |
| $I^*_{yy}$ | - modulus weighted moment of inertia about y axis |
| $M^T_y$ | - beam moment resultant about y axis due to temperature change |
| $N$ | - number of cycles of applied load |
| $n$ | - number of plies in laminate |
| $p_z$ | - beam transverse load per unit length |
| $S$ | - term used to obtain laminate damping coefficient |
| $T$ | - temperature |
| $t$ | - time |
| $U^*_L$ | - total internal energy dissipation due to matrix cracking |
| $U_S$ | - maximum strain energy of a deflected beam |
| $w_o$ | - transverse displacement of neutral surface |
| $x$ | - beam axial coordinate direction |
| $z$ | - beam transverse coordinate direction |
| $\bar{z}_i$ | - z component of distance from centroid of ith ply to modulus weighted centroid |
| $\alpha$ | - coefficient of thermal expansion |
| $\alpha_1$ | - axial component of matrix cracking damage internal state variable (ISV) |
| $\alpha_{1i}$ | - axial component of matrix cracking damage ISV in ith lamina |
| $\Delta$ | - beam tip deflection |
| $\delta$ | - logarithmic decrement |
| $\varepsilon_{xx}$ | - axial strain component |
| $\eta$ | - damping coefficient |
| $\eta_{Bi}$ | - bending damping coefficient in ith lamina |
| $\mu_{Bi}$ | - bending stiffness loss coefficient in ith lamina |
| $\omega_1$ | - modal frequency of the 1st resonant mode |
| $\rho$ | - mass density |
| $\sigma_A$ | - stress amplitude of cyclic loading |

## Introduction

Microstructural damage in laminated fibrous composite materials has been found to alter several material properties[1-3]. Extensive modeling and testing has been performed to determine stiffness loss in laminated composites as a result of matrix cracking and interply delaminations. In addition, several investigators have noted and measured the changes in damping caused by damage[4-8]. However, no attempt has been made to quantify or model the effect of damage on material damping. The objective of this study was to define a direct relationship between microstructural damage in a laminate and the resulting change in the damping capacity of that laminate.

This paper presents and discusses the results of an experimental program which has investigated the effects of matrix cracking on material damping of laminated graphite/epoxy specimens. The effect of ply stacking sequence on material damping is also discussed. A mathematical model developed by Allen, Harris, and Highsmith[9] has been applied, and the resulting predictions of damage-dependent damping are compared to the experimental results.

## Mathematical Model

Many mathematical models have been developed which attempt to predict the material damping of composite materials[10-15]. However, none of these models are able to predict the material damping of composites as a function of microstructural damage. The model discussed in this section was developed by Allen, Harris, and Highsmith[9] at the Mechanics and Materials Center at Texas A&M University. This section provides only a brief overview of this model, as detailed derivations and explanations appear in Reference 9.

The model uses the concept of continuum damage mechanics, using internal state variables to account for damage in the constitutive equations. The internal state variables may be defined for each particular form of damage in the composite. The constitutive equation for the material system used in this study is based on a nonlinear Voigt model representation, shown in Figure 1. The general constitutive equation for this model is:

$$\sigma_{xx} = E(\varepsilon_{xx} - \frac{n\varepsilon_{xx}}{E} - E\alpha T) \qquad (1)$$

---

* Graduate Research Assistant, Aerospace Engineering, Student Member AIAA
** Professor, Aerospace Engineering, Member AIAA
*** Branch Head, NASA Langley, Member AIAA

where $\eta$ is a constant material property, $\bar{\alpha}$ is the coefficient of thermal expansion, and $\Delta T$ is the change in temperature. Experimental evidence has shown that polymeric composites are not accurately represented by this simple model. In the model development, it is shown that a Voigt model in which $\eta$ is not assumed to be constant for all loadings, but is instead a function of initial stress, $\sigma_A$, frequency, $\omega$, and the number of cycles, N, will closely approximate the actual material constitution of polymeric composites for small displacements.

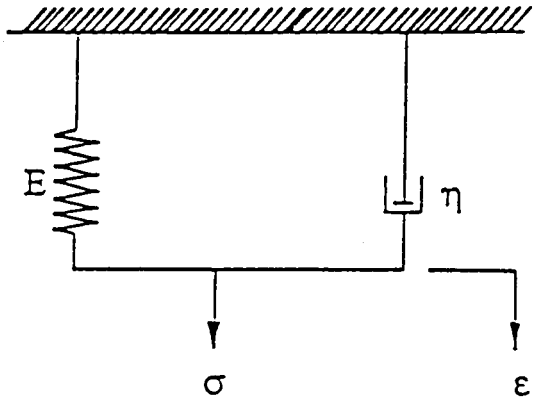


Figure 1. Voight Model

The general thermomechanical constitutive relationship for a material, including the internal state variable $\alpha_1$, is:

$$\sigma_{xx} = E(\varepsilon_{xx} - \alpha_1 - \bar{\alpha}\Delta T) \quad . \tag{2}$$

Equating (1) and (2), the internal state variable

$$\alpha_1 = \frac{\eta}{E}\varepsilon_{xx} \tag{3}$$

for a single ply within the laminate is determined.

The equation of motion for transverse displacement (bending) is developed using the constitutive equations, equilibrium, and strain displacement relationships for an Euler-Bernoulli beam.

$$\frac{\partial^2}{\partial x^2}(E_1 I^*_{yy}\frac{\partial^2 w_o}{\partial x^2} - \sum_{i=1}^{n} E_i \alpha_{1i} \bar{z}_i A_i - M^T_y) = p_z + \frac{\partial}{\partial t}(\rho A \frac{\partial w_o}{\partial t}) \quad , \tag{4}$$

where

$$I^*_{yy} = \int_A \frac{E}{E_1} dA \tag{4a}$$

and

$$M^T_y = \int_A E\,\bar{\alpha}\,(\Delta T)\,z\,dA \quad . \tag{4b}$$

Replacing $\varepsilon_{xx}$ in (3) with displacement variables, and introducing a coefficient $\mu_{bi}$ for the $i^{th}$ ply, which describes the loss in stiffness caused by matrix cracking, $\alpha_{1i}$ for a pure bending case becomes:

$$\alpha_{1i} = \mu_{bi}\,\bar{z}_i \frac{\partial^2 w_o}{\partial x^2} + \frac{\eta_{bi}}{E_i}\bar{z}_i \frac{\partial^3 w_o}{\partial t \partial x^2} \quad . \tag{5}$$

The model development also accounts for axial displacement, but will not be considered in this study since only the bending case has been investigated experimentally.
Substituting (5) into (4) yields:

$$\frac{\partial^2}{\partial x^2}[(1-\bar{\mu}_{B2})E_1 I^*_{yy}\frac{\partial^2 w_o}{\partial x^2}] + \frac{\partial^2}{\partial x^2}[\bar{\eta}_{B2} I^*_{yy}\frac{\partial^3 w_o}{\partial t \partial x^2}] + \frac{\partial}{\partial t}(\rho A \frac{\partial w_o}{\partial t}) = p_z + \frac{\partial^2 M^T_y}{\partial x^2} \quad , \tag{6}$$

where

$$\bar{\mu}_{B2} = \frac{\sum_{i=1}^{n} \mu_{Bi} E_i A_i \bar{z}_i^2}{E_1 I^*_{yy}} \tag{6a}$$

and

$$\bar{\eta}_{B2} = \frac{\sum_{i=1}^{n} \eta_{Bi} A_i \bar{z}_i^2}{I^*_{yy}} \quad . \tag{6b}$$

The determination of the laminate damping coefficients is accomplished by calculating the energy dissipated per cycle of vibration, $U^c_L$. Assuming that Zener and shear damping effects can be neglected, that the damage distribution is uniform over the length of the specimen, and that additional damage is not introduced during the cycle of interest, the bending damping constant, $\bar{\eta}_{B2}$, is approximated by

$$\bar{\eta}_{B2} = -\frac{U^c_L}{I^*_{yy} S} \tag{7}$$

where

$$U^c_L = -S \sum_{i=1}^{n} \eta_{bi} A_i \bar{z}_i^2 \tag{7a}$$

and

$$S = \int_{\tau_1}^{\tau_1 + 2\pi/\omega} \int_0^L \frac{\partial^2 w_o}{\partial x^2}\frac{\partial^4 w_o}{\partial t^2 \partial x^2} dx\,dt \quad . \tag{7b}$$

For a cantilevered beam vibrating in the first mode, $w_o$ is derived as

$$w_o(t,x) = \frac{\Delta}{3.2734}\cos\omega_1 t[0.7341(\sinh 1.875\frac{x}{L} - \sin 1.875\frac{x}{L}) + \cosh 1.875\frac{x}{L} - \cos 1.875\frac{x}{L}] \tag{8}$$

where the constants were determined by the boundary conditions. Substituting (8) into (7b) and integrating,

$$S = 20.12 \frac{\omega_1 \Delta^2}{L^3} \quad . \qquad (9)$$

where $\Delta$ is the initial beam tip deflection and L is the length of the beam. Substituting (9) into (7) yields the following expression:

$$U_L^c = 20.12\, \eta_{B2}\, I_{yy}^* \frac{\omega_1 \Delta^2}{L^3} \quad . \qquad (10)$$

The logarithmic decrement, $\delta$, is defined to be one-half of the energy dissipated per cycle, $U_L^c$, divided by the maximum strain energy of the deflected beam, $U_s$. For the given configuration,

$$U_s = 3.2016 \frac{\Delta^2}{L^3} \sum_{i=1}^{n} E_i\, A_i\, \bar{z}_i^2 \quad . \qquad (11)$$

Therefore,

$$\delta = 3.142\, \omega_1 \frac{\sum_{i=1}^{n} \eta_{Bi}\, A_i\, \bar{z}_i^2}{\sum_{i=1}^{n} E_i\, A_i\, \bar{z}_i^2} \quad , \qquad (12)$$

which is a first order approximation of the logarithmic decrement for a symmetric, cantilevered laminate, vibrating in the first mode. Additionally, this form assumes that the displacements are small, that the beam is not shear deformable, and that lamina property $\eta_{Bi}$ is a function of $\sigma_A$, $\omega$, N, and ply orientations.

The values of $\eta_{Bi}$ for a given damage state, initial stress level, and frequency are determined by measuring the logarithmic decrement and extracting $\eta_{Bi}$ for each ply. It is also assumed in this model that, for cross-ply laminates, $\eta_{Bi}$ for 0 degree plies does not change when matrix cracks are introduced in the 90 degree plies. Therefore, for this study, $\eta_{Bi(0)}$ will be assumed constant for all damage levels. However, $\eta_{Bi(90)}$ will be defined as a function of matrix cracking, and will be determined experimentally.

## Experimental Program

### Specimen Preparation

In order to meet the objectives of this study—to isolate matrix cracking as the only damage mode—cross-ply laminates were chosen to be tested. 12 inch square plates were prepared from Hercules AS4/3502 Graphite/Epoxy preimpregnated tape, and 1 inch wide specimens were subsequently cut from these plates using a high speed diamond-edge cutting wheel. Table 1 lists the ply properties of the material which have been obtained from appropriate testing methods. Table 2 lists the laminates selected for testing in this study.

To minimize undesirable damage caused by the grips of the loading machine, a thin coating of epoxy was spread over the ends of the specimens. The specimen edges were then polished to insure high quality edge replicas. 1000Ω single element strain gages, aligned with the beam axis, were bonded to the specimens to measure the response signal during the damping measurements. The final specimen configuration is seen in Figure 2.

Table 1. Lamina Properties for AS4/3502 Graphite/Epoxy

| Property | Value |
|---|---|
| $E_{11}$ | $21.0 \times 10^6$ psi |
| $E_{22}$ | $1.39 \times 10^6$ psi |
| $G_{12}$[1] | $0.694 \times 10^6$ psi |
| $\nu_{12}$ | 0.310 |
| Fiber Volume Fraction[2] | 62% |

[1] Calculated from test data for a $[\pm 45]_{2s}$ laminate

[2] Manufacturer's Pre-Cure Value

Table 2. AS4/3502 Laminate Types Tested

| Laminate | Stacking Sequence |
|---|---|
| A | $[0/90/0]_s$ |
| B | $[90/0/90]_s$ |
| C | $[0/90_3]_s$ |
| D | $[90_3/0]_s$ |
| E | $[0/90]_{2s}$ |
| F | $[90/0/90_2]_s$ |

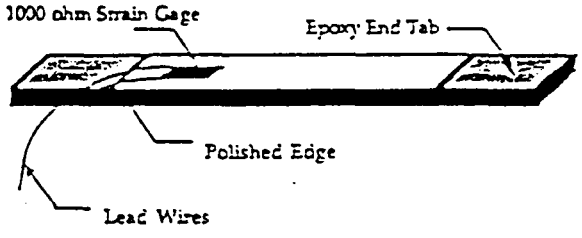


Figure 2. Specimen Configuration

### Damping Measurements

Because of its simplicity, a cantilevered beam configuration was chosen for the damping apparatus. A support was designed which minimized specimen slippage at the boundary, and avoided inducing damage in the specimen. Figure 3 is a scale drawing of the fixture. To conduct damping tests, the specimen was placed in the slot with a predetermined length extending from the support. This length was chosen to produce a desired beam frequency.

Many experimental techniques have been employed in the past to study the material damping of composites. One concern in these studies has been the effect on damping caused by external factors[5,6,16-18]. Some of the undesirable damping contributions encountered in past investigations are atmospheric pressure, friction caused by contacting instruments and/or boundaries, and additional masses. Regardless of the method used for damping measurement, considerable difficulty has been encountered by almost all experimentalists in obtaining repeatable and accurate results. Since this study focused on the effect of damage on material damping, all other damping contributions were minimized and held constant to establish an exact correlation between damping and damage. Atmospheric pressure has been found to influence damping. To eliminate this effect from measured damping, all tests were conducted inside a vacuum chamber. To study the effect of the epoxy end tabs on material damping, tests were conducted first without the end tabs, and then with the end tabs on the specimen. The measured damping for a given

configuration decreased with the addition of the epoxy end tabs. This was attributed to the resulting decrease in frequency caused by the small mass at the free end, and did not affect the actual material damping capacity of the specimens.

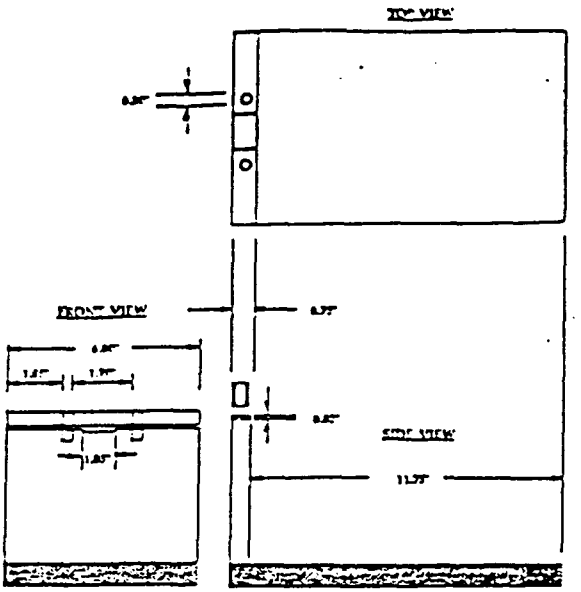

Figure 3. Boundary Support

In order to excite the beam at a prescribed amplitude, a mechanical system was developed to "pluck" the free end of the beam to a given deflection. An electric motor is attached to an aluminum mount which slides in a groove cut into the baseplate of the specimen support. Also attached to the mount is a rotating wheel which is powered by the motor. An arm extends from the wheel and is used to contact the free end of the specimen. The excitation source and support are shown in Figure 4. Upon initiation of a damping experiment, the wheel is rotated until the arm contacts the specimen. The arm then continues to rotate, causing the beam to deflect, and eventually releases the specimen into a free vibrating motion. The tip deflection of the beam is adjusted by moving the contact point of the arm to the specimen.

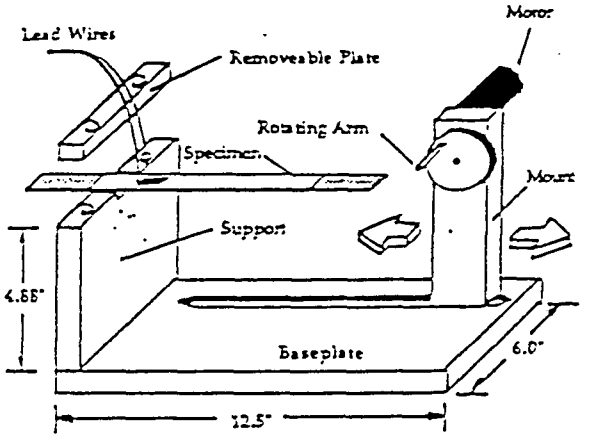


Figure 4. Damping Excitation Apparatus

The strain response signal was transmitted to a half bridge contained in a Micro Measurements EAM-1, which was also used to indicate static strain values. In order to obtain an initial strain level that produces a signal of sufficient amplitude for the damping measurements, the arm-to-specimen contact point is moved by adjusting the position of the wheel mount on the baseplate. Figure 5 is a schematic of the test system. The entire process of specimen excitation and data collection is controlled by a personal computer. An analog and digital interface board was installed into the computer. The control of the motor and the collection of the data is provided by software. The data sampling rate was adjusted for each test to collect exactly 50 data points per cycle of beam vibration.

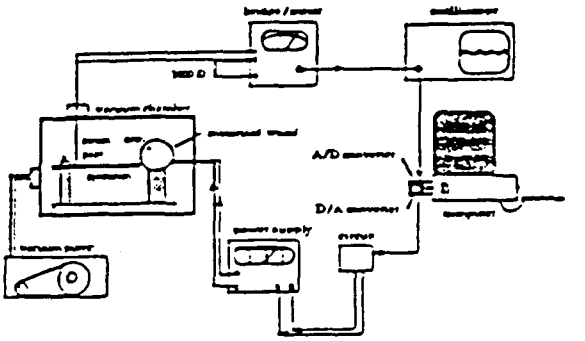

Figure 5. Schematic of Damping Test System

To accurately measure the damping and frequency of the specimen, a sufficient number of cycles had to be captured. Since data was collected at 50 points per cycle, capturing 9000 data points results in recording 180 cycles. This number of cycles was adequate to describe the decay of the specimen response in vacuum. With the number of data points and the sampling rate prescribed, the computer was prepared to start the damping experiment. An initial zero load strain reading was made which was subtracted from the output signal. After this value was recorded, a 5 volt analog signal, generated by the D/A interface board, was supplied to an external circuit board. This circuit then directed a 12 volt power supply to transmit a signal to the motor, causing the mechanical arm to rotate. At this point, the computer began to read the data signal from the stationery beam. As the rotating arm contacted the specimen and deflected downward, the resulting tensile strain was read by the computer as a positive voltage. When the arm released the specimen free end and the beam deflected upward, the strain approached the initial unloaded value. Once the beam crossed this initial deflection plane, the strain became compressive, and was read as a negative value. As soon as the computer recognized the negative value, it ceased to supply a voltage to the external circuit, causing the wheel to stop rotating. Then the computer collected data at the prescribed sampling rate. By collecting data only after the motor had been turned off, the electrical signal and vibration caused by the motor, would not influence the data.

One measure of the logarithmic decrement, $\delta$, is given by

$$\delta = -\ln\left(\frac{x_{j+1}}{x_j}\right) \quad , \qquad (13)$$

where $x_j$ is the peak strain amplitude of the $i^{th}$ cycle. For most materials, however, the peak decay of consecutive cycles is extremely small, and difficult to resolve from experimental data. Another approach is to measure the logarithmic decrement between a finite number of cycles. The logarithmic decrement becomes:

$$\delta = -\left(\frac{1}{N}\right)\ln\left(\frac{x_{j+N}}{x_j}\right) \quad . \qquad (14)$$

However, if the $N^{th}$ data point is not a valid representation of the response at that particular cycle, error in $\delta$ can be very significant. If the decaying response is not greatly influenced by the presence of shear deformation, friction, or atmospheric

pressure (as discussed earlier), the free decay will be exponential, and independent of strain levels. By determining these effects to be negligible, the logarithmic decrement was measured by fitting a straight line through the natural log of the peak values. This was done for the positive (tension) and negative (compression) peak values. Figure 6 is the positive peak value decay for a $[0/90/0]_s$ specimen plotted on a semi-log scale. The degree of "linearity", and the small amount of experimental data scatter of the decay can easily be seen in this graph.

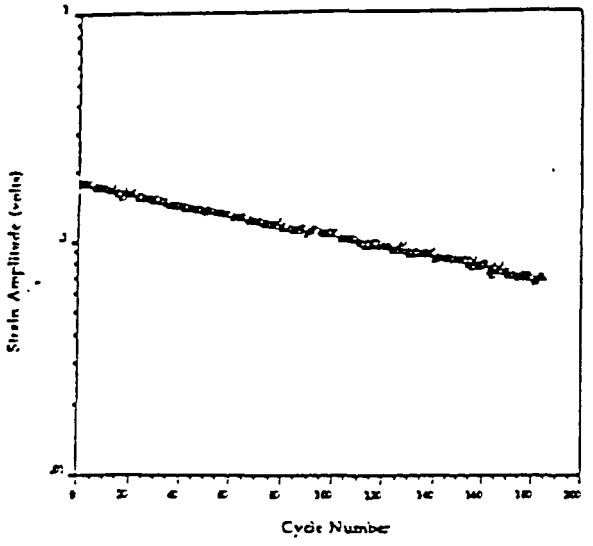


Figure 6. Peak Value Decay for $[0/90/0]_s$ Gr/Ep

Damage Inducement

The objectives in the damage inducement phase of this study were to introduce matrix cracking in the specimens, and to quantify the resulting damage. A 20 kip MTS 810 testing machine was used to load the specimens. All of the specimens were loaded at a rate of 20 pounds per second as recommended by ASTM Standard 3039-76. A uniaxial extensometer which was attached to the specimen with Tesafix double-stick tape was used to measure strain in the specimens.

Edge replication was used to document matrix cracking. Since matrix cracks generally extend across the width of the specimen, as indicated by x-ray radiographs, visible cracks can be detected on both sides of the specimen. Edge replicas indicate the location of cracks with respect to the thickness dimension, information which is not easy to obtain using radiography. However, edge replicas do not reveal matrix cracks in the 0 degree plies (axial splits), or areas of delamination. Previous studies of AS4/3502 cross-ply laminates show a distinct damage progression for monotonic loadings, in which matrix cracks form only in the 90 degree plies at relatively low loads. As the load is increased, the number of matrix cracks in the 90 degree plies grows substantially, until a matrix crack saturation level is reached. Higher load levels will not produce additional cracks in the 90 degree plies. However, axial splits and interlaminar delaminations may form, depending upon the cross-ply stacking sequence. Since this study was focused on matrix cracking, all tests were conducted below the matrix crack saturation level, determined for each laminate, minimizing the presence of higher damage modes.

Several measurements of the stiffness of the undamaged specimen were made by loading the specimen to the 500 pound level, and recording the resulting stress and strain. Subsequently, the load was slowly increased, and edge replicas were taken at several intervals. When matrix cracks first became detectable, the load was reduced and the stiffness was measured again. Because matrix cracks are not always spaced uniformly along the length of the specimen, and since spacing may be different in non-consecutive 90 degree plies, the number of cracks per inch in each ply was averaged over a 2 inch gage length. The gage section was the two inches closest to the root of the specimen when in the clamped damping apparatus. The ply dimensions varied slightly from specimen to specimen. Therefore, damage was quantified by crack surface area per inch of length. A numerical value was determined by multiplying the cracks per inch of a ply by the cross-sectional area (thickness x width) of the ply containing the crack. The surface area is approximately twice this value since each crack has two faces. A diagram of a matrix crack in a single ply appears in Figure 7, which indicates the dimensions of crack surface area.

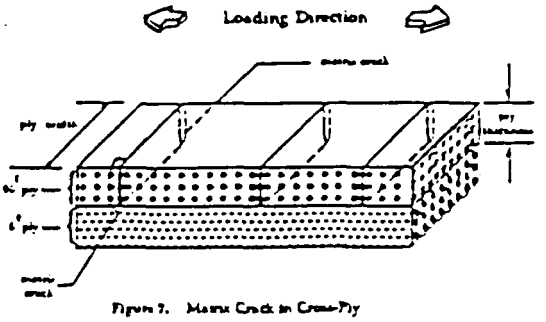


Figure 7. Matrix Crack in Cross-Ply

## EXPERIMENTAL RESULTS

The first step in conducting the damping and damage experiments was to measure damping for $[0]_8$ and $[90]_8$ laminates, which would be used to develop the undamaged damping constants for 0 and 90 degree plies. Using the average damping and frequency values of 5 tests, as well as the specimen dimensions and properties, the model constants for 0 and 90 degree plies were calculated. The constants are in units of lb-sec/in$^2$, and are:

$$\eta_{Bi(0)} = 164.625$$
$$\eta_{Bi(90)} = 196.948 \quad .$$

To illustrate the difference in the damping of these laminates, the peak value decays are plotted together in Figure 8.

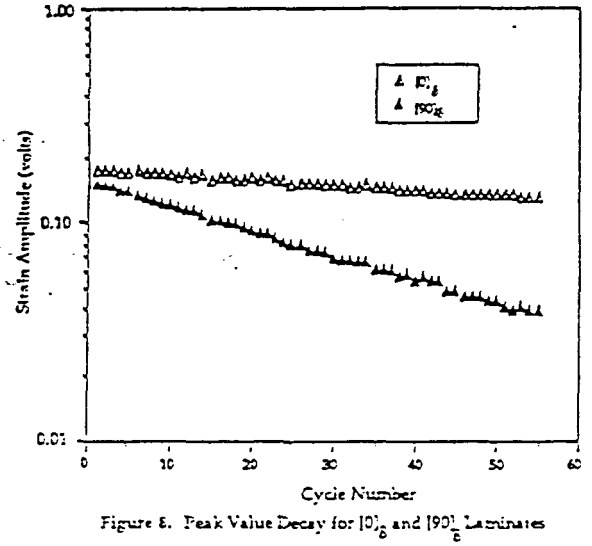


Figure 8. Peak Value Decay for $[0]_8$ and $[90]_8$ Laminates

These values were used in the model to predict the undamaged damping values for each of the specimens tested in this study. Figure 9 compares the measured and predicted damping values for each of the specimens. The measured values represent the average of 5 damping measurements taken for each specimen. The next step in the experimental procedure was to measure the logarithmic decrement for a $[0/90/0]_s$ specimen as a function of damage in order to develop a relationship between $\eta_{Bi(90)}$ and the matrix crack surface area, S.

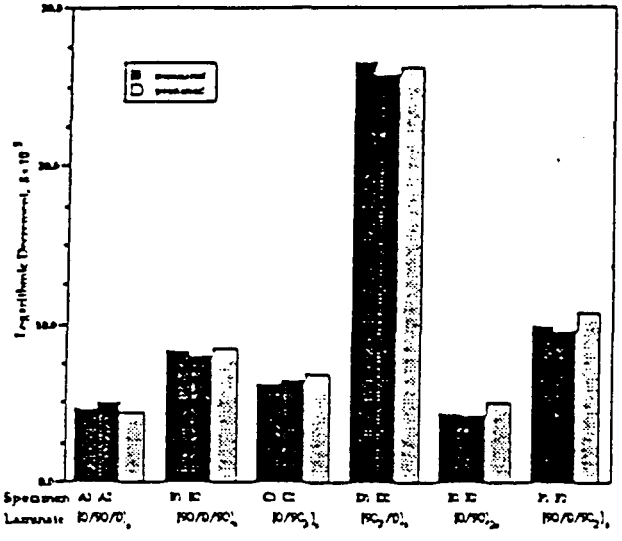

Figure 9. Undamaged Logarithmic Values for Gr/Ep Laminates

Laminate A, $[0/90/0]_s$

This particular stacking sequence was chosen to develop the damage-dependent damping relationship for matrix cracking in a single 90 degree ply because the 90 degree ply was not adjacent to any other 90 degree plies, thereby restricting the size of the matrix cracks to one ply thickness. Once a relationship was obtained for the damping of the specimen, the mathematical model parameter, $\eta_{Bi}$, was calculated as a function of matrix cracking, and subsequently used to predict damping for other AS4/3502 Graphite/Epoxy cross-ply laminates at various levels of matrix crack damage. Figure 10 is a plot of the measured logarithmic decrement vs. crack surface area for this laminate. The value $\eta_{Bi(90)}$ as a function of crack surface area was calculated from the model at each damage state for this specimen, and is seen to follow a curve of the form $y=Ax^b$. A power law curve fit was applied, and is shown in Figure 11. This approximation is valid for crack surface area values greater than 0.005 $in^2$, which corresponds to 1 crack per 12 inches of specimen length. Damage below this level was assumed to indicate an "undamaged" specimen. Therefore, for the case in which matrix cracks could not be detected, $\eta_{Bi(90)}$ was assumed to be the value extracted from the damping test of the $[90]_8$ laminate. This approximation was then used to predict damping of all of the cross-ply specimens at any given matrix crack damage state, including the undamaged state.

The reduction in stiffness was extremely small for this laminate. Because the data scatter was great in the stiffness measurements, and the reduction was minimal, no quantitative relationship between axial stiffness and matrix cracking was established. Figure 12 is a plot of normalized stiffness as a function of matrix crack surface area for this $[0/90/0]_s$ specimen. Matrix cracking in a laminate is seen to cause only a slight decrease the axial modulus (less than 1% for this laminate at saturation), whereas the damping increase is very significant (37% for the same level of damage). Therefore, damping can be considered to be a superior method of non-destructively evaluating the matrix cracking in a laminate.

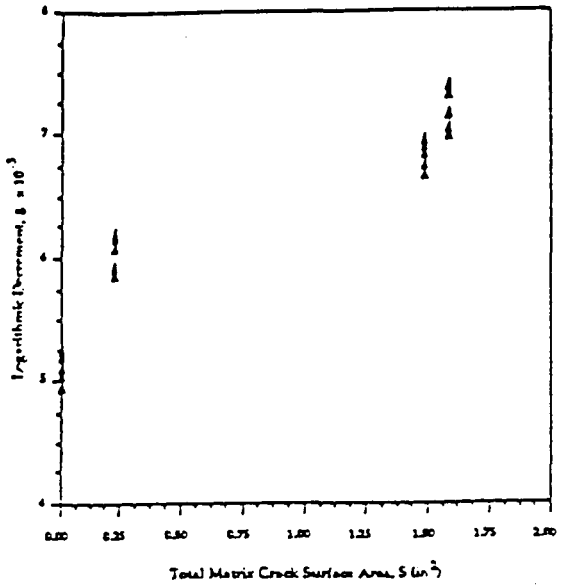

Figure 10. Logarithmic Decrement vs. Total Matrix Crack Surface Area $[0/90/0]_s$

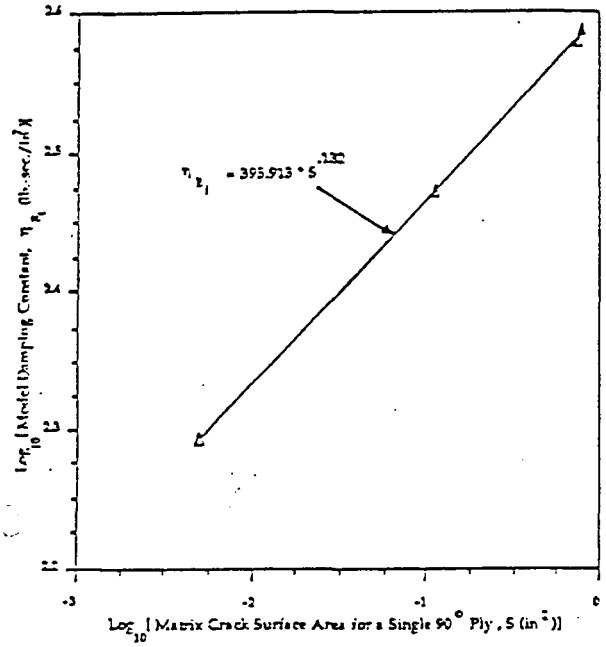


Figure 11. Model Damping Constant vs. Matrix Crack Surface Area for a Single 90° Ply

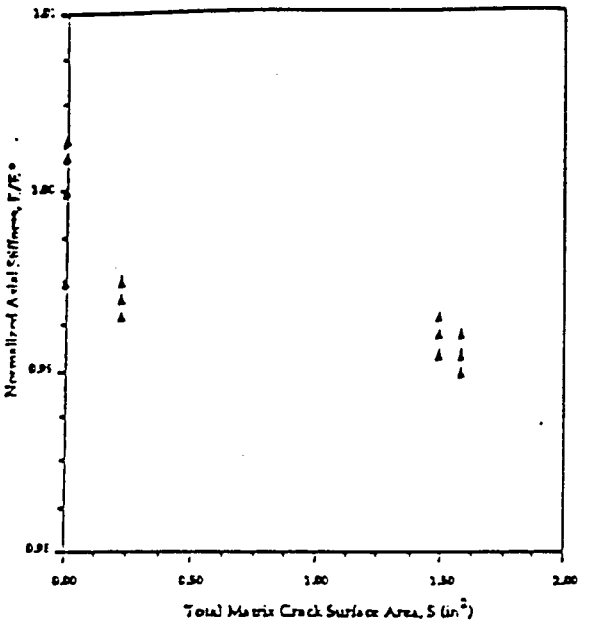


Figure 12. Normalized Axial Stiffness vs. Total Matrix Crack Area $[0/90/0]_s$

Laminate B $[90/0/90]_s$

The next laminate tested was also a six ply laminate, with a single 0 degree ply between two 90 degree plies in each half-plane. The undamaged bending stiffness was predicted to be significantly less than that of the $[0/90/0]_s$ laminate, which resulted in a smaller fundamental frequency for the same length beam. Therefore, the length of the $[90/0/90]_s$ beams was shortened to increase the frequency, in an attempt to match it with that of the $[0/90/0]_s$ laminate. However, the specimen had to be long enough to minimize the presence of shear deformation[15]. The frequency for the undamaged $[0/90/0]_s$ specimen was 20.7 Hz, and the frequency of the $[90/0/90]_s$ beam was 14.7 Hz.

The mathematical formulation for the logarithmic decrement in (14) includes a term which defines the damping to be a linear function of frequency, for a constant value of $\eta_{Bi}$. Closer inspection of the model development reveals, however, that $\eta_{Bi}$ is not constant with frequency, and in fact, the logarithmic decrement is predicted to follow a Zener like curve with respect to frequency. The damping test apparatus does not provide for testing a single specimen at a wide range of frequencies. Since the differences in frequency for all of the tests are not dramatic (less than 8 Hz difference), the differences in damping for the various frequencies are approximated by the linear relationship of the model. Therefore, for this study, $\eta_{Bi}$ was assumed to be constant with respect to frequency. If specimens at much higher frequencies, i.e., greater than 50 Hz had been measured, this assumption would not necessarily be valid.

The measured and predicted damping values for the undamaged $[90/0/90]_s$ laminate can be seen in Figure 9. Matrix crack initiation was found to occur at approximately 1200 lbs. for this stacking sequence. In this laminate the initial damage state was one in which matrix cracks were abundant in the outer 90 degree plies, and minimal at the mid-plane at a load of 1405 lbs. At a slightly higher load of 1496 lbs., the cracks in the inner 90 degree plies increased by a factor of 12, while the cracks in the outer plies increased by less than a factor of 3. At the saturation level, all of the 90 degree plies had approximately the same crack spacing (about 30 cracks per inch).

The mathematical model predicts that the damping will be affected more by matrix cracks far away from the mid-plane, than matrix cracks which are near the mid-plane. Therefore, it would not be an accurate depiction of damage-dependent damping to relate the damping strictly to the total crack surface area in a laminate. The location of the cracks with respect to the mid-plane must be taken into account when reporting the data. The reported crack surface area was therefore weighted by a non-dimensional factor $(\bar{z}_j/t)^2$, where $\bar{z}_j$ is the distance from the centroid of the crack to the mid-plane, and t is the laminate thickness. The equation for this weighted crack surface area, S*, is

$$S^* = 2w \sum_{j=1}^{N} c_j t_j \left(\frac{\bar{z}_j}{t}\right)^2 \qquad (17)$$

where $c_j$ is the number of cracks per inch of length in the $j^{th}$ ply, and $t_j$ is the thickness of the $j^{th}$ ply, and w is the width of the specimen. The factor of 2 accounts for the number of crack faces per matrix crack. It is stressed that this value was not used in the model to make damping predictions, but is simply used to identify the amount and location of matrix cracks in a laminate. Figure 13 indicates the relationship of measured and predicted damping to S* for this specimen.

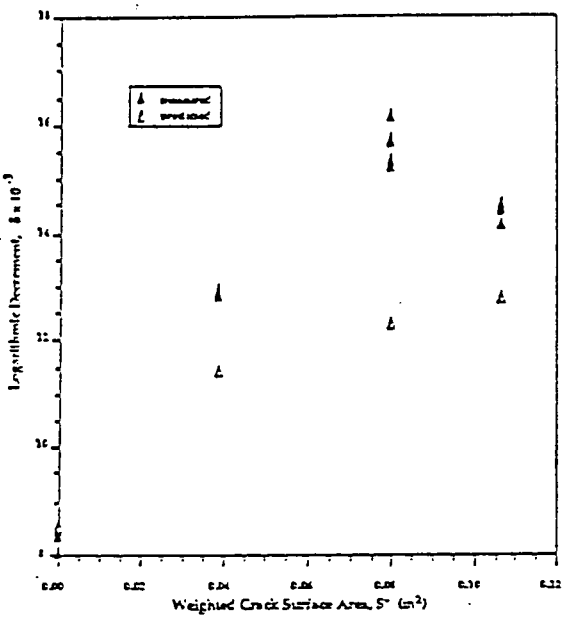


Figure 13. Logarithmic Decrement vs. Weighted Matrix Crack Area $[90/0/90]_s$

Laminate C $[0/90_2]_s$

This laminate contained 6 consecutive 90 degree plies sandwiched by single 0 degree plies on each outer surface. The damage progressed steadily from crack initiation at 32 ksi, to saturation at 62 ksi. The damping values increased significantly for this specimen, and the measured and predicted logarithmic decrement is plotted against S* in Figure 14. Although at first glance there appears to be a great deal of data scatter in the damping measurements taken at the higher damage levels, further inspection of the scaling reveals that the greatest amount of variation in damping measurements at a single damage state is less than 4 percent. The model predicts the increase in logarithmic decrement accurately for this laminate at all of the damage levels.

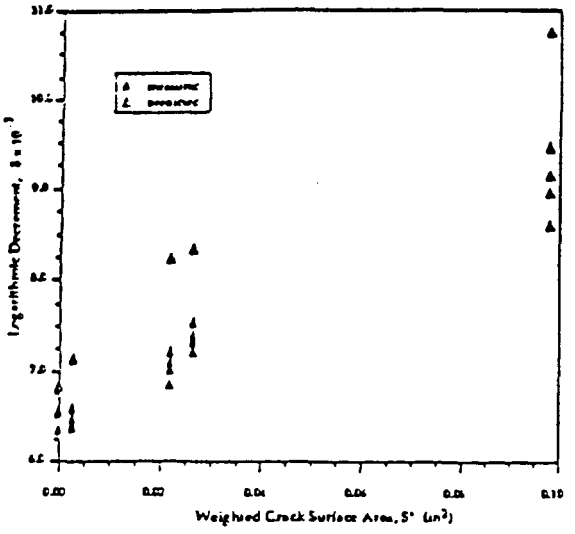


Figure 14. Logarithmic Decrement vs. Weighted Matrix Crack Area $[0/90_3]_s$

Laminate D, $[90_3/0]_s$

This laminate series had the smallest bending stiffness of all of the laminates considered. The natural frequency for the undamaged specimens was 12.7 Hz, which was also lower than that of all of the other laminates. The undamaged damping value was by far the highest of the specimens tested (the $[90]_8$ laminate was higher, but was only tested to obtain model constants), and was closely predicted by the mathematical model as seen in Figure 9. The plot of the logarithmic decrement vs. S* this laminate appears in Figure 15, with the corresponding model predictions. The initial and final predictions correspond very well to the measured values. The measured value at the middle damage state is slightly higher than the final measurement, and is attributed to experimental error.

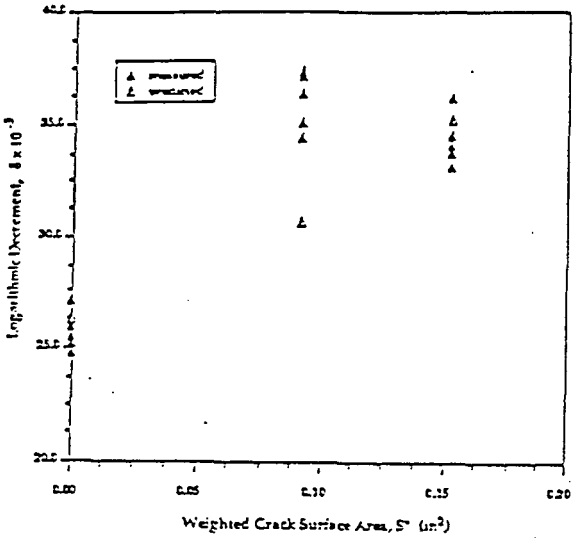


Figure 15. Logarithmic Decrement vs. Weighted Matrix Crack Area $[90_3/0]_s$

Laminate E, $[0/90]_{2s}$

The $[0/90]_{2s}$ (equivalently $[0/90/0/90]_s$) stacking sequence is similar to that of the $[0/90/0]_s$ except for the addition of two 90 degree plies adjacent to the laminate mid-plane. The damping for the undamaged $[0/90]_{2s}$ specimens was found to be almost identical to that measured for the $[0/90/0]_s$ specimens, and was closely predicted by the model. The damage progressed very rapidly for this particular stacking sequence in the 90 degree plies. This laminate began to show matrix cracking at 77.5 ksi and quickly reached a matrix crack saturation level at a stress level of 85 ksi, and failed at 87.5 ksi. The damping increased dramatically in these specimens, and is seen in Figure 16. This increase is predicted very well by the model.

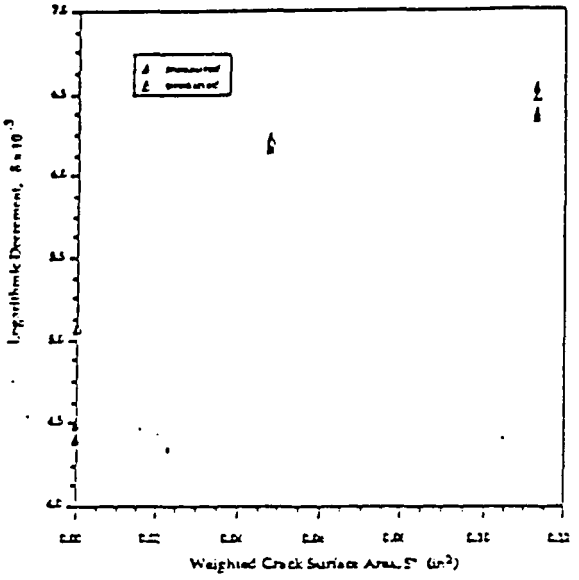


Figure 16. Logarithmic Decrement vs. Weighted Matrix Crack Area $[0/90]_{2s}$

Laminate F, $[90/0/90_2]_s$

The stacking sequence for laminate F was similar to the $[0/90_3]_s$ series, except for one of the 90 degree plies being outside the 0 degree ply. This difference has no effect on axial stiffness, but it does affect the bending stiffness. The damping of the undamaged $[90/0/90_2]_s$ specimen is seen to be significantly higher than the $[0/90_3]_s$ in Figure 9. For the $[90/0/90_2]_s$ stacking sequence, the matrix cracks grew very quickly in the outer 90 degree plies, and more slowly in the inner 90 degree plies. This laminate showed a very large increase in damping with increased damage, which was closely predicted by the model. This resulting function is plotted in Figure 17.

Laminate Comparisons

The results which have been presented indicate a strong dependence of damping on laminate stacking sequence and matrix cracking. It was postulated in the model development that the damping of a laminate would be greatly dependent upon the 90 degree plies, and only slightly dependent upon the 0 degree plies. This assumption is supported by the fact that the damping of the $[90]_8$ laminate was found to be 7 times greater than the damping of the $[0]_8$ laminate. However, the extensive testing of cross-ply laminates indicated that the percentage of 90 degree plies in a specimen has very little effect on the material damping of the laminate. Figure 18 is a plot of the measured logarithmic decrement for all of the undamaged specimens against the corresponding percentage of 90 degree plies in the specimen. For example, the $[0/90/0]_s$ laminate contains 33.33 percent 90 degree plies. No trend can be seen in this plot which would indicate that the damping changes with the percentage of 90 degree plies.

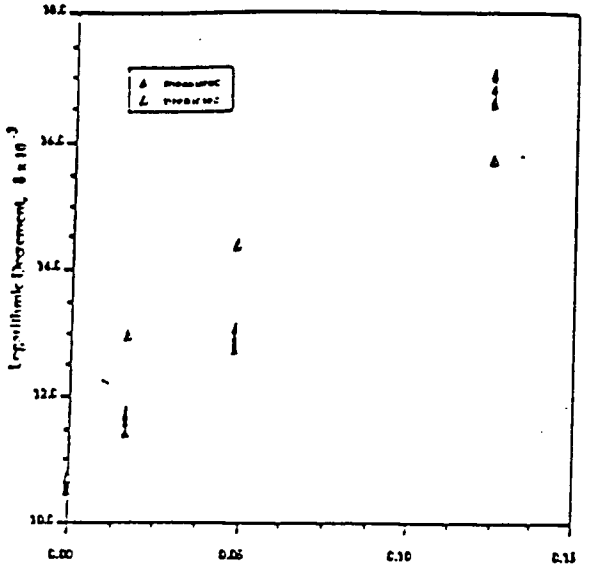


Figure 17. Logarithmic Decrement vs. Weighted Matrix Crack Area $[90/0/90_2]_s$

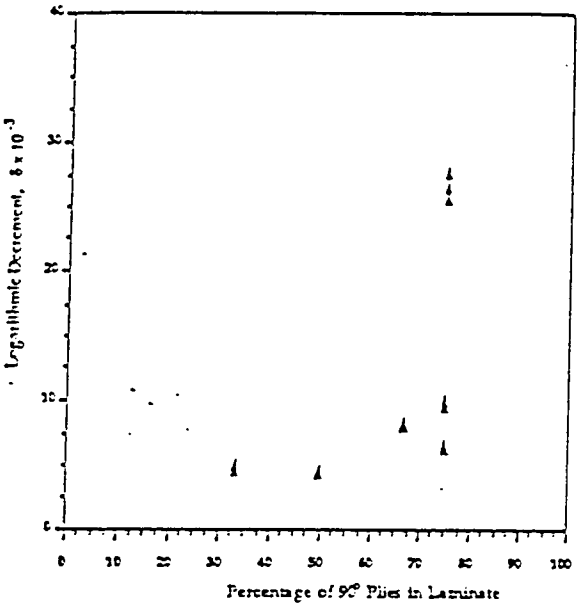


Figure 18. Measured Logarithmic Decrement vs. % 90° Plies

The major factor contributing to the relative damping magnitudes for the undamaged specimens was seen to be the placement of the 90 degree plies with respect to the mid-plane. A plot similar to Figure 18 was created which weighted each 90 degree ply by the distance from the mid-plane, and related this value to the measured logarithmic decrement. The value used for the domain is a weighted percentage of 90 degree plies given by the following formula:

$$\Psi = \frac{J}{N} \sum_{i=1}^{J} \left(\frac{\bar{z}_i}{t}\right)^2 \qquad (18)$$

where J is the number of 90 degree plies and N is the total number of plies in the laminate. A laminate with a significant fraction of the 90 degree plies far away from the mid-plane will have a high value of $\Psi$, while a laminate with the same percentage of 90 degree plies closer to the mid-plane, will have a low value of $\Psi$. The graph of this relationship is shown in Figure 19, and indicates an interesting function of the logarithmic decrement with respect to the number and location of 90 degree plies in a laminate. The trend appears to be exponential in form, although since no exact correlation can be made to account for this function, a curve fit was not applied.

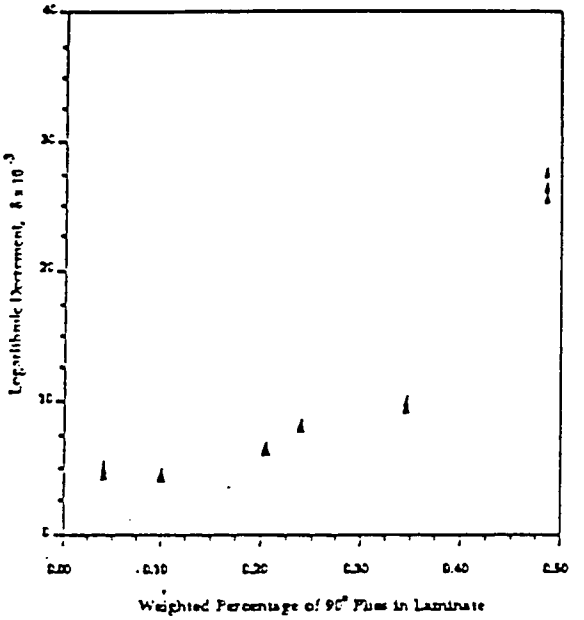


Figure 19. Measured Logarithmic Decrement vs. Weighted % 90° Plies

Figure 20 is a plot of the increase in the logarithmic decrement for each stacking sequence, from the undamaged state, to the matrix crack saturation damage state. The corresponding increase predicted by the model is also shown for each specimen. In all of the specimens except the $[90_3/0]_s$ specimen, the predicted increase is lower than the measured increase. This difference is possibly due to the presence of additional damage which may have been introduced during the loading process. The stacking sequences which were greatly underpredicted, $[90/0/90]_s$ (23 percentage points under), and the $[90/0/90_2]_s$ (25.7 percentage points under), both had 90 degree plies on the outer layer. As the number of matrix cracks directly under the strain gage increased for both of these laminates, the movement of the crack faces against the strain gage resulted in an increased damping measurement. This did not occur in the $[90_3/0]_s$ laminate because the damping was not measured at a damage level which contained a great number of matrix cracks. From the damage-dependent damping plots of the individual laminates given throughout the results section, it can be seen that for these specimens with the 90 degree plies at the outer surface, the model makes accurate predictions at earlier matrix crack damage states. For specimens with 90 degree plies at the outer surface containing a large number of matrix cracks, the model does not seem to correspond well with the experimental measurements. For all of the laminates with 0 degree plies at the outer surface, the model provides reasonable predictions of the increase in damping at all matrix crack levels.

## Conclusions

The material damping of several graphite/epoxy cross-ply laminates was measured as a function of matrix cracking. The testing configuration was a cantilevered beam, mechanically excited to vibrate in the first mode. The free response was captured, and the logarithmic decrement was calculated from the peak decay of the strain amplitude. Six different laminates were tested at several levels of matrix

crack damage. A mathematical model was used to predict the damping at all levels of damage, including the undamaged specimens.

The damping values for all of the undamaged specimens were predicted by the mathematical model. The percent error for this set of measurements and predictions was less than ± 15% for all of the specimens tested. The measured increases were very significant in all of the specimens. It was seen that matrix cracks in 90 degree plies which were far away from the mid-plane caused a greater increase in laminate damping values, than matrix cracks near the mid-plane.

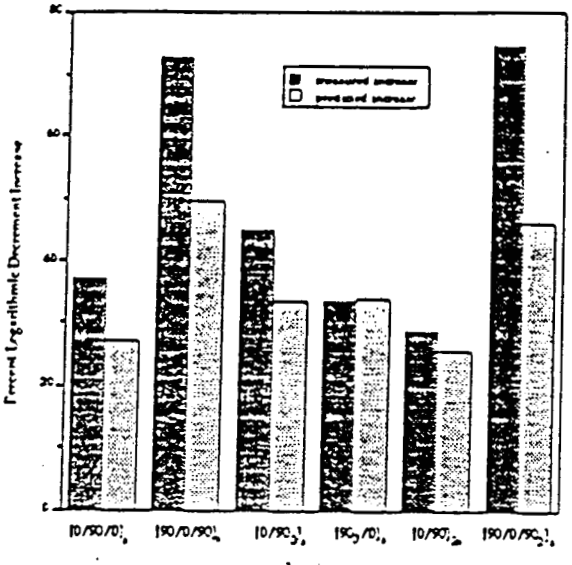


Figure 20. Percent Increase in Logarithmic Decrement at Matrix Crack Saturation Level

## References


1. Highsmith, A.L., Stinchcomb, W.W., and Reifsnider, K.L., "Stiffness Reduction Resulting from Transverse Cracking in Fiber-Reinforced Composite Laminates," Virginia Polytechnic Institute and State University, VPI-E-81.33, (November, 1981).

2. O'Brien, T.K., "An Evaluation of Stiffness Reduction as a Damage Parameter and Criterion for Fatigue Failure in Composite Materials," Ph.D. Dissertation, Virginia Polytechnic Institute and State University, (October 1978).

3. Norvell, R.G., "An Investigation of Damage Accumulation in Graphite/Epoxy Laminates," Texas A&M University Thesis, (August 1985).

4. Raju Mantena, T. Alan Place, and R.F. Gibson, "Characterization of Matrix Cracking in Composite Laminates by the Use of Damping Capacity Measurements," Mechanical Engineering Department, University of Idaho, Moscow, Idaho (October 1985).

5. D.G. Mohr and Edward F. Crawley, "Experimental Measurements of Material Damping of Aluminum and Graphite/Epoxy in Free-Fall Tuneable Excitation," Space Systems Laboratory, Dept. of Aeronautics and Astronautics, Massachusetts Institute of Technology, #11-82 (June 1982).

6. D.L. Edberg, "Measurement of Material Damping in a Simulated Space Environment," Ph.D. Dissertation, Stanford University (Dec. 1984).

7. A.T. DiBendetto, J.V. Gauchel, R.L. Thomas, and J.W. Barlow, "Nondestructive Determination of Fatigue Crack Damage in Composites Using Vibration Tests," Journal of Materials, JMLSA, 7.211-215 (June 1972).

8. Dahsin Liu, C.T. Sun, and L.E. Malvern, "Structural Degradation of Impacted Graphite/Epoxy Laminates," The Shock and Vibration Bulletin, Bulletin 56, Part 2, 51-60 (August 1986).

9. D. H. Allen, C.E. Harris, and A.L. Highsmith, "Prediction and Experimental Observation of Damage Dependent Damping in Laminated Composite Beams," Texas A & M University Mechanics and Materials Center (June 1987).

10. Albert B. Schultz and Stephen Tsai,"Dynamic Moduli and Damping Ratios in Fiber-Reinforced Composites," J. Composite Materials, 2:368-379 (July 1968).

11. R.D. Adams and D.G.C. Bacon, "Effect of Fibre Orientation and Laminate Geometry on the Dynamic Properties of CFRP," J. Composite Materials, 7:402-428 (October 1973).

12. D.X. Lin, R.G. Ni, and R.D. Adams, "Prediction and Measurement of the Vibrational Damping Parameters of Carbon and Glass Fibre-Reinforced Plastic Plates," J. Composite Materials, 18:132-153 (March 1984).

13. C.W. Bert and C.C. Sin, "Vibration and Damping of Laminated Composite-Material Plates Including Shear Effects," School of Aerospace, Mechanical, and Nuclear Engineering, The University of Oklahoma (March 1972).

14. R.F. Gibson and Robert Plunkett, "Dynamic Mechanical Behavior of Fiber-Reinforced Composites: Measurement and Analysis," J. Composite Materials, 10:325-341 (October 1976).

15. S. Kalyanasundaram, D.H. Allen, and R.A. Schapery, "Dynamic Response of a Viscoelastic Timoshenko Beam," Texas A & M University Mechanics and Materials Center (1987).

16. Albert B. Schultz and Stephen Tsai, "Dynamic Moduli and Damping Ratios in Fiber-Reinforced Composites," J. Composite Materials, 2:368-379 (July 1968).

17. R.D. Adams and D.G.C. Bacon, "Measurement of the Flexural Damping Capacity and Dynamic Young's Modulus of Metals and Reinforced Plastics," J. Phys. D: Appl. Phys., 6:27-41 (1973).

18. S.A. Suarez and R.F. Gibson, "Improvement and Optimization of Internal Damping in Fiber Reinforced Composite Materials," Mechanical Engineering Dept., University of Idaho (March 1986).

## 8.4 A Model for Predicting Damage Dependent Damping in Laminated Composites

Computers & Structures Vol. 30, No. 1/2, pp. 113–118, 1988
Printed in Great Britain.

0045-7949/88 $3.00 + 0.00


# A MODEL FOR PREDICTING DAMAGE DEPENDENT DAMPING IN LAMINATED COMPOSITES

S. KALYANASUNDARAM and D. H. ALLEN
Aerospace Engineering Department, Texas A&M University, College Station, TX 77843, U.S.A.

**Abstract**—A constitutive model has been developed for predicting the dynamic properties of composite beams which accounts for the influence of microstructural damage. The model assumes the damage state to be fixed. The model can account for both the damping increase and stiffness loss due to microstructural damage. Damage dependent material constants obtained from a baseline data set can be used to predict damping changes for several composite layups. The validity of the model has being verified by comparing the experimental results to model predictions for crossply laminates with a variety of stacking sequences.

## NOTATION

| | |
|---|---|
| $A$ | cross sectional area of the beam |
| $E$ | Young's modulus of elasticity |
| $N$ | total number of plies in the laminate |
| $s$ | total surface area of matrix cracks |
| $U$ | maximum strain energy of defiected beam |
| $w$ | defiection of the beam |
| $\delta$ | logarithmic decrement |
| $\rho$ | mass density/unit length |
| $l$ | length of the beam |
| $\hat{\rho}$ | complex curvature |
| $\lambda_n$ | frequency parameter |
| $\eta$ | loss factor |
| $\omega_n$ | complex frequency |
| $E_0^*$ | complex extensional modulus of the central ply |
| $I_{xx}$ | area moment of inertia of the cross section |
| $E^*$ | complex Young's modulus |
| $E'$ | storage modulus |
| $E''$ | loss modulus |
| $M^*$ | complex bending moment |
| $E_j^*$ | complex extensional modulus of $j$th ply |
| $E_j'$ | extensional storage modulus of the $j$th ply |
| $E_j''$ | extensional loss modulus of the $j$th ply |
| $E_L^*$ | complex modulus of 0° plies |
| $E_T^*$ | complex modulus of 90° plies |
| $\tan \phi_E$ | flexural loss tangent |

## INTRODUCTION

The process of ultimate failure of advanced composite materials is preceded by a sequence of microstructural and macrostructural events termed as damage. These events may be due to transverse matrix cracking, delamination, fiber breaking and fiber matrix debonding[1–4]. This damage results in stiffness loss which in turn may have a significant effect on the dynamic response of structural components[5]. Experimental results indicate that material damping may be more sensitive to damage development than stiffness loss. Damping in the presence of damage has been observed as high as 350% greater than the reference undamaged damping although the corresponding reduction in resonant frequencies is only about 5%.

Schultz and Warwick[6] used oscillatory flexural loads of zero mean value to fatigue cantilever beam specimens of scotchply laminates. During this fatiguing, the vibration response of the specimens was measured to determine if the response changes were indicative of fatigue. It was found that the increase in damping correlated fairly well with damage. For specimens which exhibited significant crack damage the damping ratio increased by 100%. In a closely related investigation[7] similar results were reported for oscillatory tensile loads of non-zero mean value. A torsional pendulum was used to measure the torsional storage modulus and damping capacity of carbon fiber reinforced bars before and after cracks were introduced through static torsion testing[8]. The specific damping capacity increased by nearly 80% after the introduction of damage. Chandra *et al.*[9] measured damping in crossply glass/epoxy composite beams before and after the introduction of damage due to static and fatigue loads. It was found that there was a considerable increase in damping with the increase in number of cycles of fatigue loading and the level of prestressing. For the fatigue load the reduction in storage modulus was very small after five cycles, but the damping showed a monotonic increase with increasing cycles. The damping was found to be independent of amplitude of oscillation up to about 0.04% strain.

Plunkett[10] measured damping factors of cantilever beams made of crossply glass/epoxy laminates as they were vibrated at different strain levels in the first and second bending mode simultaneously. It was found that the damping factor was substantially increased by large strain induced matrix cracking in laminae with transverse fibers. The damping factor was independent of current strain history or mode shape and was a function of damage. It was concluded that this behavior makes it possible to use a linear superposition method for

dynamic analysis. Smith *et al.*[11] have measured material damping of laminated graphite/epoxy specimens as a function of matrix cracking. It was found that damping increased significantly for various stacking sequences due to transverse matrix cracks. Allen *et al.*[12] have developed a theoretical model for predicting the damage dependent damping based on the theory of internal state variables to account for damage. Weitsman[13] has developed a continuum damage model for viscoelastic material. The special cases of uniaxial damage under uniaxial stress and interaction of damage with moisture diffusion have been considered.

In this paper a model is developed for predicting the structural dynamic response of composite beams in the presence of transverse matrix cracks. The validity of the theoretical formulation is verified by comparing the theoretical results with the experimental results obtained in [11] for different stacking sequences.

## MATHEMATICAL MODEL

The determination of damping properties of beams usually employs the Euler–Bernoulli assumption. In this theory it is assumed that the beam element is in pure bending and shear effects are neglected. For highly anisotropic materials and in the presence of interply delaminations, the dynamic properties obtained on the basis of the Euler–Bernoulli beam theory may exhibit significant errors. Since the current study will concentrate on crossply laminated beams with transverse matrix cracks, the Euler–Bernoulli beam theory is assumed to be adequate for obtaining the dynamic properties. The governing differential equation for the dynamic response of an elastic Euler–Bernoulli beam is given by

$$EI_{yy}\frac{\partial^4 w}{\partial x^4}+\rho A\frac{\partial^2 w}{\partial t^2}=0. \tag{1}$$

The solution for free vibrations can be written in the form

$$w_n(x,t)=W_n(x)\exp(i\omega t). \tag{2}$$

For sufficiently small damping, free vibrations are also approximately harmonic and from the correspondence principle of viscoelasticity, the elastic Young's modulus may be replaced by the corresponding complex modulus, $E^*$, where

$$E^*=E'+iE''=E'(1+i\eta) \tag{3}$$

and the flexural damping is given by

$$\tan\theta_E=\frac{E''}{E'}=\eta. \tag{4}$$

The complex frequency equation is given by

$$\lambda_n^4=\frac{\rho A l^4\omega_n^2}{E^* I_{yy}}, \tag{5}$$

where $\lambda_n$ is given by the boundary condition. Since $E^*$ is complex, the frequency values are also complex and can be written as

$$\omega_n=\omega_n'+i\omega_n''. \tag{6}$$

Separating the real and imaginary parts of eqn (5) results in

$$E'=\frac{\rho A l^4}{\lambda_n^4 I_{yy}}\omega_n'^2\left(1-\frac{\omega_n''^2}{\omega_n'^2}\right). \tag{7}$$

If $(\omega_n''/\omega_n')^2 \ll 1$

$$E'=\frac{\rho A l^4}{\alpha_n^4 I_{yy}}\omega_n'^2 \tag{8}$$

$$\tan\phi_E=\frac{2\omega_n''}{\omega_n'}$$

$$\tan\phi_E=\frac{\delta}{\pi}, \tag{9}$$

where $\delta$ is the logarithmic decrement obtained from a free vibration decay experiment.

The uniaxial constitutive equation for matrix cracking of elastic-composites under isothermal conditions is modelled by[14, 15].

$$\sigma_{xx}=E\epsilon_{xx}+I\alpha_1, \tag{10}$$

where $\alpha_1$ is an internal state variable representing matrix cracking in each ply. The changes in damping and stiffness due to microstructural damage are history dependent and spatially variable. For a fixed damage state the dynamic properties are slowly varying functions of time so that the composite material behaves like a linear viscoelastic body. Under sinusoidal loading, experimental results[10] indicate that the principle of superposition is valid for a damage state that is fixed and subjected to small amplitude vibrations. Based on these observations it is proposed that eqn (10) can be modified for sinusoidal loading at fixed damage state to

$$\tilde{\sigma}_{xx}=E^*\tilde{\epsilon}_{xx}+I^*\tilde{\alpha}_1, \tag{11}$$

where

$$E^*=E'+iE''$$

$$I^*=I'+iI''$$

$$\tilde{\epsilon}_{xx} = \epsilon_A e^{i\omega t}$$

$$\tilde{\alpha}_1 = \alpha_{1A} e^{i\omega t}.$$

Further insight into the effects of fixed damage on damping can be gained by studying the energy dissipated in a cycle of sinusoidal motion. Therefore,

$$\Delta w = \int \tilde{\sigma}_{xx}\, d\tilde{\epsilon}_{xx} \tag{12}$$

$$\Delta w = \int_0^{2\pi} \tilde{\sigma}_{xx} \frac{d\tilde{\epsilon}_{xx}}{d(\omega t)} d(\omega t). \tag{13}$$

In order to obtain a meaningful expression for energy dissipation the real part of $\tilde{\sigma}_{xx}$ and $\tilde{\epsilon}_{xx}$ should be used in the evaluation of (13). Thus,

$$\text{real}\left[\frac{d\tilde{\epsilon}_{xx}}{d(\omega t)}\right] = -\epsilon_A \sin \omega t \tag{14}$$

$$\begin{aligned}\text{Real}(\tilde{\sigma}_{xx}) &= \text{Real}[(E' - iE'')\epsilon_A e^{i\omega t} \\ &\quad + (I' - iI'')\alpha_{1A} e^{i\omega t}] \\ &= [E' \sin \omega t - E'' \cos \omega t]\epsilon_A \\ &\quad + [I' \sin \omega t - I'' \cos \omega t]\alpha_{1A}.\end{aligned} \tag{15}$$

Using (15) and (14) in (13) the energy dissipated per cycle is given by

$$\Delta w = \pi E'' \epsilon_A^2 + \pi I'' \alpha_{1A} \epsilon_A. \tag{16}$$

Note that for $\alpha_{1A} = 0$ (no damage) the above expression reduces to the case of energy dissipation in a linear viscoelastic body with no damage.

The strain energy stored during the peak displacement is

$$U = [E' \epsilon_A^2 + I' \epsilon_A \alpha_{1A}]/2. \tag{17}$$

The loss factor is

$$\eta = \frac{E'' \epsilon_A^2 + I'' \alpha_{1A} \epsilon_A}{E' \epsilon_A^2 + I' \alpha_{1A} \epsilon_A}. \tag{18}$$

Furthermore, it will be assumed that

$$I'' \alpha_{1A} = \Delta E'' \epsilon_A \tag{19a}$$

$$I' \alpha_{1A} = \Delta E' \epsilon_A, \tag{19b}$$

where $\Delta E''$ is the increase in loss modulus and $\Delta E'$ is the decrease in storage modulus due to damage. This assumption is made based on the experimental evidence that damping increases with microstructural damage and the resonant frequencies decrease. Equation (18) can therefore be written as

$$\eta = \frac{E'' + \Delta E''}{E' + \Delta E'}. \tag{20}$$

*Application of the model to crossply laminates*

The moment–curvature relationship for a viscoelastic Euler–Bernoulli beam vibrating sinusoidally with frequency $\omega$ can be written as

$$\frac{\tilde{M}}{E^* I} = \frac{1}{\tilde{\rho}}. \tag{21}$$

For plies of uniform thickness the complex flexural modulus is given in terms of the complex ply moduli and stacking geometry by[16]:

$$\begin{aligned}E^* &= \frac{8}{N^3}\left[\sum_{j=1}^{N/2} E_j^*(3j^2 - 3j + 1)\right] \quad \text{for even } N \\ &= \frac{8}{(N)^3}\left[\frac{E_0^*}{8} + \sum_{j=1}^{(n-1)/2} E_j^*(3j^2 - 3j + 1)\right] \quad \text{for odd } N.\end{aligned} \tag{22}$$

In this work symmetric laminated beams composed solely of longitudinal and transverse plies will be considered. For this case eqn (22) reduces to

$$E^* = \frac{8}{N^3}[aE_L^* + bE_T^*], \tag{23}$$

where $a$ and $b$ are functions of stacking geometry.

The flexural damping is given by

$$\tan \phi_E = \eta = \frac{aE_L'' + bE_T''}{aE_L' + bE_T'}. \tag{24}$$

In the presence of transverse matrix cracks in the 90° plies, it is assumed here that $E_T'$ and $E_T''$ will be affected by damage and the values of $E_L'$ and $E_L''$ remain unchanged since no cracking occurs in the 0° plies.

Comparing eqns (20) and (24), the loss factor in the presence of transverse matrix cracks is thus given by

$$\eta = \frac{aE_L'' + C\Delta E_T'' + bE_T''}{aE_L' + C\Delta E_T' + bE_T'}, \tag{25}$$

where $C\Delta E_T''$ and $C\Delta E_T'$ are functions of the total surface area of matrix cracks and the location of the cracks. $\Delta E_T''$ and $\Delta E_T'$ as functions of crack damage can be extracted from a single simplified stacking sequence. This information may then be utilized in (25) to predict the damping as a function of damage for different stacking sequences.

## DISCUSSION OF RESULTS

Experimental results[11] obtained from crossply laminates with different stacking sequences will be used to verify the validity of the model developed in the previous section. By testing laminates built from 0 or 90° plies, the values of $E'_L$ and $E'_T$ can be obtained from resonant frequency measurements through eqn (8). Using the damping measurements, the values of $E''_L$ and $E''_T$ can be obtained from eqn (4). These values can be used to predict the damping of any crossply laminates with various combinations of 0 and 90° plies. Figure 1 is a comparison of experimental and theoretical damping values for different laminates. For polymer matrix composites the viscoelasticity of the matrix is the major source of energy dissipation. Hence, the material damping of a crossply laminated beam is dominated by the location and the number of 90° plies. The predicted and experimental damping values indicate that the flexural damping increases with distance from the midplane of the beam.

For predicting the damage dependent damping for different stacking sequences, the increase in loss modulus as a function of matrix crack damage can be constructed by experimentally measuring the damping increase in a [0/90/0], laminate. The change in loss factor as a function of transverse matrix crack surface area is given experimentally by

$$\Delta\eta(s) = 0.0002(s) - 1.7108\times10^{-5}s^2. \quad (26)$$

For this laminate the damping increased by 35%, while the reduction in the resonant frequency was about 0.07%. Using eqn (25) for a [0/90/0], laminate, the change in the loss modulus as a function of surface area of matrix cracks is given by

$$\Delta E''_T(s) = 57.97\times10^{-6}[0.0002(s) - 1.7108\times10^{-5}s^2]. \quad (27)$$

The experimental change in the storage modulus is negligible.

The experimental and theoretical predictions of damping of a [90/0/90], laminate at two different damage states are illustrated in Fig. 2. The descriptions of the damage states are given in Table 1. For this laminate there are more transverse matrix cracks at the outer 90° plies than the 90° plies near the midplane. The damping increases by nearly 100%. The agreement between theoretical and experimental results is good. The reduction in the first mode resonant frequency (an indication of stiffness loss) is only about 7%. This trend clearly indicates that damping changes are more sensitive to the microstructurally induced damping changes than the stiffness loss. Figure 3 depicts the effect of the matrix damage on a [0/90/0/90], laminate. The corresponding damage states are given in Table 2. The theoretical model predicts the increase in damping due to transverse matrix cracks to be a function of both total matrix crack area and the location of the 90° ply in the laminate. It is interesting to note that for approximately the same amount of total matrix crack area the damping change in a [90/0/90], laminate is several times higher than the change in the [0/90/0/90], laminate. This is due to the fact that the matrix crack damage in 90° plies farther away from the midplane of the beam will lead to a larger increase in damping than the 90° plies near the midplane. This trend is captured by both the theoretical and

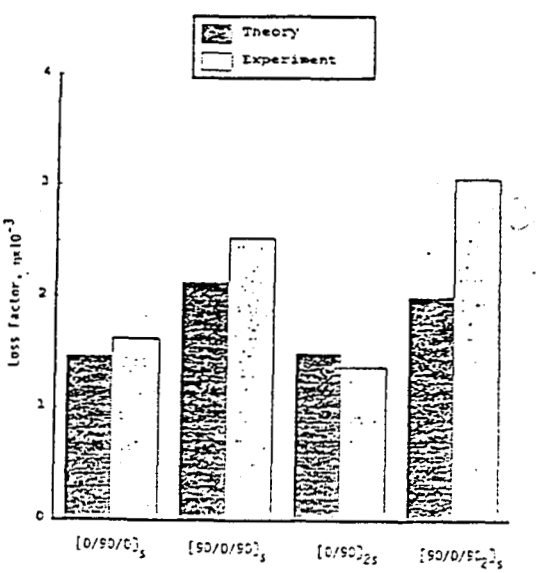


Fig. 1. Damping values for various laminates.

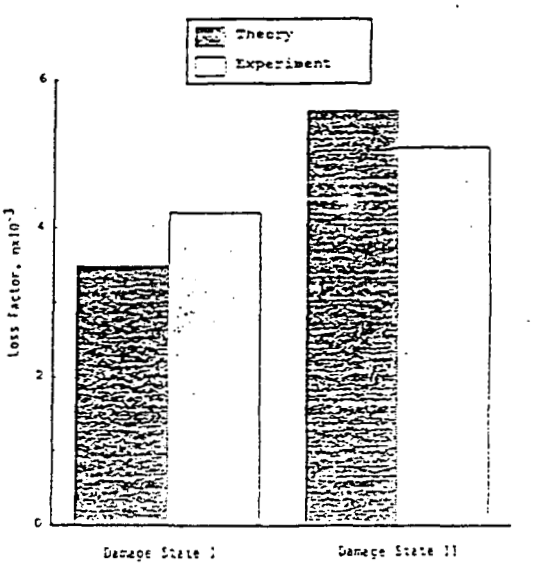


Fig. 2. Damage dependent damping values for [90/0/90], laminate.

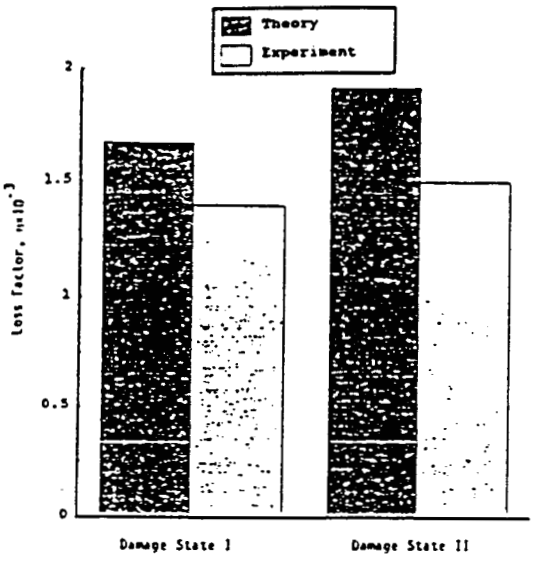


Fig. 3. Damage dependent damping values for $[0/90]_2$, laminate.

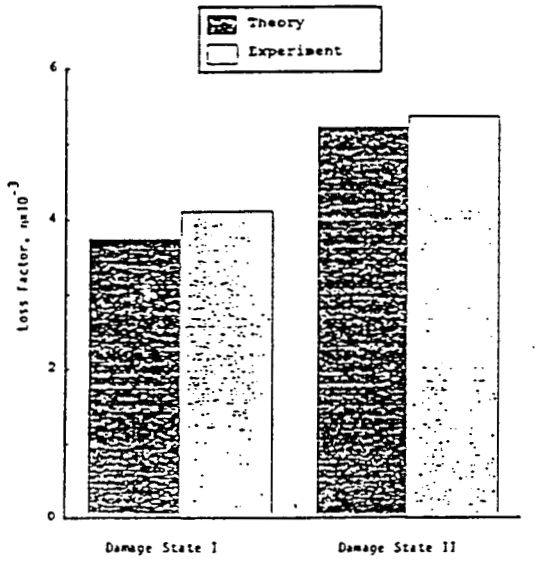


Fig. 4. Damage dependent damping values for $[90/0/90_2]$, laminate.

experimental results. Figure 4 illustrates the effect of matrix cracks on a $[90/0/90_2]$, laminate (see Table 3). The agreement between the theoretical and experimental damping values for the damage states is good. However, the theoretical model tends to overpredict the increase in damping from undamaged damping values as compared to the experimental results.

## CONCLUSIONS

A constitutive model has been developed for including the effect of microstructural damage on the dynamic response of laminated composites.

Table 1. Description of damage state for [90/0/90], alminate

| Stacking geometry | Damage state I (cracks/in.) | Damage state II (cracks/in.) |
|---|---|---|
| 90 | 7.9 | 21.3 |
| 0 | – | – |
| 90 | 0 | 2.9 |
| 90 | 0 | 2.9 |
| 0 | – | – |
| 90 | 7.9 | 30.2 |

Table 2. Description of damage state for $[0/90]_2$, laminate

| Stacking geometry | Damage state I (cracks/in.) | Damage state II (cracks/in.) |
|---|---|---|
| 0 | – | – |
| 90 | 5.0 | 10.3 |
| 0 | – | – |
| 90 | 6.3 | 13.0 |
| 90 | 6.3 | 13.0 |
| 0 | – | – |
| 90 | 3.7 | 6.7 |
| 0 | – | – |

Table 3. Description of damage state for $[90/0/90_2]$, laminate

| Stacking geometry | Damage state I (cracks/in.) | Damage state II (cracks/in.) |
|---|---|---|
| 90 | 10.9 | 24.7 |
| 0 | – | – |
| 90 | 3.9 | 27.2 |
| 90 | 3.9 | 27.2 |
| 90 | 3.9 | 27.2 |
| 90 | 3.9 | 27.2 |
| 0 | – | – |
| 90 | 11.9 | 26.7 |

This model is valid for a fixed damage state and small amplitude vibrations. Under these assumptions the composite material behaves like a quasi-linear viscoelastic body. The validity of the theoretical formulation has been verified for crossply graphite–epoxy laminates with a variety of stacking sequences. Damage dependent material constants obtained from [0/90/0], laminate have been used to predict the increase in damping in [90/0/90],, [0/90/0/90], and $[90/0/90_2]$, laminates for different damage states. Damping is found to be more sensitive to microstructural damage than the stiffness loss. Thus, damping holds some promise for further studying the damage development in composite structural components.

*Acknowledgements*—The authors wish to acknowledge the financial support provided by NASA Johnson Space Center under grant number NAG 9-140.

## REFERENCES


1. K. L. Reifsnider and K. Jamison, Fracture of fatigue-loaded composite laminates. *Int. J. Fatigue* 4, 187–197 (1982).
2. H. L. Highsmith, W. W. Stinchcomb and K. L. Reifsnider, Stiffness reduction resulting from transverse cracking in fiber reinforced composite laminates. Virginia Polytechnic Institute and State University, Blacksburg, VA, VPI-E-81.33 (1982).
3. J. E. Masters and K. L. Reifsnider, An investigation of cumulative damage development in quasi-isotropic graphite/epoxy. In *Damage in Composite Material* (Edited by K. L. Reifsnider), pp. 40–62. ASTM STP775, American Society for Testing and Materials, Philadelphia, PA (1982).
4. R. G. Norvell, An investigation of damage accumulation in graphite/epoxy laminates. Texas A&M University thesis (1985).
5. S. Kalyanasundaram, J. D. Lutz, W. E. Haisler and D. H. Allen, Effect of degradation of material properties on the dynamic response of large space structures. *J. Spacecraft Rockets* 23, 297–302 (1986).
6. A. B. Schultz and D. N. Warwick, Vibration response: A non-destructive test for fatigue crack damage in filament-reinforced composites. *J. Comp. Mater.* 5, 394–404 (1971).
7. A. T. DiBenedtto, J. V. Gavehel, R. L. Thomas and J. W. Barlow, Nondestructive determination of fatigue crack damage in composites using vibration tests. *J. Materials* 7, 211–215 (1972).
8. R. D. Adams, J. E. Flitcroft, N. L. Hancox and W. N. Reynolds, Effect of shear damage on the torsional behavior of carbon fibre reinforced plastics. *J. Comp. Mater.* 7, 68–75 (1973).
9. R. Chandra, A. K. Mallik and R. Prabhakaran, Damping as a measure of damage in composites. *J. Tech. Councils ASCE* 108, 106–111 (1982).
10. R. Plunkett, Damping in fiber reinforced laminated composites at high strain. *J. Comp. Mater. Suppl.* 14, 109–117 (1980).
11. S. A. Smith, D. H. Allen and C. E. Harris, An experimental investigation of damage-dependent material damping in laminated composites. In *Proceedings AIAA 29th Structures, Structural Dynamics and Materials Conference*, pp. 1501–1510. American Institute of Aeronautics (1988).
12. D. H. Allen, C. E. Harris and A. L. Highsmith, Prediction and experimental observation of damage dependent damping in laminated composite beams. In *The Role of Damping in Vibration and Noise Control* (Edited by L. Rogers and J. C. Simonis), DE-Vol. 5, pp. 253–264. American Society of Mechanical Engineers (1987).
13. Y. Weitsman, A continuum damage model for viscoelastic materials. Mechanics and Materials Center, Texas A&M University, MM 4762-87-17 (1987).
14. D. H. Allen, C. E. Harris and S. E. Groves, A thermomechanical constitutive theory for elastic composites with distributed damage — Part I: theoretical development. *Int. J. Solids Struct.* 23, 1301–1318 (1987).
15. D. H. Allen, C. E. Harris and S. E. Groves, A thermomechanical constitutive theory for elastic composites with distributed damage — Part II: application to matrix cracking in laminated composites. *Int. J. Solids Struct.* 23, 1319–1338 (1987).
16. R. F. Gibson and R. Plunkett, Dynamic mechancial behavior of fiber-reinforced composites: measurement and analysis. *J. Comp. Mater.* 10, 324–341 (1976).